To the Graduate council:

I am submitting herewith a thesis written by Daniel Max Sherman entitled "Manipulating aerodynamic boundary layers using an electrohydrodynamic effect generated by a One Atmosphere Uniform Glow Discharge Plasma." I have examined the final copy of this thesis for form and content and recommend that it be accepted in partial fulfillment of the requirements for the degree of Master of Science, with a major in Physics.

J. Reece Roth

J. Reece. Roth, Major Professor

We have read this dissertation
And recommend its acceptance:

A. J. Baker

Marshall Pace

Stuart Bolston

Accepted for the Council:

Anne Mayhew

Associate Vice Chancellor and
Dean of The Graduate School

MANIPULATING AERODYNAMIC BOUNDARY LAYERS USING AN ELECTROHYDRODYNAMIC EFFECT GENERATED BY A ONE ATMOSPHERE UNIFORM GLOW DISCHARGE PLASMA

A Thesis
Presented for the
Master of Science
Degree
The University of Tennessee, Knoxville

Daniel Max Sherman
August 1998

STATEMENT OF PERMISSION TO USE

It is the author's intent that this thesis may be allowed to be copied for use in any way that promotes education or research, as long as the material used is cited.

DEDICATION

This thesis is dedicated to the memory of my grandmother

Mrs. Letha Nell Sherman

who taught me the value of education.

ACKNOWLEDGEMENTS

There are several people to whom I am grateful for enriching my educational experience at the University of Tennessee. I have benefited greatly from the educational and research instruction of Professor J. Reece Roth, whose ideas will shape my thoughts for years to come. I would also like to thank Stephen Wilkinson, for making my time at NASA such an enjoyable one. I would also like to express my appreciation to my Dissertation Committee, Professor J. Reece Roth, Mr. Stephen P. Wilkinson of the NASA Langley Research Center, Professor A. J. Baker, Professor Marshall O. Pace, and Professor Stuart B. Elston, for their support and comments.

There are a number of people whose assistance should be recognized. I would like to thank Professor Geoffrey Canright for encouragement and guidance in attaining my educational goals. I would also like to thank Albert and Rosetta White for the tremendous amount of emotional support they have given me over so many years.

Lastly, this work was sponsored by NASA grant NCC-1-223 and conducted at the NASA Langley Research Center and the University of Tennessee Plasma Sciences Laboratory.

ABSTRACT

In this study the ability of a One Atmosphere Uniform Glow Discharge Plasma (OAUGDP) to modify aerodynamic boundary layers is demonstrated. In early 1996, the staff at the University of Tennessee's Plasma Sciences Laboratory designed and had fabricated circuit board electrodes capable of producing thin, flat sheets of its proprietary One Atmosphere Uniform Glow Discharge Plasma (OAUGDP). Since then, these OAUGDP panels have been repeatedly and successfully operated in the NASA Langley Research Center's 7 x 11 (17.8 x 27.9 cm) Low Speed Wind Tunnel. Experimental results will be presented from exploratory investigations of the OAUGDP panel's aerodynamic properties utilizing an air bearing drag balance, pitot tube velocity profiles, smoke-wire flow visualization, and a hot-wire anemometer.

The OAUGDP panels consist of parallel linear arrays of RF electrode strips on opposite sides of standard circuit board material. The OAUGDP panels have been energized by a RF power supply operating at frequencies between 0.4 - 6.0 kHz, and RMS voltages between 2.2 - 5.6 kV. These panels have had a variety of electrode geometries with different electrode spacings and electrode widths, and with the strip electrodes oriented both parallel and perpendicular to the airflow. While the number of possible electrode geometries is limitless, our investigations have identified two types of electrode strips with interesting aerodynamic properties.

Symmetric OAUGDP panels (plasma panels in which the plasma is generated on each side of the electrode strips) are found to increase the aerodynamic drag and boundary layer thickness by creating vortical structures and inducing turbulence.

Asymmetric OAUGDP panels (plasma panels in which the plasma is generated predominately on one side of an electrode) are found to be capable of either increasing or decreasing the aerodynamic drag and boundary layer thickness by inducing a unidirectional airflow immediately above the surface of the OAUDGP panel, either against (counter-flow) or with (co-flow) the free stream airflow, respectively.

In either case, the degree to which the aerodynamic boundary layer is affected is dependent on the electrode strip's orientation with respect to the airflow (parallel or perpendicular), relative electrode spacing, electrode width, and applied voltage. The data also suggest that the frequency of the applied RF voltage and the plasma power also strongly influence the panel's performance.

TABLE OF CONTENTS

LIST OF FIGURES

Figures | Page

Part I

INTRODUCTION

Motivation

Since the Wright brothers' airplane first took off, more efficient methods of flight have been sought. For nearly a hundred years, advances in aviation have been achieved by improving the shape of aircraft and the propulsion and control systems. An aerodynamic body is generally designed so that a gas flows over its surface with minimized drag. But is there a way in which the airflow over existing, well-known aerodynamic bodies can be made more efficient and the drag reduced further without changing the basic shape? By what means can one reach beyond a surface to provide an effector mechanism to affect the airflow?

Previous Attempts

According to Dennis Bushnell, Chief Scientist of the NASA Langley Research Center, any method of controlling the airflow above a surface is useful only when the concept is both 1.) technically sound, and 2.) technologically feasible (Bushnell, 1997). These two stages in the development of a concept he refers to as *filters*. He related the *technical filter* to how well a concept functions to accomplish a particular aerodynamic goal (including net power balance and complete theoretical understanding of the concept), and the *technological filter* to such issues as cost, complexity, reliability, retrofittability, and performance flexibility.

Attempts to modify aerodynamic boundary layers without reshaping the surface can be divided into three categories: 1.) mass flow injection/removal; 2.) active surface enhancements; and 3.) energizing the mass flow. These three types of boundary layer control can be summarized as follows.

(1.) Mass flow injection/removal is still being actively pursued. In these approaches injection or removal of air (or some other gas) into or from the free stream airflow is accomplished by a single or series of holes or slits in the surface. Sucking or blowing presents technological difficulties, particularly with complexity and retrofittability because of the required internal piping and mechanical pumps (Hefner & Bushnell, 1989). Some current research uses this approach by inducing periodic oscillations in the boundary layer (by alternating between blowing and sucking through a rectangular slit or hole in the surface) to achieve both drag reduction and delaying airflow separation (Lachowicz et al, 1998, and Wygnanski, 1997).

(2.) One can also manipulate the passing airflow by modifying the skin of an aircraft. Two examples of methods of surface modification are riblets and MEMS (MicroElectronic Mechanical Systems). Riblets act passively, and are a series of narrow, parallel streamwise grooves on the skin of the aircraft in contact with the airflow. These grooves channel the airflow as it passes over the surface, suppressing turbulence close to the surface (Walsh, 1989). MEMS or "microelectronic" surfaces achieve active control of a boundary layer by utilizing a multitude of shear stress sensors and micro-sized actuators linked to a neural network. The neural network is then taught to sense and alter the aerodynamic boundary layer in such a way as to suppress the formation of vorticity and turbulence, leading to reductions in the drag (Kimura, et al, 1989).

Both active and passive concepts are technically feasible, though all have distinct technological disadvantages. Riblet technology, while producing a significant decrease in drag, (up to 10 percent) has problems with cost and maintenance. Due to the small width of the grooves, which are easy to fill with dirt and contaminants, continuous maintenance is required to keep the grooved surfaces clean. Along with the initial cost (relative to the benefits), this issue has prevented the riblet concept from gaining widespread acceptance. Microelectronic surfaces are not retrofitable, may not be reliable, and are both complex and costly. Any form of impact, by birds, hail, or any other object, not to mention walking on them or lightning, may destroy the delicate sensors and actuators on the surface. Additionally, the issues of cost and complexity, which arise from covering the surface area of an aircraft with specialized microelectronics, make this particular concept economically unattractive.

(3.) Energizing the mass flow by means other than blowing or suction (of which the present method is an example) modifies aerodynamic boundary layers by adding energy or momentum to the boundary layer airflow. These methods can be subdivided by the means of energy addition, which include energizing the flow by acoustic, microwave, or laser sources, or by momentum addition, which can be accomplished by a plasma source. Acoustic disturbances can be used to trip a boundary layer from laminar to turbulent flow, with a resultant increase in drag. Both direct microwave heating and laser addition of energy/heat to the airflow may also increase the level of turbulence and the thickness of the aerodynamic boundary layer, but in any case, these approaches appear to be useful only for velocities greater than Mach 1.

A variety of plasma - based methods for altering aerodynamic boundary layers have been and are being studied. Plasmas are quasi-neutral collections of charged particles, which respond to electric and magnetic fields and exhibit collective behavior. Typically plasma is formed by energy input from DC or RF electric fields. Plasma based methods offer to the field of aeronautics the ability to couple momentum and energy into the neutral gas (airflow) through Lorentzian particle collisions with the charged species of the plasma. Furthermore, once generated, the plasma and the airflow can be manipulated by magnetic fields (MHD) or by electric fields (EHD).

While many types of plasma sources are available, a fundamental requirement for a plasma to be utilized in aerodynamic flow control is that it exist at one atmosphere of pressure in normal air. This greatly constrains the methods available to generate the plasma. Plasma based methods which can function at one atmosphere of pressure and be used for boundary layer control include coronas (sometimes called ion wind) (El-Khabiry and Colver, 1997), magnetohydrodynamics (MHD) (Tsinober, 1989), crossed microwave beam focusing (Kuo, 1989), and the One Atmosphere Uniform Glow Discharge Plasma (OAUGDP) (Roth, et al., 1995 a, b).

Coronas are created by very high electric fields, above the breakdown strength of the surrounding gas, near sharp points or fine wires. Recent work using coronas was done by S. El-Khabiry, and G. M. Colver (1997). Using a corona they obtained experimentally an 8 percent reduction in the drag, in the laminar regime with an airflow velocity of 2.1 m/s, and developed a preliminary numerical model for the corona. Coronas have the technical limitation of scaleability to relevant flight velocities.

In the 1950's and 1960's magnetohydrodynamic (MHD) approaches were explored as a means of using a plasma to interact with the boundary layer (Tsinober, 1989). When a magnetic field is perpendicular to the direction of a current flow, the neutral gas, which exchanges momentum with the current, will experience a body force (Lorentz force) and be accelerated in a direction normal to both the current and the magnetic field. MHD requires both that real currents be present in the boundary layer, and the use of either strong electromagnets or powerful rare earth magnets. Having a real current pass through electrodes on the surface erodes them over long times (a reliability issue), and the magnets not only have to be built into the wing (a retrofittability issue), but also are heavy (thus reducing the payload of the aircraft). Additionally, most MHD concepts assumed sufficiently high airspeeds that a surface layer of plasma would be present, or alternatively that a separate plasma source would generate the plasma.

Creating atmospheric plasmas using microwave power is technically difficult because they require high power densities (kW/cm^3). At the Polytechnic University in New York, one method of creating a microwave plasma in atmospheric air was suggested by S. Kuo (Kuo, 1989). In his approach, two beams of microwave energy with electric field intensities slightly less than that necessary to ionize air are aimed such that the beam paths cross where the plasma is desired. At this location, a plasma forms due to the high electrical fields resulting from constructive interference of the electric fields of the two beams. Because of the high power consumption, this method is not envisioned for subsonic applications, including commercial aviation.

The One Atmosphere Uniform Glow Discharge Plasma (OAUGDP) (Roth, 1995 a, b; 1997) offers a simple and direct way of creating an atmospheric plasma suitable for the modification of aerodynamic boundary layers. The OAUGDP is an electrohydrodynamic (EHD) method of generating plasma, i.e. it doesn't require magnetic fields, the induced velocities are scaleable linearly with the applied plasma voltage, and does not require large areal power densities for its generation.

Part II

The One Atmosphere Uniform Glow Discharge Plasma

Generation Mechanism

Professor J. R. Roth and co-workers at the University of Tennessee achieved the first One Atmosphere Uniform Glow Discharge Plasma (OAUGDP) in January, 1992, and received patents on this method of generating plasma in 1995 (Roth, 1995 a,b). As the name implies, the OAUGDP is an atmospheric plasma, though it can also be formed at both higher and lower pressures. It is uniform in comparison to a dielectric barrier discharge or ozonizer plasma, in which filaments are present in the plasma during operation. The OAUGDP is a glow discharge during each half-cycle of the voltage waveform, even though the plasma is generated by a RF power supply instead of a DC power supply and operated at one atmosphere of pressure. Independent research has confirmed the presence of the classical structures of a normal DC glow discharge plasma (cathode fall, negative glow, Faraday dark space, and positive column) during each half-cycle of operation of the OAUGDP. (Massines, et al, 1998)

The OAUGDP is a capacitive plasma, which is energized by displacement currents. No real currents need to pass through the plasma. It is formed between two RF electrodes, on at least one of which a sufficiently strong dielectric coating is necessary to the mechanism of plasma formation, and to suppress the formation of RF arcs. An RF voltage with the frequency required to trap ions is applied across the gap between the electrodes. Under conditions required by the ion trapping mechanism (Roth, 1995c, Section 12.5.2) for a given gas, including the proper frequency and amplitude of the applied RF voltage, the One Atmosphere Uniform Glow Discharge Plasma will appear (figure 2.1). If the frequency of the applied RF voltage is too low, or the gap distance is

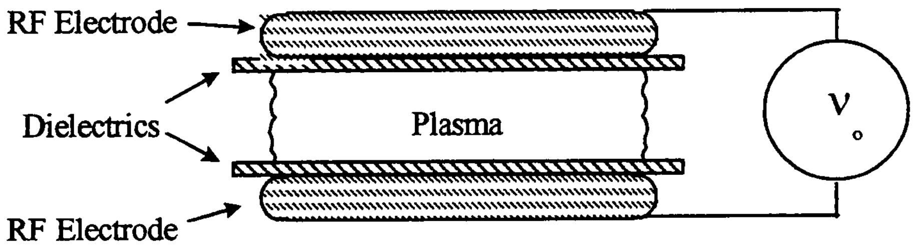

Figure 2.1 The standard volumetric configuration for a OAUGDP.

too large for a given amplitude of the applied voltage, the OAUGD plasma will either be very dilute or not form. If the frequency of the applied RF voltage is too high, then ions and electrons will both be trapped, and the OAUGDP will become polarized and filamentation will develop.

For a given applied voltage, operating gas and electrode separation distance, the applied voltage drives an oscillation of the ions between the RF electrodes with the applied frequency. This constraint on the plasma generation method has been termed *Ion trapping* (Roth, 1995c).

The equation that characterizes the ion trapping behavior of the OAUGDP, was given by J. R. Roth in his book, Industrial Plasma Engineering, Vol. 1. Section 12.5.2. The minimum driving RF frequency is as follows,

$$\nu_o \cong e\, V_{rms} / \pi\, m\, d^2\, \nu_c,$$

where ν_o is the RF frequency required to trap the ion, e is the charge of ion, V_{rms} is the RMS voltage, m is the mass of the ion, d is the gap distance, and ν_c is the collision frequency of the ions.

OAUGDP Acceleration Methods

As already stated, the charged particles comprising a plasma can be accelerated by electric fields. This can lead to a controlled acceleration of the neutral gas because the plasma exchanges its momentum and energy to the surrounding neutral gas. The magnitude and direction of the plasma induced accelerations in the neutral gas are dependent on the magnitude and direction of the surrounding electric fields. During this study three mechanisms, distinguished by the way the plasma is accelerated, have been envisioned for using the OAUGDP to control aerodynamic boundary layers: 1.) *paraelectric acceleration*, 2.) *DC acceleration*, and 3.) *peristaltic acceleration* (Roth 1998). A *paraelectric force* is a net unidirectional body force derived from a net charge density in the plasma in the presence of an electric field gradient. *Paraelectric acceleration* (acceleration due to paraelectric forces) utilizing the OAUGDP relies on the induced motion of the neutral gas (airflow) derived from Lorentzian collisions (collisions in which the ions and electrons exchange their momentum along the electric field, with the neutral gas) by ions and electrons. *DC acceleration* is accomplished by drawing a DC current through a OAUGDP in (or counter to) the direction of the airflow. The resulting electric field accelerates ions, which transfer their momentum to the neutrals in the airflow. This greatly increases the energy and momentum of the airflow. *Peristaltic Acceleration* of the gas flow using the OAUGDP is accomplished by energizing a series of OAUGDP generating strip electrodes with progressively increasing phase angles. The increasing phase on each successive electrode creates an electric field normal to the electrode strips and parallel to the surface of the panel, which can accelerate the charged species of the plasma, and through momentum exchange with the neutral gas, accelerate and control the airflow. The peristaltic method of acceleration is described in a 1997 U.S. patent (Roth, 1997) on flat panel plasmas and their application to aeronautics.

The original goal of this study was to investigate what effect the OAUGDP might have on an aerodynamic boundary layer and the resulting drag. Interaction of the OAUGDP surface layer with the boundary layer by Lorentzian collisions, momentum transfer from the charged species to the boundary layer airflow, and the production of vortical structures between parallel strip electrodes were anticipated at the beginning of this study. The detailed mechanism of paraelectric EHD flow acceleration was discovered during the course of this research, while an explanation for the observed neutral gas and plasma interaction was being sought. The DC acceleration method was briefly attempted. This method of plasma acceleration requires real currents and large potential differences on surfaces relevant to aeronautics, and though possible in principle, it appears to be technologically unfeasible for commercial use because of surface electrical breakdown (tracking) between adjacent strip electrodes at high relative potentials. The peristaltic method of acceleration, although envisioned at the beginning of this study, requires an advanced polyphase RF power supply for which funding was not available. For these reasons only the effects of paraelectric acceleration due to the OAUGDP will be discussed.

Previous Geometries

The original configuration used to generate the OAUGDP was two plane, parallel metallic electrodes with a dielectric covering either one or both electrodes as seen in figure 2.1. Other configurations operated during evolution to the flat panels can be seen in figure 2.2. These include: a.) two insulated plane electrodes with a grounded mid-

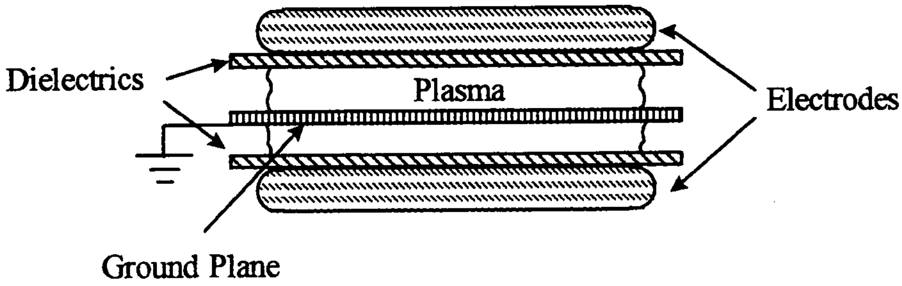

a.) A volumetric configuration utilizing a grounded mid-plane.

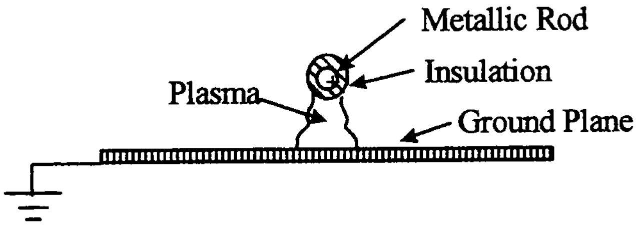

b.) A volumetric configuration utilizing a insulated rod over a metallic ground plane.

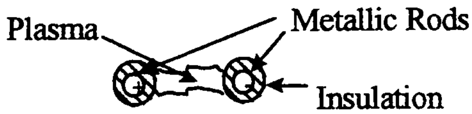

c.) A volumetric configuration utilizing two insulated rods.

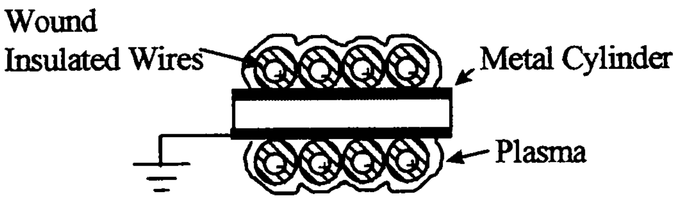

d.) A surface configuration utilizing two wound insulated wires.

Figure 2.2 Previous electrode configurations for the generation of a OAUGDP operated prior to the development of the OAUGDP flat panel.

plane electrode; b.) an insulated electrode rod above a flat metallic ground plane; c.) two insulated metallic rods; and d.) a coil wound with two adjacent, parallel insulated wires at opposite RF polarity wound around a grounded cylinder. When considering the above OAUGDP generating configurations, and the flat panel configuration discussed below, it is apparent that virtually any shape of surface can be covered or volume filled by a One Atmosphere Uniform Glow Discharge Plasma.

The Flat Panel

In October of 1995 attempts to construct a flat OAUGDP panel with both sets of parallel RF electrode strips on one side of the panel (and thus subject to surface electrical breakdown or "tracking") had met with limited success (Figure 2.3). At this time, OAUGDP panel development was focused on finding an insulator that could electrically isolate the RF electrode strips from each other so that no tracking would occur when the RF voltage was applied. Three months of testing various inexpensive and unsophisticated painted-on coatings, including high voltage corona dope, had resulted in a flat panel that could only sustain operation approximately 5 to 10 seconds in air or 40-60 seconds in helium. A constraint during these tests was to find an inexpensive insulator that could be applied and removed easily in the laboratory. The problem with such insulators is that as the panel heated up, the insulator would lift away from the panel or fail, producing an RF electrical spark in the vacated area and thereby carbonizing (burning) the surface of the test panel. While this study never did identify a cheap and

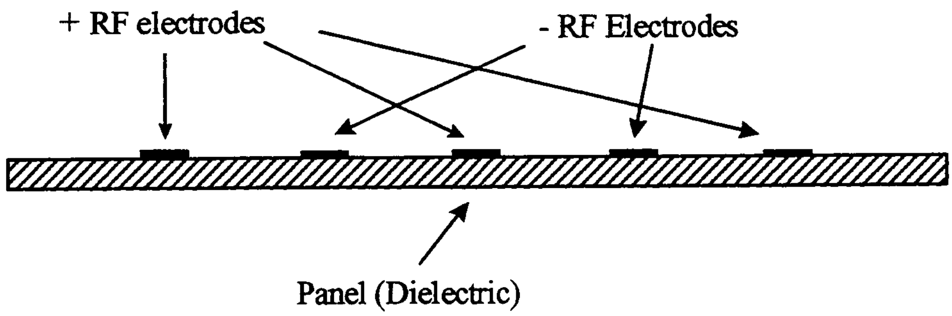

Figure 2.3 The original design for the generation of a surface layer OAUGDP with both RF electrodes on the upper surface.

removable high voltage insulator, irreversible methods of electrical insulation such as plasma flame spraying, and baked or cured epoxy products such as Hylar™ are likely to work.

The problem of insulating the gap between the electrode strips was sidestepped by separating RF electrode strips of opposite polarity to opposite sides of the test panel (fig 2.4). For sufficiently thin panels, the electrical impedance characteristics are similar to having both sets of RF electrode strips on the same side of the test panel with a layer of electrical insulation covering them. This change allowed most OAUGDP panels to be constructed from standard circuit board material (woven glass/epoxy construction, with a dielectric constant of 4.5), though in some cases, a high temperature circuit board material (polyamide, with a dielectric constant of 4.3) was used if overheating the test panel was a concern. Electrode separation to opposite sides of the test panel also increased the number of possible RF electrode designs because each RF electrode configuration could now be placed anywhere on a surface without reference to the other set of RF electrodes, even directly above or displaced from the other RF electrode.

The following design parameters defined the OAUGDP test panels used in this study: the width of the RF electrode strips, held the same in both the upper and lower RF electrode configurations on the panel; the relative distance between centerlines of the RF electrode strips; the insulating border, which is necessary to suppress RF electrical breakdown (tracking) between the top and bottom electrode arrays, around the edge of the test panel; and the panel thickness (fig. 2.5). Because of the design flexibility possible by confining one RF polarity to one side of a panel, many different panel

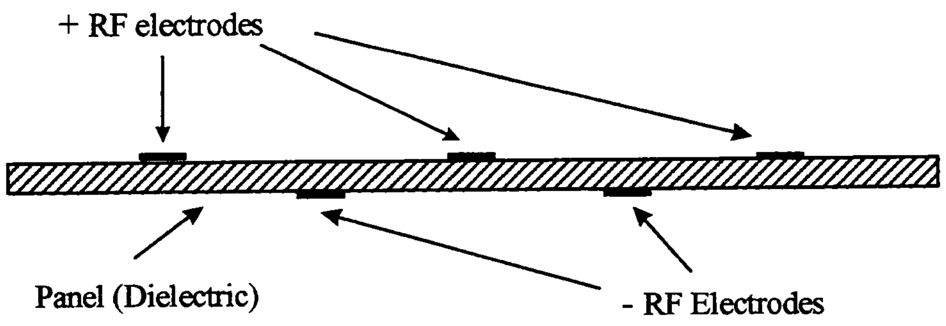

Figure 2.4 The design for the generation of a surface layer OAUGDP with RF electrodes on opposite sides of the surface.

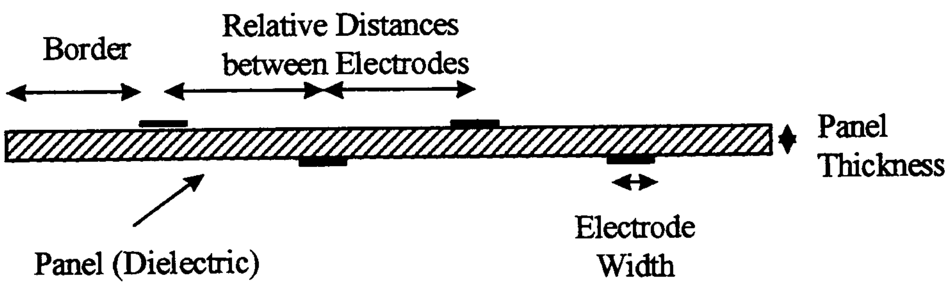

Figure 2.5 The design parameters of the OAUGDP panels.

configurations were developed, fabricated and tested during the course of this research. In order to focus the research and minimize the design parameters, only designs that used parallel strip electrodes to generate parallel strips of OAUGDP were studied. A table of OAUGDP panel designs and their parameters is located in appendix A.

Our RF electrode configurations can be classified as either symmetric or asymmetric. This distinction is due to the observed differences (symmetric or asymmetric) in the induced aerodynamic flow, which depends upon the direction of the paraelectric forces generated by the OAUGD plasma.

A *symmetric* OAUGDP test panel is designed so that the plasma is generated evenly on each side of the RF electrode strips on the upper surface of the test panel in contact with the airflow (fig. 2.6a). This results in the paraelectric forces being balanced (each plasma strip produces an induced airflow which is equal and opposite to that of the adjacent plasma strip) (Figure 2.6b). However, while the paraelectric force is balanced along the surface, there is induced airflow normal to the panel caused by the formation of vortical structures and entrainment of the surrounding air. The magnitude of the induced airflow depends on the operating conditions and parameters of the energized symmetric plasma. The airflow will be pulled down by the lower gas pressure induced by the electrostatic forces in the plasma, but will be ejected upward midway between RF electrodes strips due to interaction with the induced airflow from an adjacent RF electrode (Figure 2.6c). There are at least two methods of achieving the symmetric paraelectric arrangement, depending on the geometry of the lower RF electrode: the staggered lower electrode strips (fig. 2.6d) and a simple flat conducting sheet (fig 2.6e).

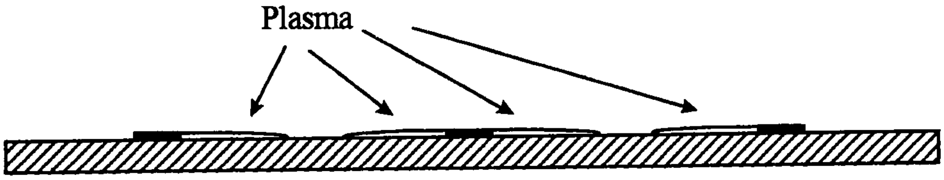

a.) The top of a symmetric panel with a plasma present.

b.) The top of a symmetric panel with arrows indicating the induced the surface airflow.

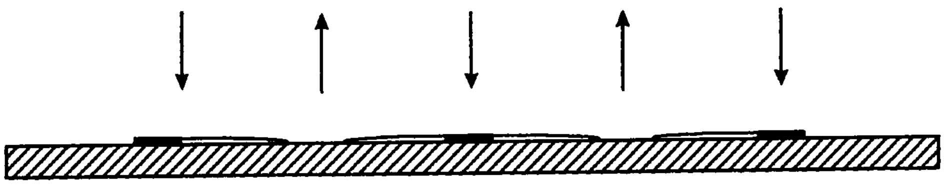

c.) The top of a symmetric panel with arrows indicating the induced the normal airflow.

d.) A symmetric panel using evenly spaced, staggeredelectrodes.

e.) A symmetric panel using a single sheet electrode.

Figure 2.6 Diagrams depicting the location of the plasma, the motion of the induced airflow, and the RF electrode configuration for the symmetric OAUGDP panel.

For most symmetric panel configurations the second design, utilizing a simple flat metallic sheet, was used for the lower RF electrode strips because it eliminated the possibility of generating a plasma on the underside of the panel.

An *asymmetric* OAUGDP test panel (a contribution of the present author) is designed in such a way that there is a net paraelectric body force on the neutral gas, normal to the electrode strips parallel to the surface of the OAUGDP panel. This net paraelectric force is created by generating the OAUGD plasma predominately on one side of the individual electrode strips that comprise the RF electrode configuration in contact with the airflow (figure 2.7a). This eliminates the equal but opposite paraelectric force generated by the plasma on the other side of the electrode strip, as in figure 2.6a, and results in the airflow from one strip being entrained and reinforced by the airflow generated by the next RF strip (figure 2.7b).

During the course of this research, asymmetric plasma generation was accomplished by displacing the lower RF electrode strips to one side of the upper RF electrode strips (figure 2.7c). It should be noted that this is not the only way to accomplish asymmetric plasma generation and the resulting directed paraelectric body force on the airflow. In this study the geometry of the asymmetric electrode array was not optimized, and improvements in the flow velocity may result from such an optimization.

Operation Conditions and Electrical Setup

Depending on the OAUGDP panel design and the RF power supply used, the OAUGDP panels are operated over appropriate ranges of applied RF voltages and

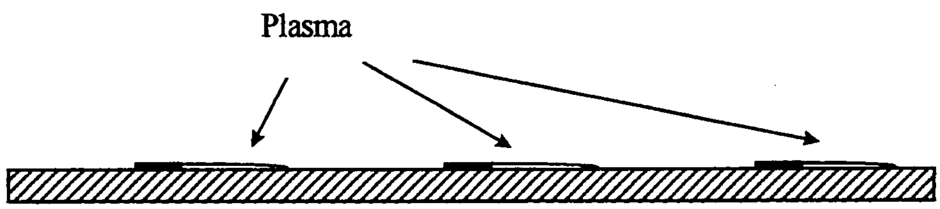

a.) An asymmetric panel with plamsa present on the surface.

b.) An asymmetric panel with arrows indicating the induced surface airflow.

c.) An asymmetric panel with plasma generated by unevenly spaced, staggered lower electrodes.

Figure 2.7 Diagrams depicting the location of the plasma, the motion of the induced airflow, and the RF electrode configuration for the asymmetric OAUGDP panel.

frequencies. The applied RF voltage has ranged from as low as 1.8 kV RMS to as high as 5.6 kV RMS. For our panels, an applied voltage of 1.5 kV RMS is the absolute minimum voltage necessary for the OAUGD plasma to appear on the surface of a panel. This threshold voltage can be higher, depending on the frequency of the applied voltage and the distance between the two sets of RF electrode strips (1.5 kV RMS corresponds to 7.0 kHz). 5.6 kV was the maximum voltage that the RF power supply could provide. The frequency of the applied RF voltage has ranged from 500 Hz up to 6.0 kHz. In most cases the frequency was 3.0 kHz. This was due to the March Instruments[1] power supply, which delivered its maximum total power at approximately 3.0 kHz for most OAUGDP test panels (because of similar values of capacitance). Figure 2.8 shows both the total power and the maximum voltages as a function of the frequency for the symmetric test panels C5-A, and C7-A.

Our early research utilized a modified 5 kVA, class C, Ling Power Amplifier[2] (model 79) driven by a signal generator to supply the RF electrical power for the OAUGDP panel. A resistive network connected in parallel to the panel was employed to load down and stabilize this class C amplifier. A block diagram of the electrical equipment is shown in figure 2.9a. Because of the inconvenient weight and size of the Ling Power Amplifier, the much smaller 2 kVA March Instruments Power Supply was employed for most of the experiments (fig. 2.9b) at the NASA Langley Research Center. In order to observe the current and voltage waveforms, a Pearson Electronics[3] Current

[1] March Instrument, Inc., (800) 326-1151, www.plasmod.com
[2] Ling Electronics, (714) 779-1900, 4890 East Lapalma, Anaheim, CA 92807
[3] Pearson Electronics, Inc., (650) 494-6716, 1860 Embarcadero Rd., Palo Alto, CA 94303

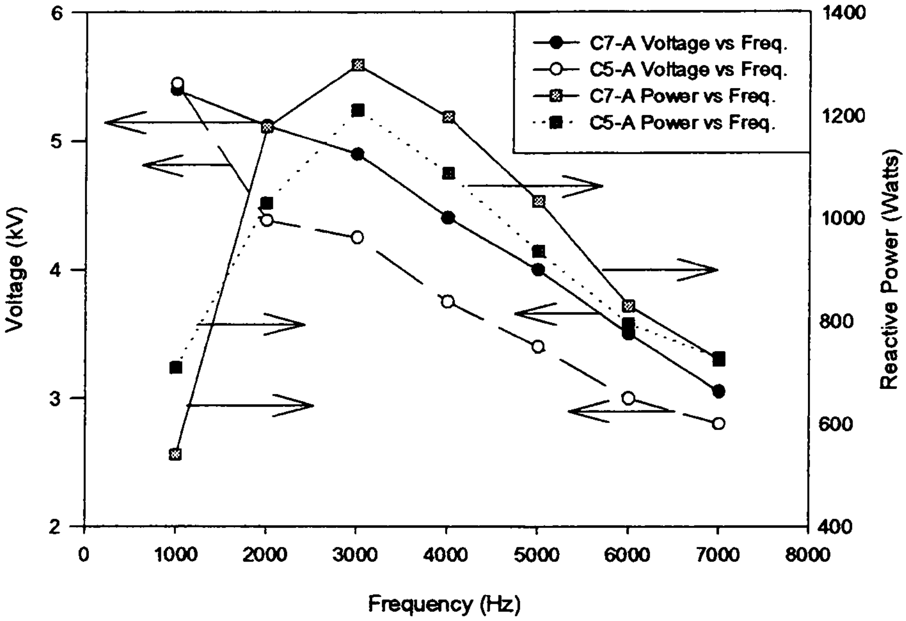

Figure 2.8 A graph of the maximum reactive power and maximum voltage versus frequency for symmetric panels C7-A & C5-A.

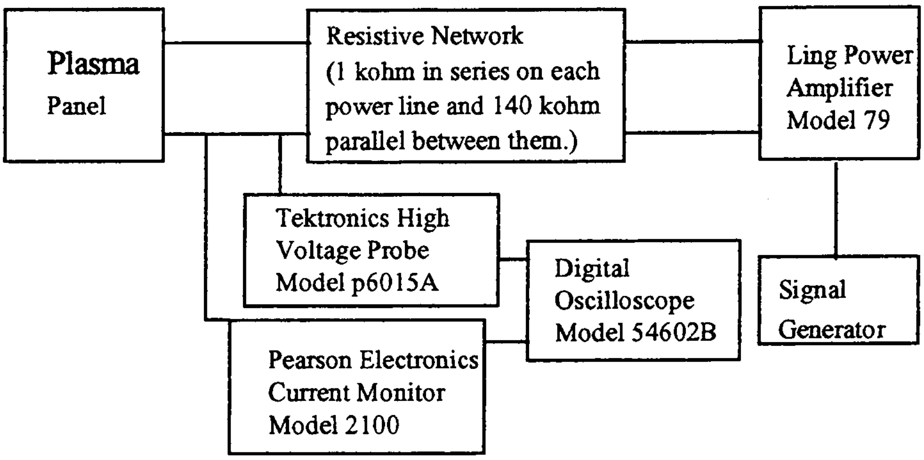

a.) The electrical equipment utilizing the Ling Power Amplifier.

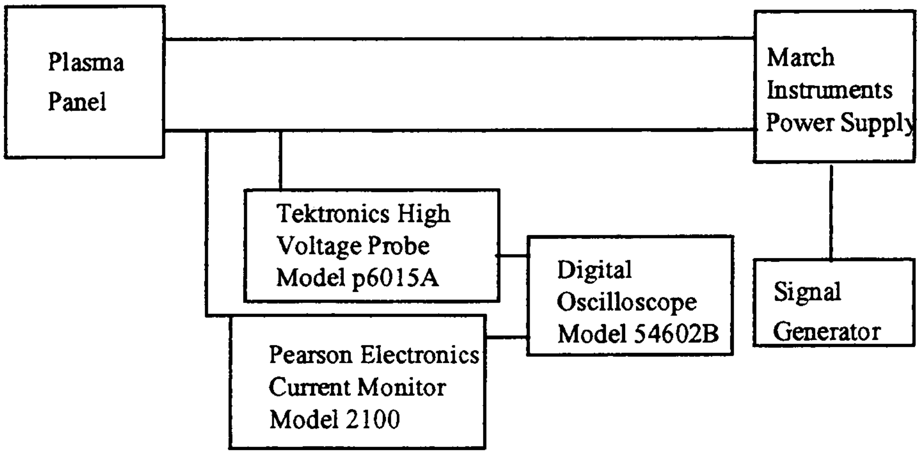

b.) The electrical equipment utilizing the March Instruments Power Supply.

Figure 2.9 Block diagrams of the electrical equipment setup for two different power supplies.

Monitor (model 2100) and a Tektronix[1] High Voltage Probe (model P6015A) were used with a Hewlett Packard[2] 150 MHz digital oscilloscope (model 54602B) and a LeCroy[3] 400 MHz digital oscilloscope.

Estimates of the Electrical Plasma Power

With the exception of the resistive network to stabilize the Ling power amplifier, both RF power supplies were utilized without impedance matching. The observed current waveforms on the digital oscilloscopes show the *total* current, which includes the component of the current due to reflected RF power caused by the impedance mismatch, which is much greater than the plasma current in this application. The impedance mismatch makes estimates of the plasma power difficult. Figure 2.10 shows a current and applied voltage waveform for the energized panel C7-A without impedance matching. Figure 2.11 shows the current and applied voltage waveform for the same panel, partially impedance matched. The data in figure 2.11 was not taken during our experimental runs at the NASA Langley Research Center. This impedance match was done by placing a 13.1 milli-Henry inductor and six 1 nF capacitors in series - parallel with the plasma panel. Note that at the time of writing, an impedance matching network capable of operating at the typical experimental run operating conditions (voltages and frequencies greater than 4.0 kV and 3.0 kHz) was not available.

Rough estimates of the plasma power can be attained by other methods, such as a current waveform subtraction method (Spence et al, 1993 or Carr & Roth, 1996a) or a

[1] Tektronix, Inc., (800) 835-9433, www.tek.com
[2] Hewlett Packard, (800) 452-4844, www.hp.com
[3] LeCroy Corp., (914) 425-2000, www.lecroy.com

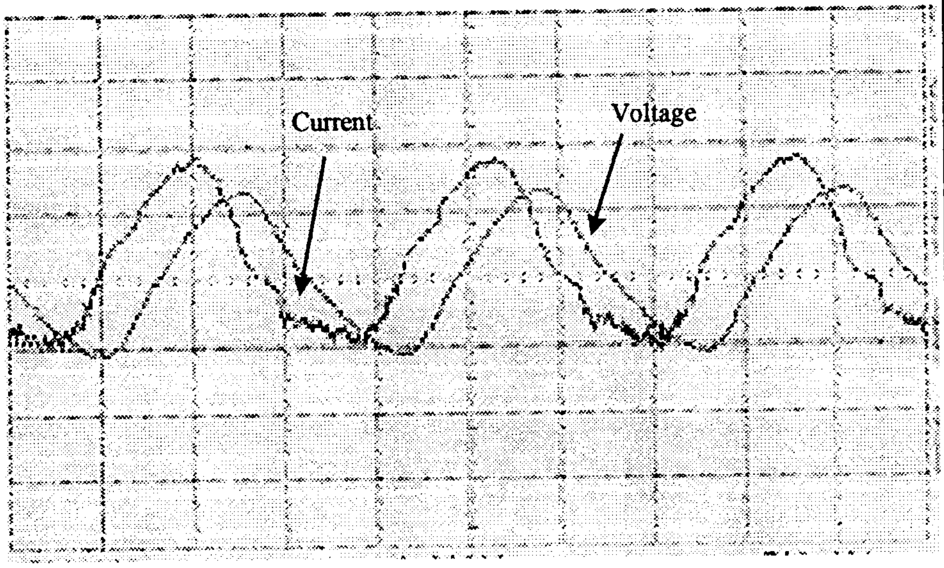

Figure 2.10 The current and voltage waveforms for symmetric panel C7-A without impedance matching (4.08 kVrms, 3.1 kHz, 189.3 mA).

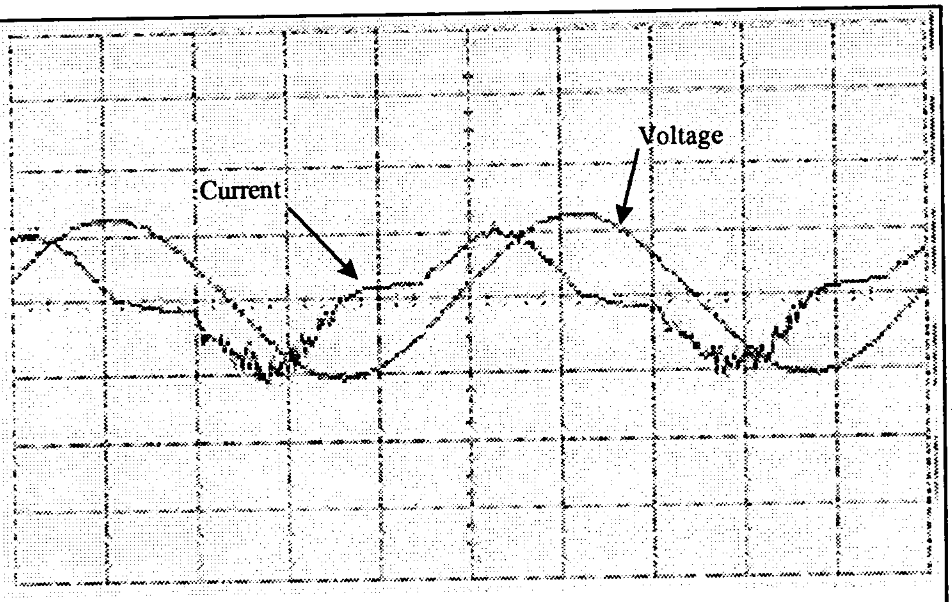

Figure 2.11 The current and voltage waveforms for symmetric panel C7-A with partial impedance matching (4.09 kVrms, 2.0 kHz, 115mA) .

capacitive charge method (Tong et al, 1995). In the first approach, a sine wave of the correct amplitude and phasing (I') is created and subtracted from the observed waveform for the total observed current (I), leaving an estimate for the current actually drawn to energize the plasma. Using this estimate for the plasma current, the observed waveform for the applied voltage (V), the phase angle between the current and voltage waveforms, θ, and an estimate of the plasma surface area, the following equation yields an estimate for the areal plasma power density:

$$\text{Power} = (I - I') \, V \cos(\theta) / \text{Area}$$

This leads to an estimate of 38 ± 7 mW/cm^2 for the symmetric panel C1-B when operated at 4.0 kV RMS and at 3.0 kHz (Carr & Roth 1996b).

The capacitive charge method for calculating the plasma power is based upon calculating the area of the charge versus voltage plot for a given RF frequency. This diagnostic has been applied to the OAUGDP configuration of two parallel plates (Tong et al, 1995), but this method has yet to be applied to the flat panel configuration.

In other University of Tennessee Plasma Sciences Laboratory experiments, the power consumption of three simultaneously energized (at half the voltage and frequency of the experimental operating conditions), electrically parallel symmetric OAUGDP panels, of a design similar to those tested in wind tunnel experiments but configured to have plasma on both sides of the test panel, were estimated to consume 187 watts, thus yielding a total of 62.3 watts per double-sided panel and ~ 45 milliwatts/cm^2 at the plasma operating conditions of 2.7 kV and 1.5 kHz. This estimate for the plasma power was found very recently by using an impedance matching network that delivered a maximum voltage of 2.7 kV at a frequency of 1.5 kHz.

Humidity

For the bulk of this study, the operating gas was normal (not commercial dry) air. This is not to imply that humidity does not influence with the characteristics of the OAUGDP. If the power of the OAUGDP is low, then a person's breath is sufficient to briefly disturb or partially extinguish the OAUGD plasma on a surface. A heavy mist has been applied to surface covered by the OAUGDP operating at a high areal power density and it was found to recover rapidly after initial quenching. A study examining the effects of water vapor on a silent discharge (a filamentary dielectric barrier discharge) shows that water vapor decreases the total charge transferred each half-cycle of the RF power cycle (Falkinstein and Coogan, 1996).

Part III

Experimental Apparatus and Methods of Observation

The 7" x 11" Wind Tunnel

For over three decades the NASA Langley Research Center has conducted a wide variety of drag reduction and boundary layer control experiments using their 7 x 11 inch (17.8 x 27.9 cm) Low Speed Wind Tunnel. The sustained research commitment to this device has produced an instrument that is both highly accurate and reliable, as well as possessing a wide variety of aerodynamic diagnostic technology. The test section of this tunnel was used to mount the OAUGDP test panels, and to study their effects on aerodynamic boundary layers.

The 7 x 11 inch (17.8 x 27.9 cm) Low Speed Wind Tunnel is an unpressurized apparatus, consisting of a tunnel contraction, diffuser, propeller, closed return, and an enclosed test section, (figure 3.1). The maximum airflow velocity was 26 m/s (56 mph). A small 1.07 mm diameter trip wire is located in the tunnel contractor (575 mm upstream of the leading edge of the test panel). Experiments were conducted in three distinctive boundary layer regimes: laminar, transition, and turbulent. The wind tunnel test section is a rectangular box, 915 mm long, 178 mm tall, and 279 mm wide (36.6 inches x 7 inches x 11 inches), assembled from removable, 1.25 cm thick clear acrylic plastic side walls and top (figure. 3.2). The bottom of the test section consists of three test plates: the fore (upstream), central, and aft (downstream) plates. A large airtight wooden box (approximately 1.5 m long x 1.0 m wide x 1.5 m tall) with a clear acrylic sliding door encloses the entire test section. This allows the pressure outside the wind tunnel test section to be adjusted relative to the pressure inside, to prevent leakage airflow into or out

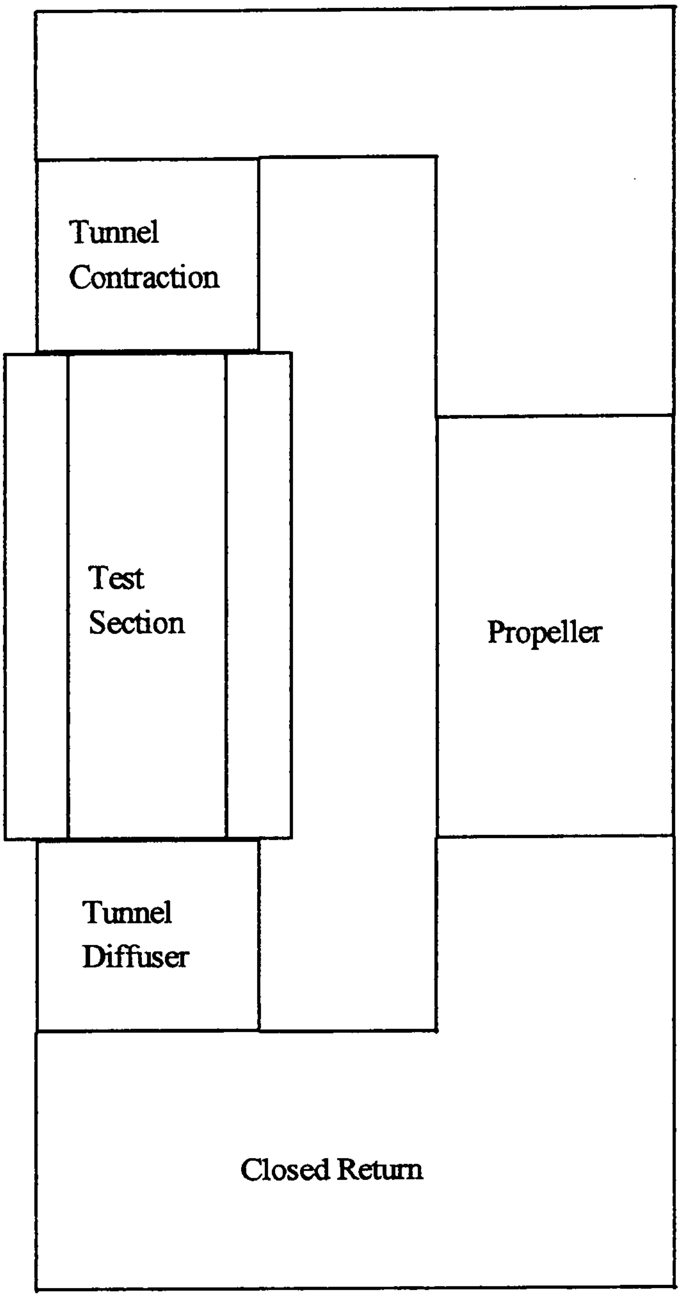

Figure 3.1 A Block diagram of the 7 x 11 Inch Low Speed Wind Tunnel.

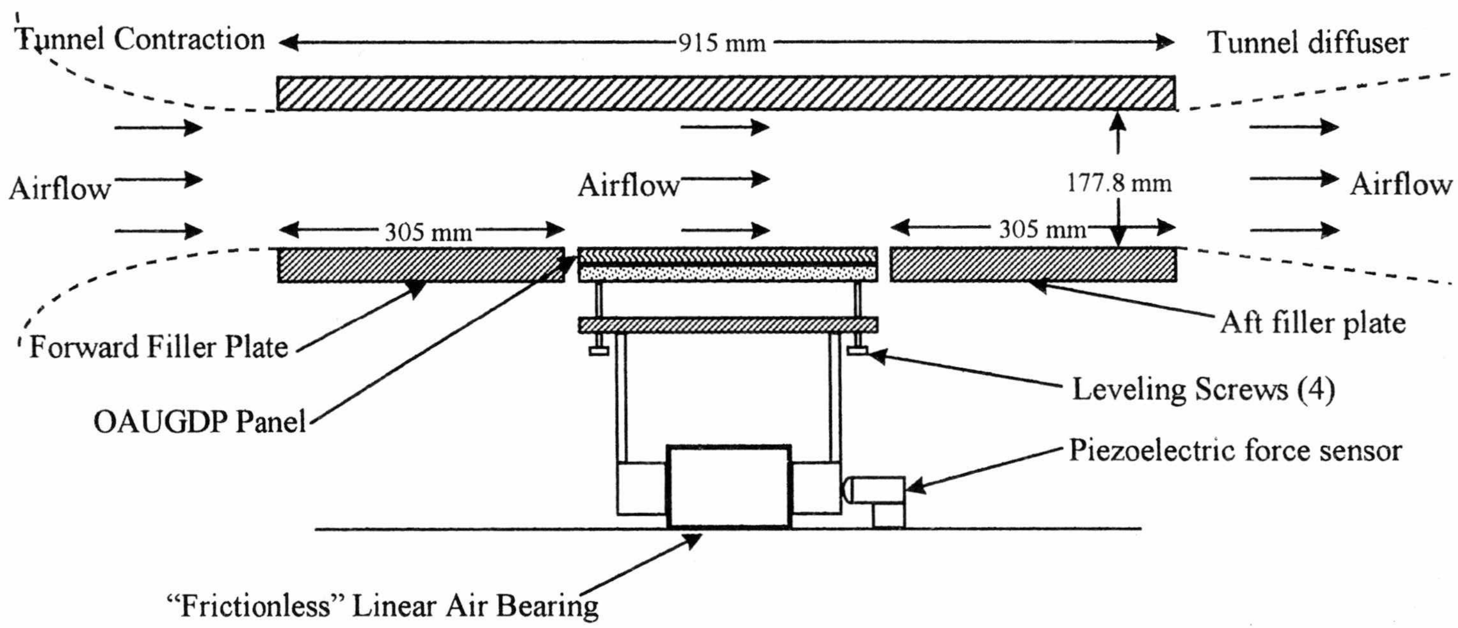

3.2 A streamwise cross-section detail of the 7 x 11 Inch Low Speed Wind Tunnel.

of the gaps around the model, which would affect drag readings. Additionally, the rear wall of the test section was adjustable to allow correction for the streamwise pressure gradient (figure 3.3).

The Drag Balance

For the tests conducted during this study, the OAUGDP test panels occupied the central third of the bottom wall of the test section (fig 3.2). In this central portion, the OAUGDP panels were mounted on a piece of 1.25 cm thick fiberglass board of equal size. This insured that the test panels would lie flat and would not be lifted into the wind tunnel test section by sudden pressure differences that might occur during testing. Surrounding this central test area was a narrow air gap (on the order of .5 mm both between the fore and aft filler plates and the sidewalls), which allowed free movement of the linear air bearing on which the central test area and OAUGDP panel rested. Located on the floor of the enclosure around the wind tunnel test section, and directly adjacent to the structural components of the linear air bearing, was a piezoresistive force transducer. The combination of the linear air bearing, the piezoresistive force sensor, and an analog-to-digital converter comprised the drag balance system used for measuring the viscous drag of the OAUGDP panels. The drag system had a minimum observable drag of 10 mg.

Figure 3.4 is characteristic of the data taken with the drag balance and illustrates the drag versus velocity for panel C1-B with the plasma off. The drag is shown in grams, and airflow velocity is shown in meters per second. Figure 3.4 is plotted on logarithmic

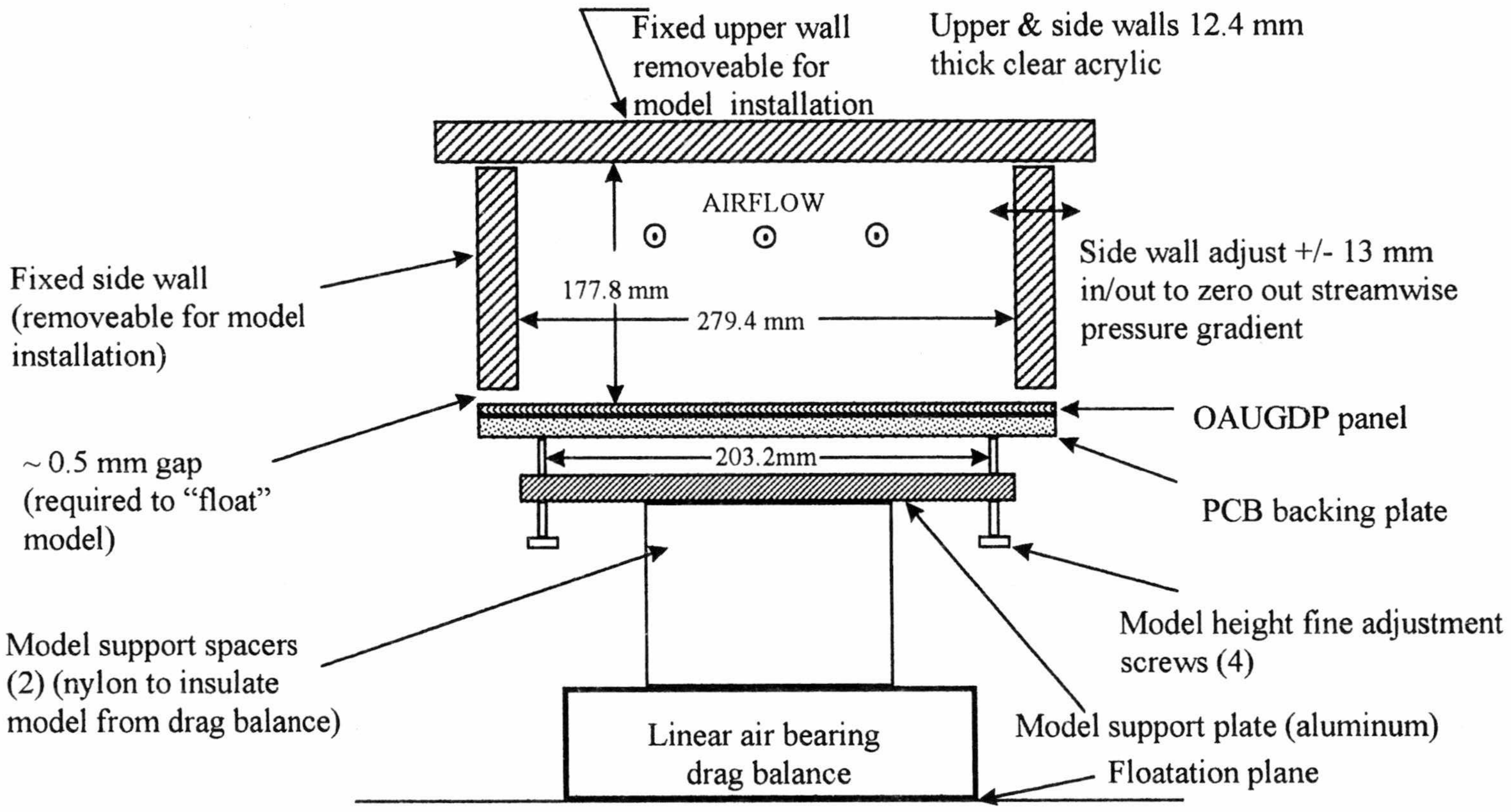

3.3 An axial cross-section detail of the 7 x 11 Inch Low Speed Wind Tunnel.

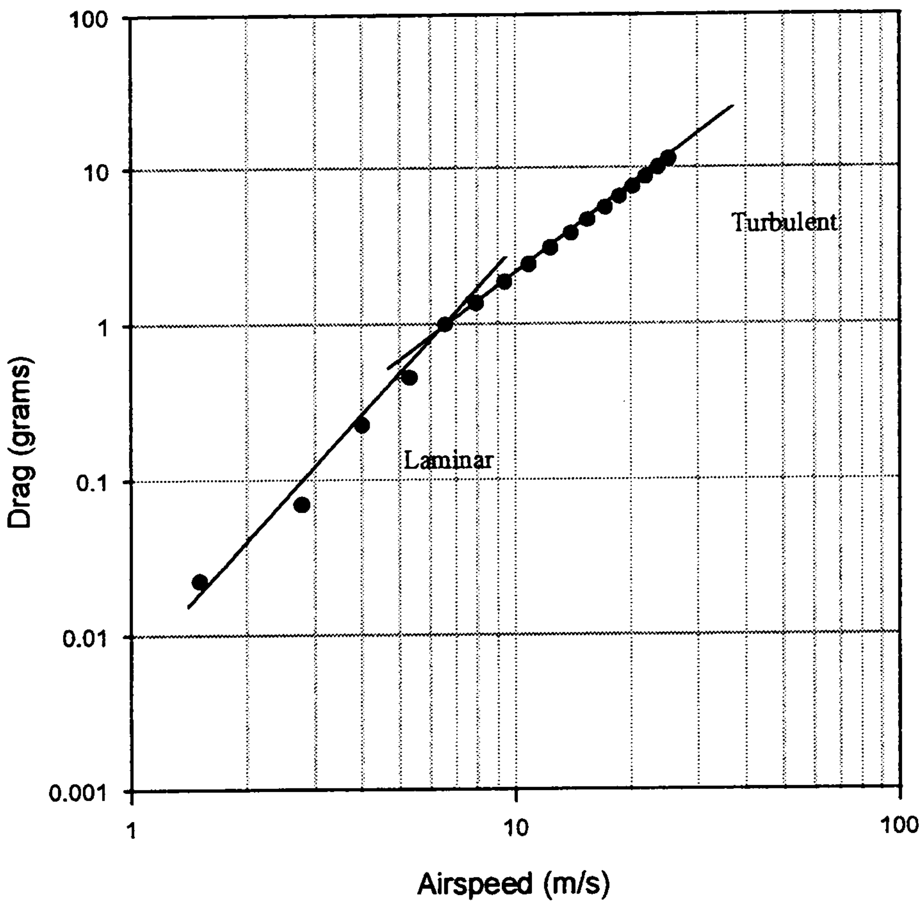

Figure 3.4 A graph of the drag versus airspeed for symmetric panel C1-B without plasma present.

coordinates to illustrate the power-law relationships expected for flat plate drag under these conditions. Three distinct airflow regimes, laminar, transition, and turbulent, are evident in figure 3.4, based on the slope of the data. For each data run using the drag balance, both plasma on and plasma off data points were taken at each airflow velocity.

The Electrostatic Correction

Initial results from the drag balance required correction for an electrostatic force which results from the electric field lines, terminating not only on the OAUGDP panel, but also on surrounding grounded objects. This is not to be confused with the electrostatic thrust or drag due to paraelectric forces. Figure 3.5a,b illustrates the electrostatic force (electrostatic drag) as a function of panel voltage for a symmetric OAUGDP panel C1-C mounted on the drag balance with no airflow. It is significant that the drag balance detects an induced "drag" at voltages less than that necessary for the plasma to form (~2.0 kV depending on the frequency). Paraelectric forces can be present only when the plasma is present. Given that the symmetric OAUGDP panels have the paraelectric forces balanced, the observed drag at a given voltage is due to the electric field lines terminating on surrounding grounded surfaces.

The electrostatic correction for a symmetric panel was found by mounting it in place, and with the wind tunnel airspeed at zero, the apparent drag was measured as a function of voltage. Then, the value of the apparent drag for a given voltage (the electrostatic correction factor) was subtracted from the drag observed during a

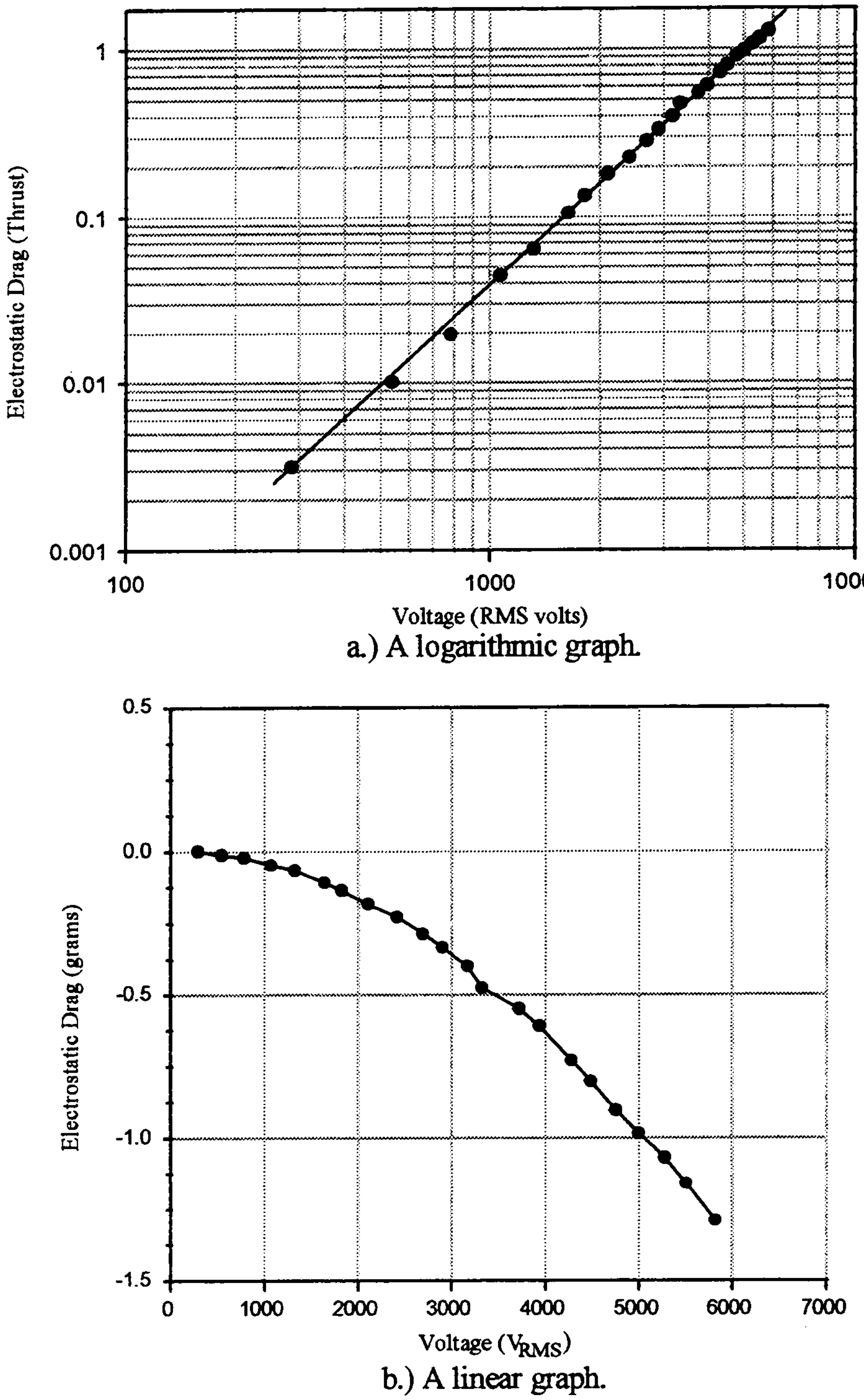

Figure 3.5 Graphs of the electrostatic drag versus the voltage for symmetric panel C1-C with no tunnel airflow.

subsequent normal wind tunnel experiment. This correction was confirmed at the beginning of each run with the first few data points taken with the plasma on, but before the wind tunnel airspeed was raised. Later investigation found that most of the electric field lines were terminating on the grounded aluminum fore and aft filler plates. By replacing these plates with 1.25 cm thick fiberglass panels, the magnitude of the electrostatic correction became negligible.

The Pitot Probe

The tip of the pitot tube probe was located ~2.8 centimeters downstream from the edge of the last RF electrode strip on the test panel near the approximate center of the wind tunnel. During testing, the pitot tube was raised in 0.5 mm increments from the surface of the aft plate to a height of 30 mm (figure 3.6). The tip of the pitot tube was a flattened hypodermic needle with a cross-sectional opening 0.28 mm high and 0.65 mm wide. The pitot tube velocity profiles were measured as quickly as possible to minimize the addition of heat to the airflow by the plasma on the panel. A MKS Industries [1] Model 150 Baratron capacitive manometer measured the pressure difference between the pitot probe tip and a reference static pressure on the test section wall. The differential pressure was converted to velocity using Bernoulli's equation:

$$\Delta P = \tfrac{1}{2} \rho v^2,$$

where ΔP is the differential pressure, ρ is the density of air, and v is the velocity.

[1] MKS Industries, Inc., (508) 975-0093, Six Shattack Rd., Andover, MA 01810

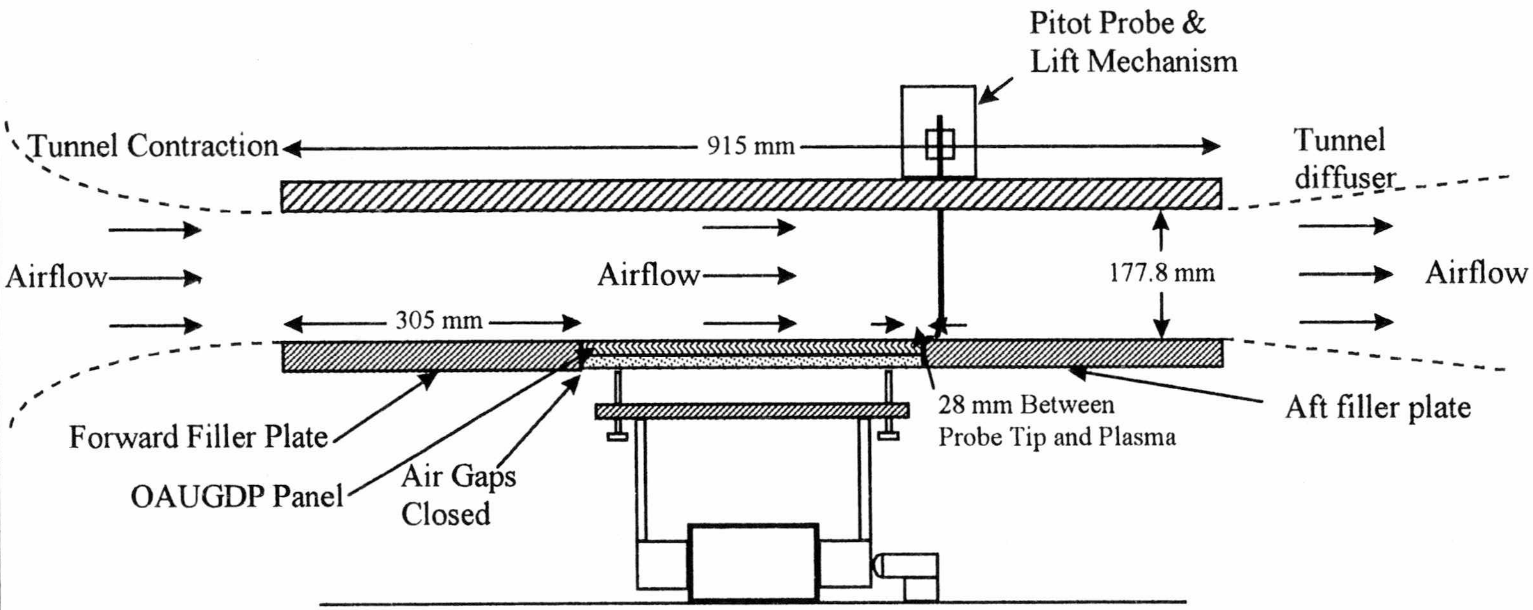

Figure 3.6 Diagram of Pitot Tube for the 17.8 x 27.9cm (7 x 11 inch) Low Speed Wind Tunnel.

Shown in figure 3.7 is a graph depicting the boundary layer air velocity for the laminar, transitional, and turbulent regimes as a function of height above the aft plate of the test section, and with the plasma turned off. The free stream velocities were 4.0 m/s, 7.0 m/s, and 26 m/s, in the laminar, transitional, and turbulent regimes, respectively. The height at which the pitot probe measures 99% of the free stream air velocity is generally considered the boundary layer thickness. The presence of the plasma alters the boundary layer thickness, sometimes profoundly. Also with the plasma turned off, there are no inflection points in the boundary layer velocity profile. This too changes in the presence of a plasma.

Smoke-Wire Visualization System

A digital smoke wire system was designed and installed in the wind tunnel by Stephen Wilkinson of the NASA Langley Research Center. A schematic of the Smoke Wire Visualization System is shown in figure 3.8. This system included the following components: a Strobex[1] light source (Model 122B), a signal conditioner, a Pulnix[2] Digital Camera, a 0.1 mm diameter type 304 stainless steel wire, a dual DC Power Supply (50 V and 20 Amp each) to heat the wire, a solid state relay, a delay timer, a Digital 488 I/O[3] converter, and a computer with Bitflow[4] Data Raptor and IEEE[5] 488 bus cards. The Strobex Lamp was located on a stand outside the front sidewall of the test section. The Pulnix digital camera was mounted on a two-directional track on the ceiling of the wind

---

[1] Chadwick – Helmuth Co., (818) 575-6161, 4601 N. Arden Dr., El Monte, CA
[2] Pulnix, (800) 445-5444, www.pulnix.com
[3] IO Tech, (216) 439-4091, 25971 Cannon Rd., Cleveland, OH
[4] Bitflow, Inc., (617)-932-2900, 21 G- Olympia Ave. #80, Woburn, MA
[5] National Instruments, Inc., (512) 433-8000, 11500 N. Mopac, Austin, TX

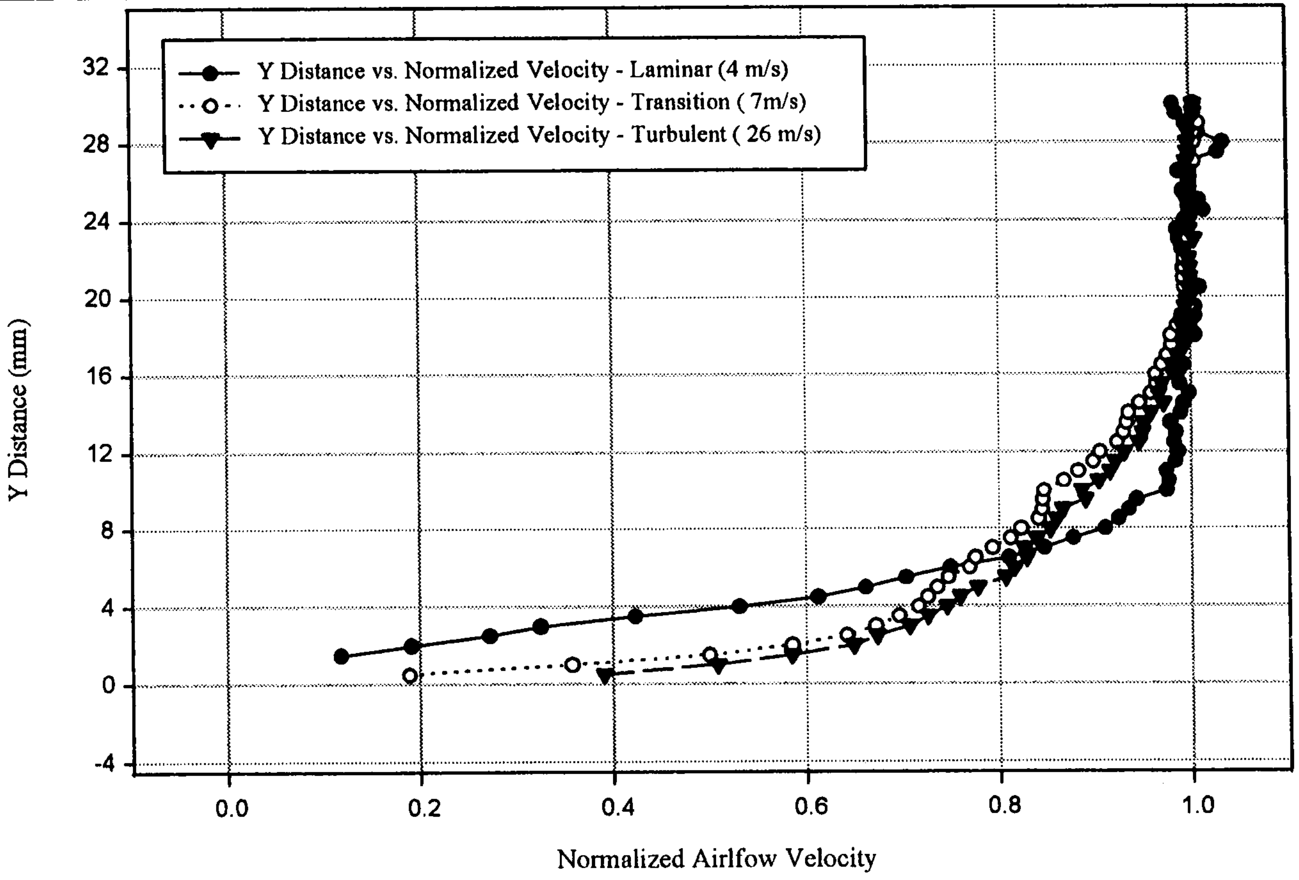

Figure 3.7 Pitot tube velocity profiles for laminar, transition,and turbulent airflow without the plasma present.

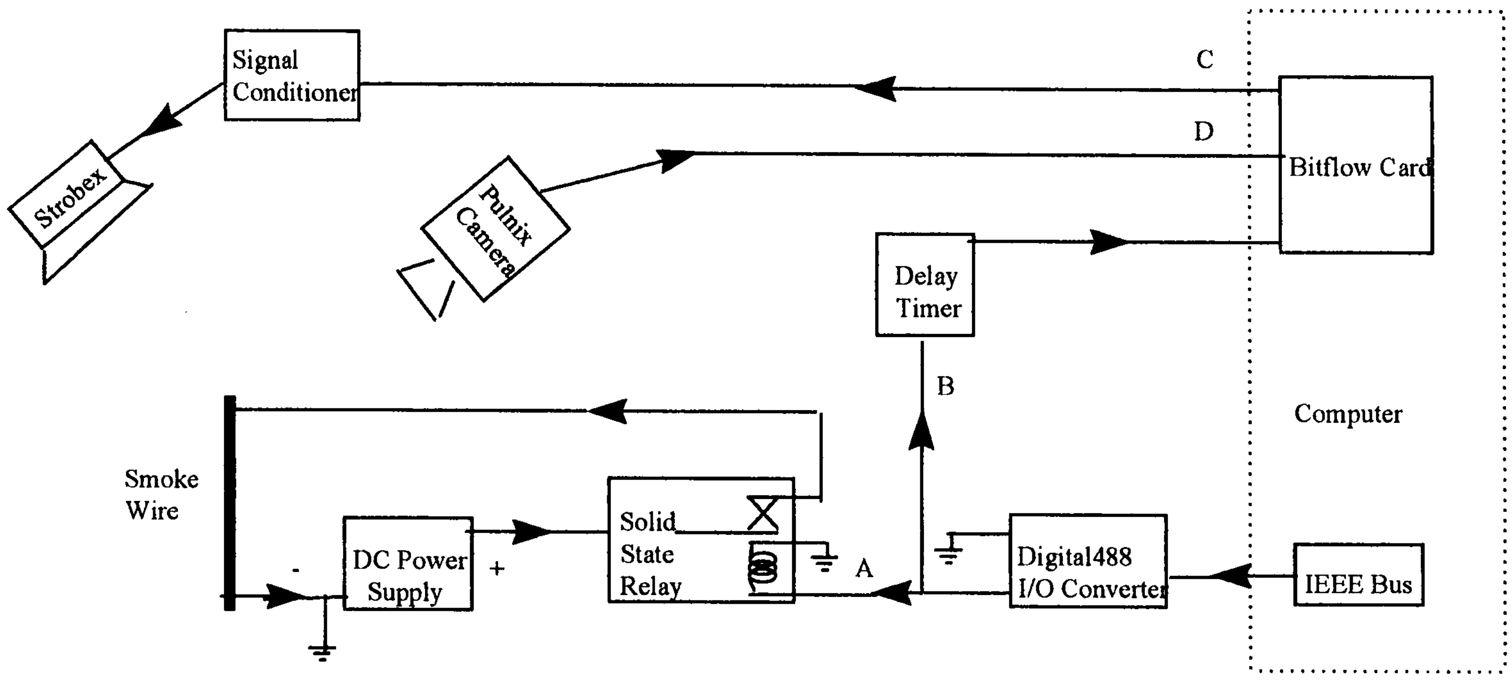

Figure 3.8 A diagram of the components of the smoke wire visualization system. The letters (A,B, C, D) refer to the time delays of figure 3.10.

tunnel test section enclosure (figure 3.9). The smoke wire was weighted at one end to keep the wire taunt as it was heated, and to ensure that if the wire broke, the wire would be removed from the test section rather than being blown on the energized panel where it could short out and/or damage the timing electronics. The DC power supply, relay, and delay were all located outside the wind tunnel test section enclosure. In order for this system to function properly, the delay between the flash of the Strobex light source and the capture of the digital image of the smoke by the Pulnix camera had to be optimized. The system was initialized with a command to the IEEE 488 bus which began heating the smoke wire (which had previously been fed through two hypodermic mountings covered by a droplet of mineral oil and located in thin slots on opposite walls of the test section) and started the delay timer. The delay time was necessary to allow the beads of mineral oil (formed by the wire being pulled through the droplet of mineral oil and the hypodermic mounting) to vaporize and the resultant smoke trails to cover the area of the panel both viewed by the camera and illuminated by the strobe light. The arrows in figure 3.8 show the flow of information. Figure 3.10 shows a timing diagram for (a.) the wire heating time, (b.) the delay timer, (c.) the strobe pulse and (d.) the image acquisition.

Figures 3.11 a & b are horizontal and vertical digital images of an unenergized OAUGD plasma panel with smoke trails. The horizontal digital images are from mounting the smoke wire through the sides of the wind tunnel test section, and the vertical images are from mounting the smoke wire through the top and bottom of the wind tunnel test section.

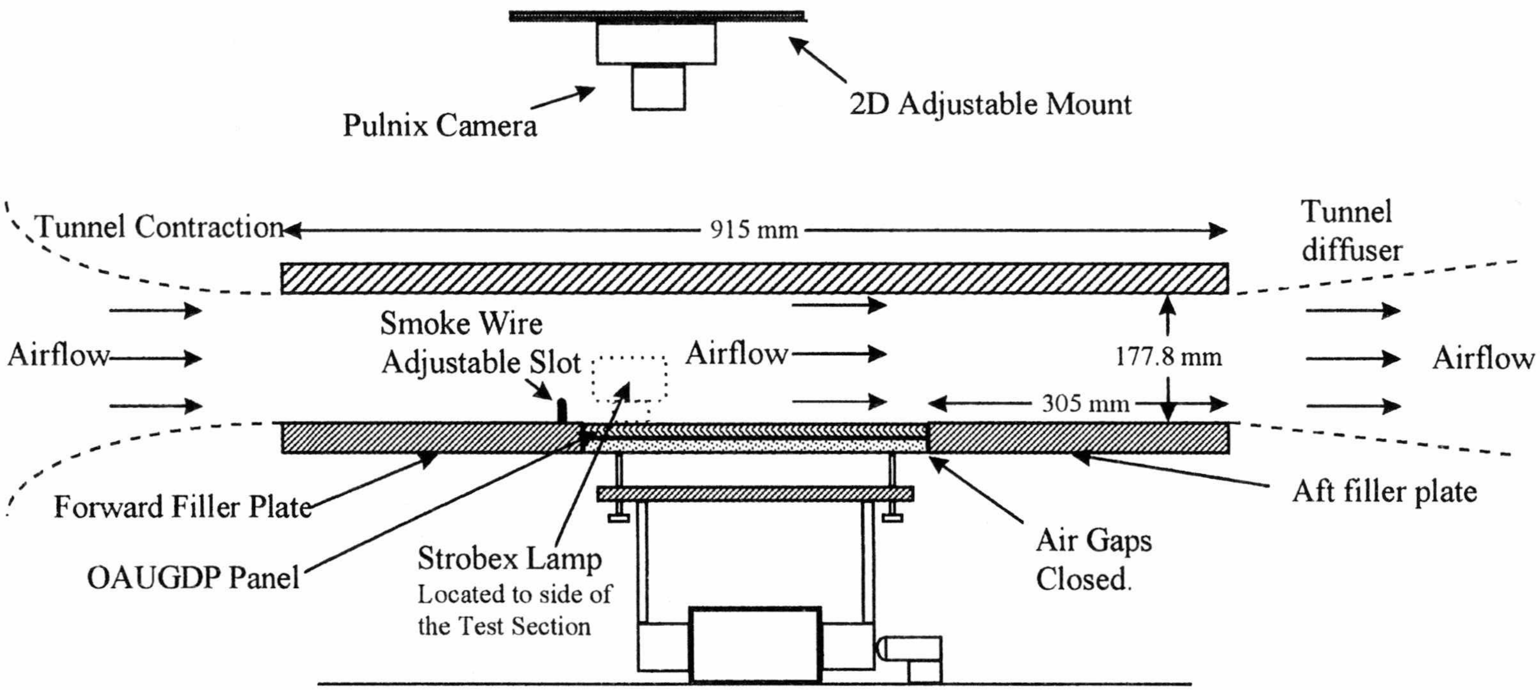

Figure 3.9 Diagram of Smoke Wire System for the 17.8 x 27.9cm (7 x 11 inch) Low Speed Wind Tunnel.

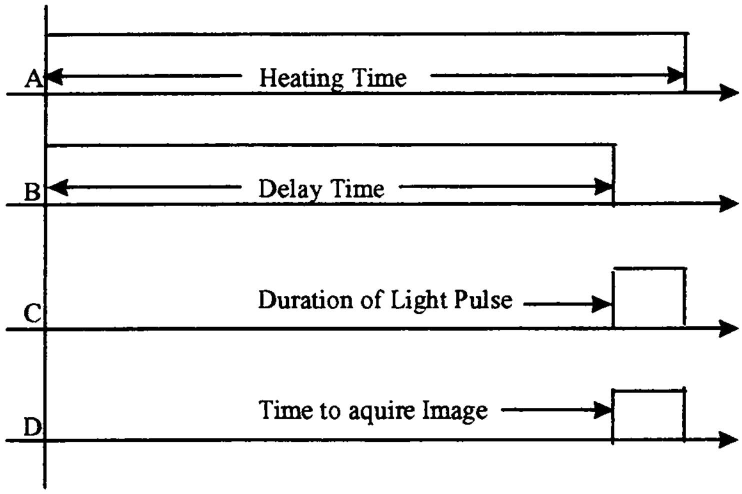

Figure 3.10 A timing diagram for (a) the wire heating time, (b) the delay timer, (c) the strobe light pulse, and (d)the image acquisition.

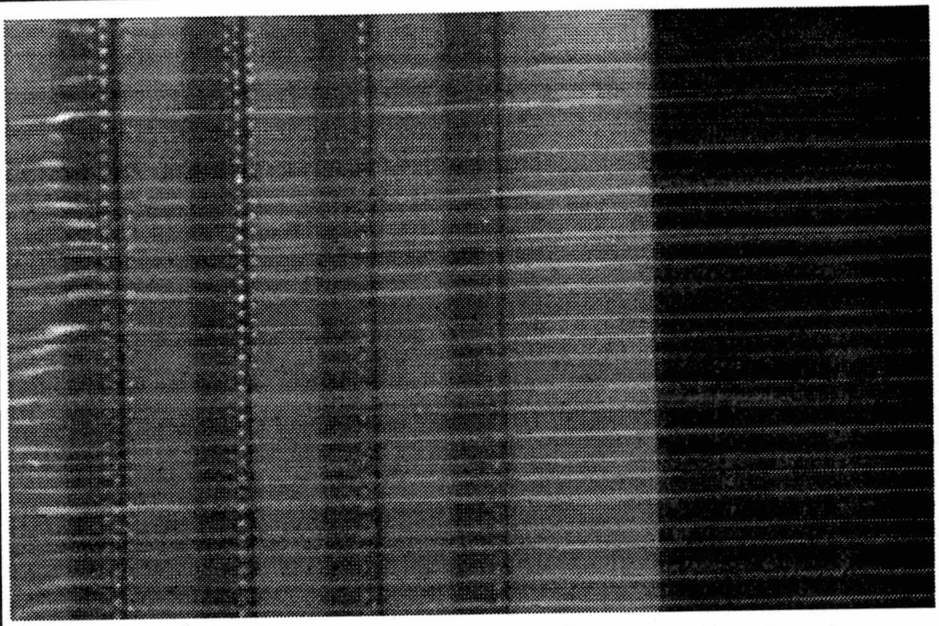

a.) Horizontal digital image.

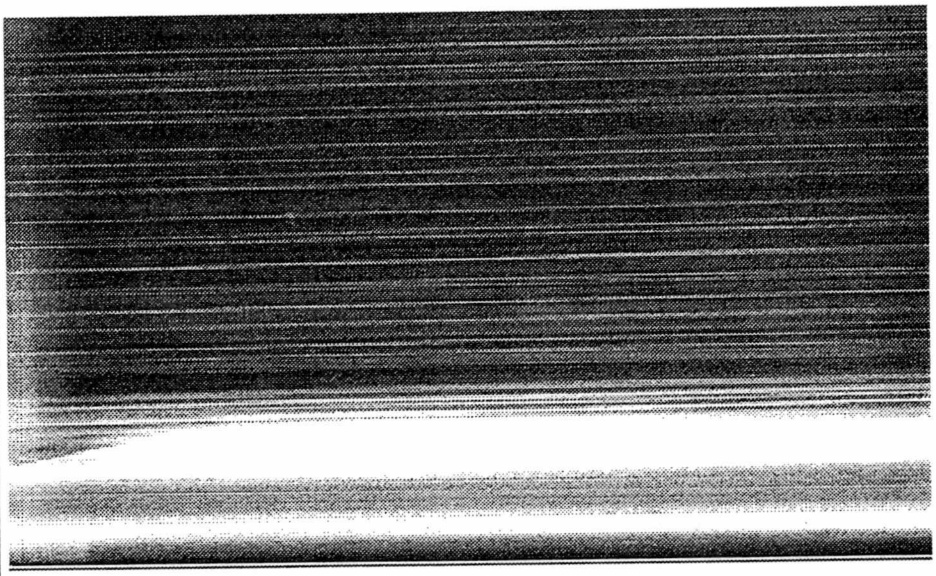

b.) Vertical digital image.

Figure 3.11 Horizontal and vertical digital images of the smoke trails over asymmetric panel without plasma present.

Hot - Wire Anemometry

There were a few instances in which a hot-wire anemometer was used during the research program. The key concern, which prevented the device from being used more often, was concern about getting this very sensitive electrical instrument too close to the plasma. Given that the plasma is energized by several thousand volts, even at a distance greater than several centimeters the RF interference was substantial. For this reason, the hot wire anemometer was used more for qualitative purposes rather than quantitative measurements. Instances of such measurements were to confirm which airflow regime (laminar, transition, or turbulent) the boundary layer was in.

Smoke Injection Videos

Though they cannot be included in the written version of this thesis, there were several instances in which the plasma panels were videotaped. By using smoke injection of titanium tetrachloride over an OAUGDP panel located in a separate small box, videos of the bulk smoke flow movement were made. The panels were placed in a box to ensure that the air was still prior to testing, and to contain any active species that the plasma generated, including ozone. These videos provided crucial demonstrations of the airflow – plasma interaction. The information derived from these videos will be presented through schematics.

Part IV

Results and Observations

Part I. – Symmetric OAUGDP panels

As mentioned in chapter two, the OAUGDP panels are covered by a series of parallel electrode strips that are either parallel or perpendicular to the airflow. For the symmetric panel these plasma strips resulted in the creation of a pair of vortical airflow structures between each pair of RF electrodes. The results which follow can be understood by imagining how an airflow would interact if the airflow encountered paired sets of counter-rotating aerodynamic vortices aligned with the airflow (figure 4.1a) or a series of co-rotating vortices perpendicular to the airflow (figure 4.1b). The orientation of the symmetric OAUGD plasma panel is a crucial parameter for manipulating the aerodynamic boundary layer.

Drag Balance Results

Figure 4.2 shows a characteristic graph of the drag versus airspeed for symmetric panel C7-A with the plasma strips parallel to the airflow for both plasma on and plasma off. In this example, the panel was operated at 4.0 kV and 3.0 kHz. The panel had a separation between centerlines of the RF electrodes of 10.5 mm. The effect of gap size will be discussed below. A significant result evident in figure 4.2 at this voltage and frequency is the near power-law relation of the drag as a function of airspeed over all three airflow regimes, laminar, transition, and turbulent.

Figure 4.3 shows a characteristic graph of the drag versus airspeed for a symmetric panel C7-C, which has the same design parameters as C7-A except the RF electrode pattern is perpendicular instead of parallel to the airflow. For this particular example, the panel was operated at 4.0 kV and 3.0 kHz. From this figure, a significant

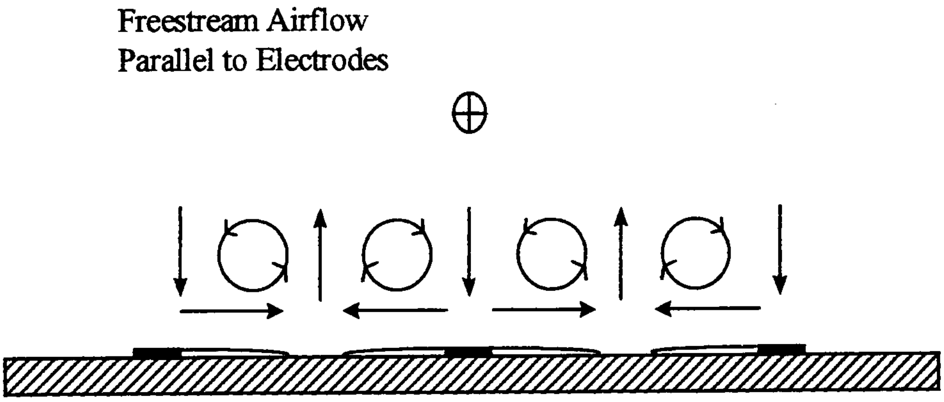

a.) Paired sets of counter-rotating vortices parallel to the airflow.

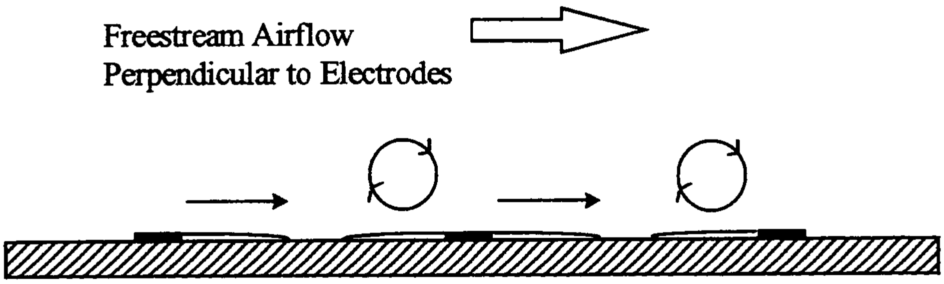

b.) A series of co-rotating vortices perpendicular to the airflow.

Figure 4.1 Diagrams depicting orientation dependent induced vortices on a symmetric panel.

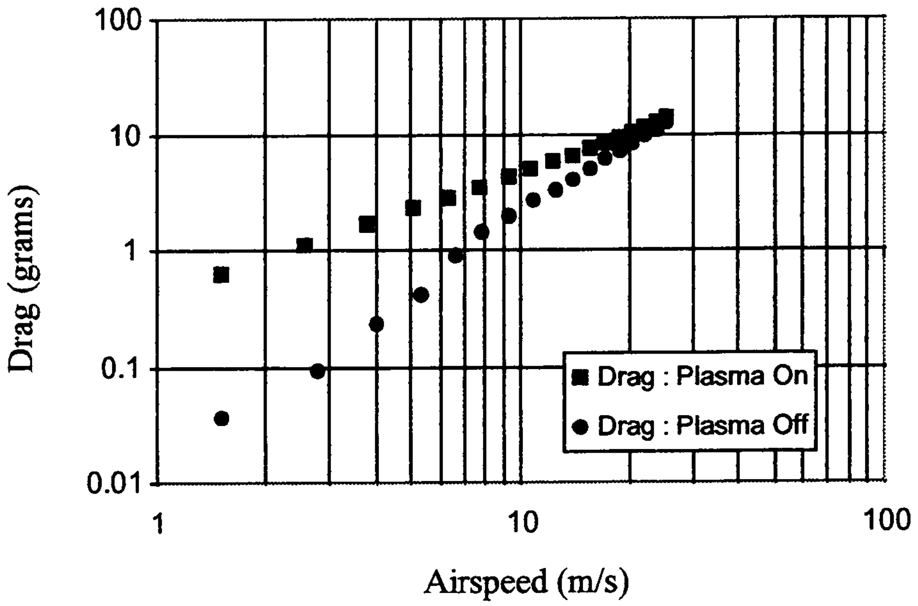

Figure 4.2 A graph of the drag versus airspeed for the symmetric panel C7-A, with streamwise electrodes, operated at 4.0 kV and 3.0 kHz.

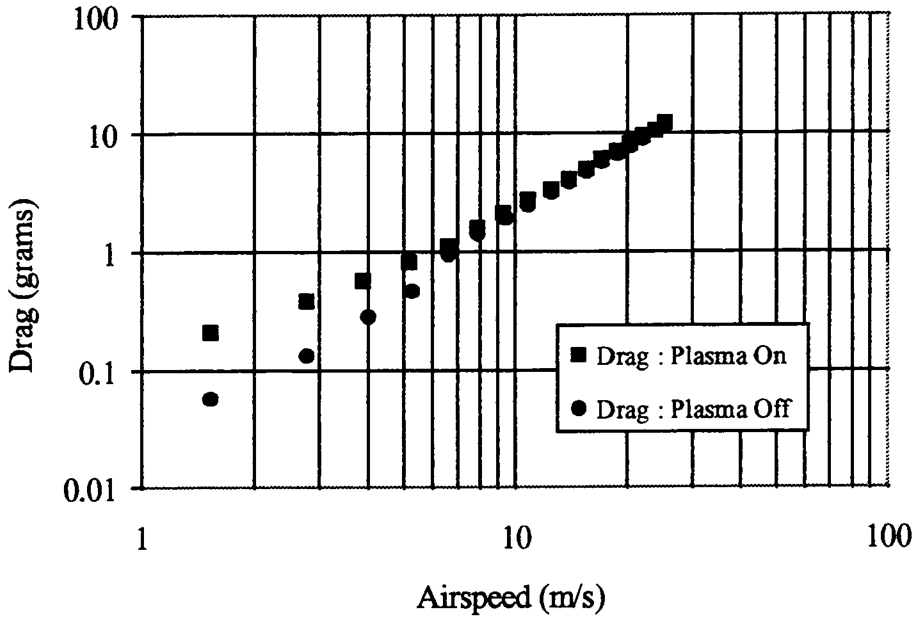

Figure 4.3 A graph of the drag versus airspeed for the symmetric panel C7-A, with spanwise electrodes, operated at 4.0 kV and 3.0 kHz.

increase in drag occurs over the laminar airflow regime, but is nearly equal to drag associated with the "plasma-off" airflow in the turbulent airflow regime. This behavior suggests that when the airflow is oriented parallel to the RF electrode strips (and their associated twin vortices), the OAUGDP acts as an airflow trip, i.e. it changes the airflow from laminar to turbulent.

Figure 4.4 shows the effect of voltage on the drag for the symmetric panel. A minimum voltage is required, which depends on the frequency, to form the plasma. For this particular panel, the March Instruments power supply delivers a maximum voltage of 5.6 kV at 3000 Hz. An increase in the applied voltage strengthens the twin vortices in the symmetric panel with parallel orientation, or trips into turbulence the laminar flow over symmetric panels with a perpendicular orientation.

The distance between the RF electrode strip centerlines, and the gap distance control the maximum possible width of each OAUGDP strip. The width of the RF electrode strips themselves seems only to utilize panel surface area that could be used for additional strips, and to unnecessarily increase the panel capacitance. For this reason, while the gap distance was increased up to 10 mm, the electrode width was reduced to 0.5 mm for all panels subsequent to the C5-A. Because a pair of vortices is generated by opposite facing OAUGDP strips between the RF electrodes, the gap distance between the RF electrodes provides an estimate of the diameter of the induced vortices (half the gap distance or less) for the parallel RF electrode arrangement.

Figure 4.5 shows a graph of drag as a function of airspeed for symmetric panels operated at approximately the same voltage and frequency, but with different electrode

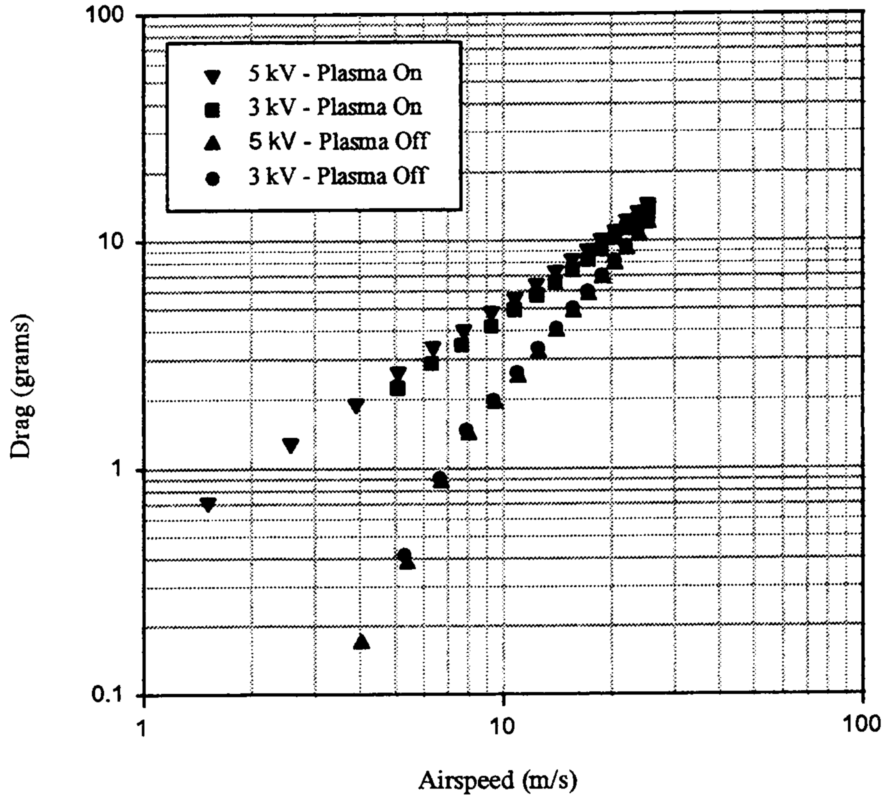

Figure 4.4 A graph of drag versus airspeed for the symmetric panel C7-A, operated at 5.0 kV and 3.0 kV at 3.0 kHz.

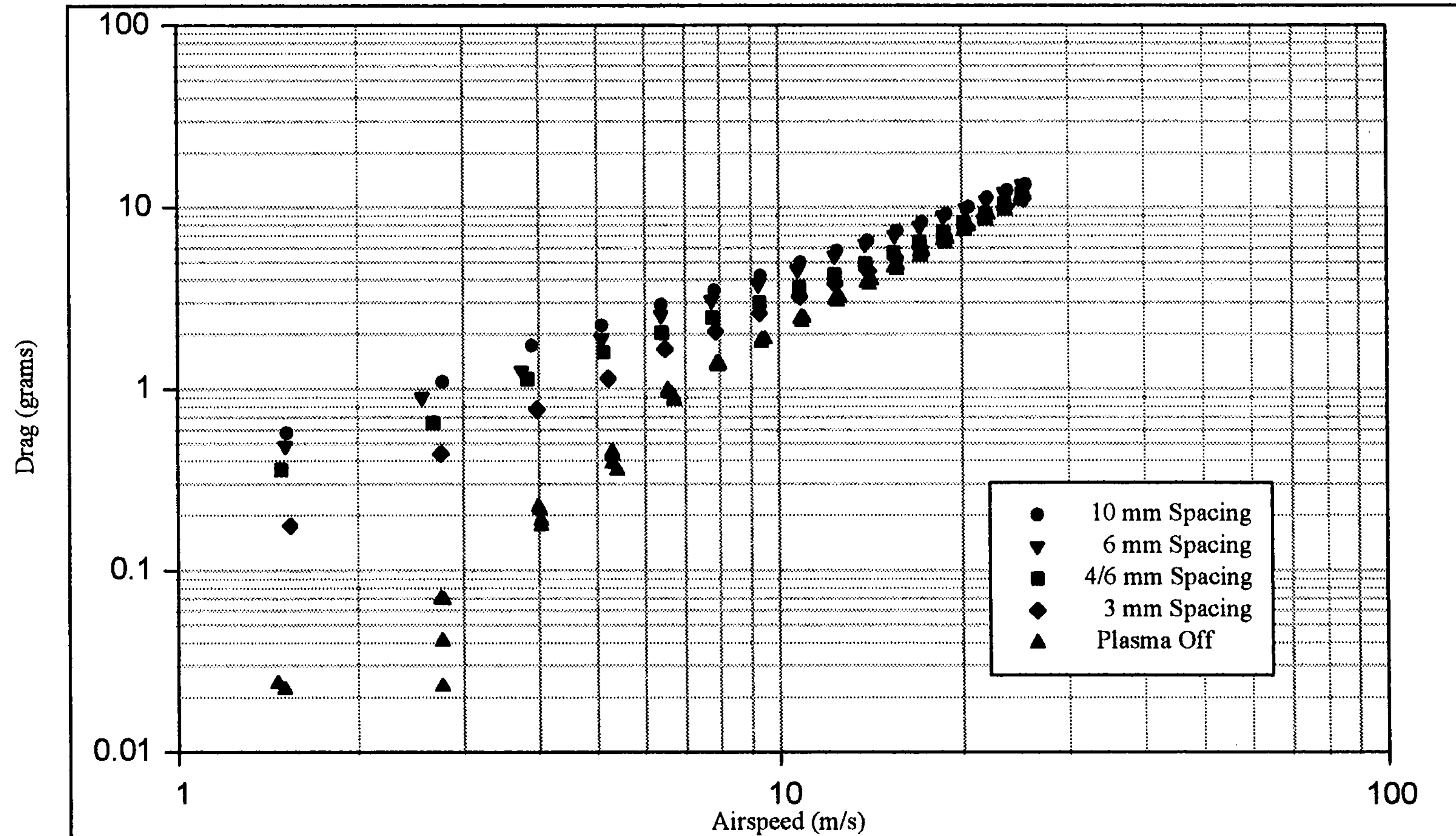

Figure 4.5 A graph of drag versus airspeed for symmetric panels, operated at 5.4 kV and 1.5 kHz with relative RF electrode spacing of of 3 mm, 4/6 mm, 6 mm, and 10 mm.

gap distances. It is evident from this figure that as the gap distance increases, the induced addition to drag also increases, even though the total number of electrode strips is decreasing because of the fixed total width of the panel. While our investigation did not exceed an electrode spacing of 10 mm, it is unlikely that for these OAUGDP operating conditions, the drag would continue to increase indefinitely.

Pitot Probe Results

Figures 4.6 a, b, c and 4.7 a, b, c show pitot tube boundary layer velocity profiles for two lateral pitot tube locations, one between a central pair of RF electrode strips, and the other behind a centrally located RF electrode strip, respectively. As noted in chapter three, the pitot tube was located 28 mm downstream from the edge of the last RF electrode strip (a RF bus bar). Note that to further minimize possible errors, the air gap required for the drag balance to move freely was closed (figures 3.2 and 3.3), since drag measurements were not taken simultaneously with the pitot tube profiles.

In both cases, the symmetric panel, C7-A, was operated at 5.1 kV, 3.0 kHz, and with the wind tunnel air velocity approximately 4 m/s (laminar airflow regime), 7 m/s (transitional airflow regime), and 26 m/s (turbulent airflow regime). In both of these figures, as well as the figures to follow, the experimental data are shown with reference to the "plasma off" pitot data.

For both of these locations span-wise to the airflow, the structure of the induced velocity profiles are nearly identical, but the magnitudes are different. Both figures show that the plasma increases the aerodynamic boundary layer thickness and alters the airflow velocity profiles, depending on the velocity of the free stream airflow. As the velocity of

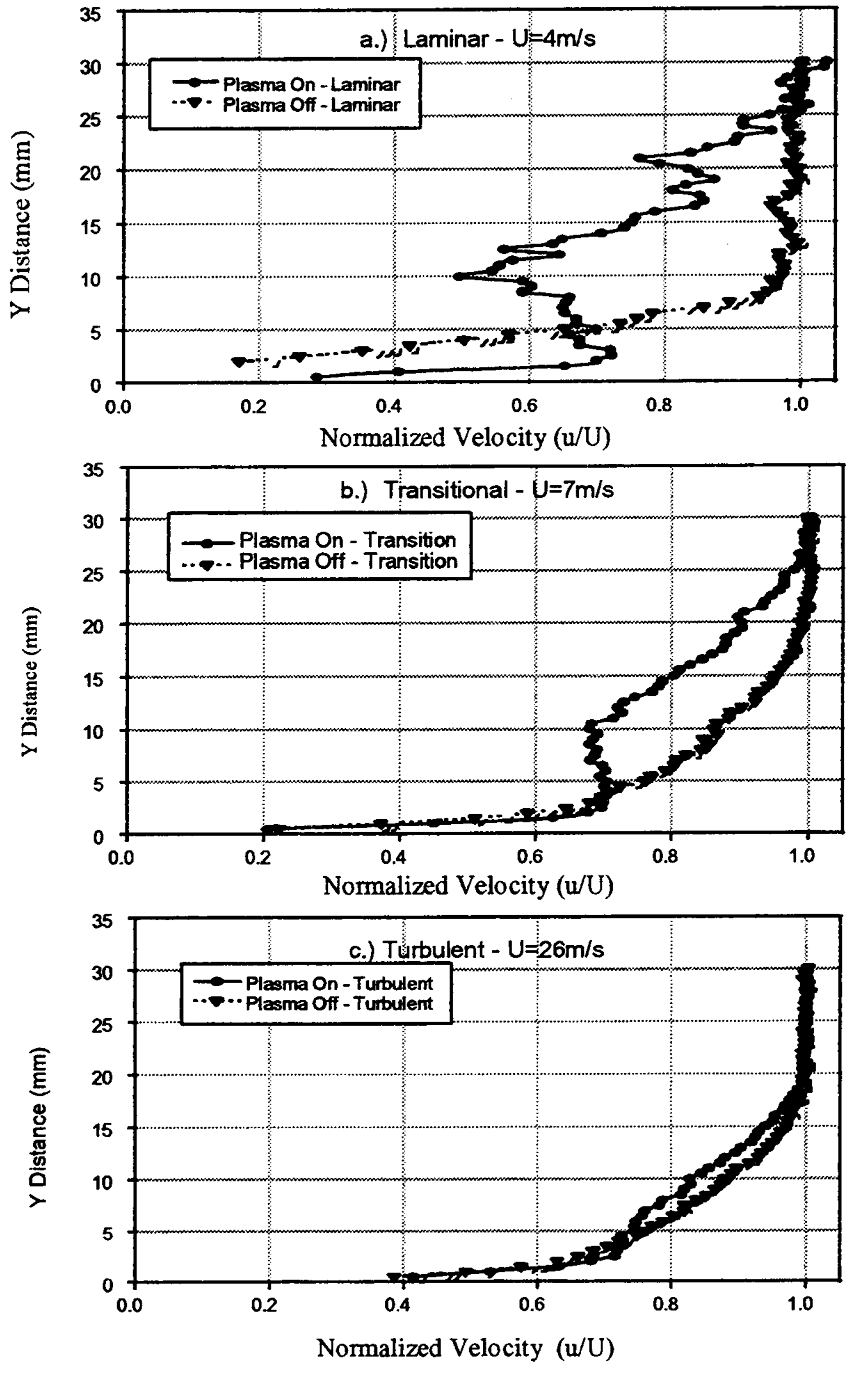

Figure 4.6 Pitot tube velocity profiles for symmetric panel C7-A with the pitot tube located downstream and between a streamwise central pair of RF strips operated at 5.1 kV and 3.0 kHz.

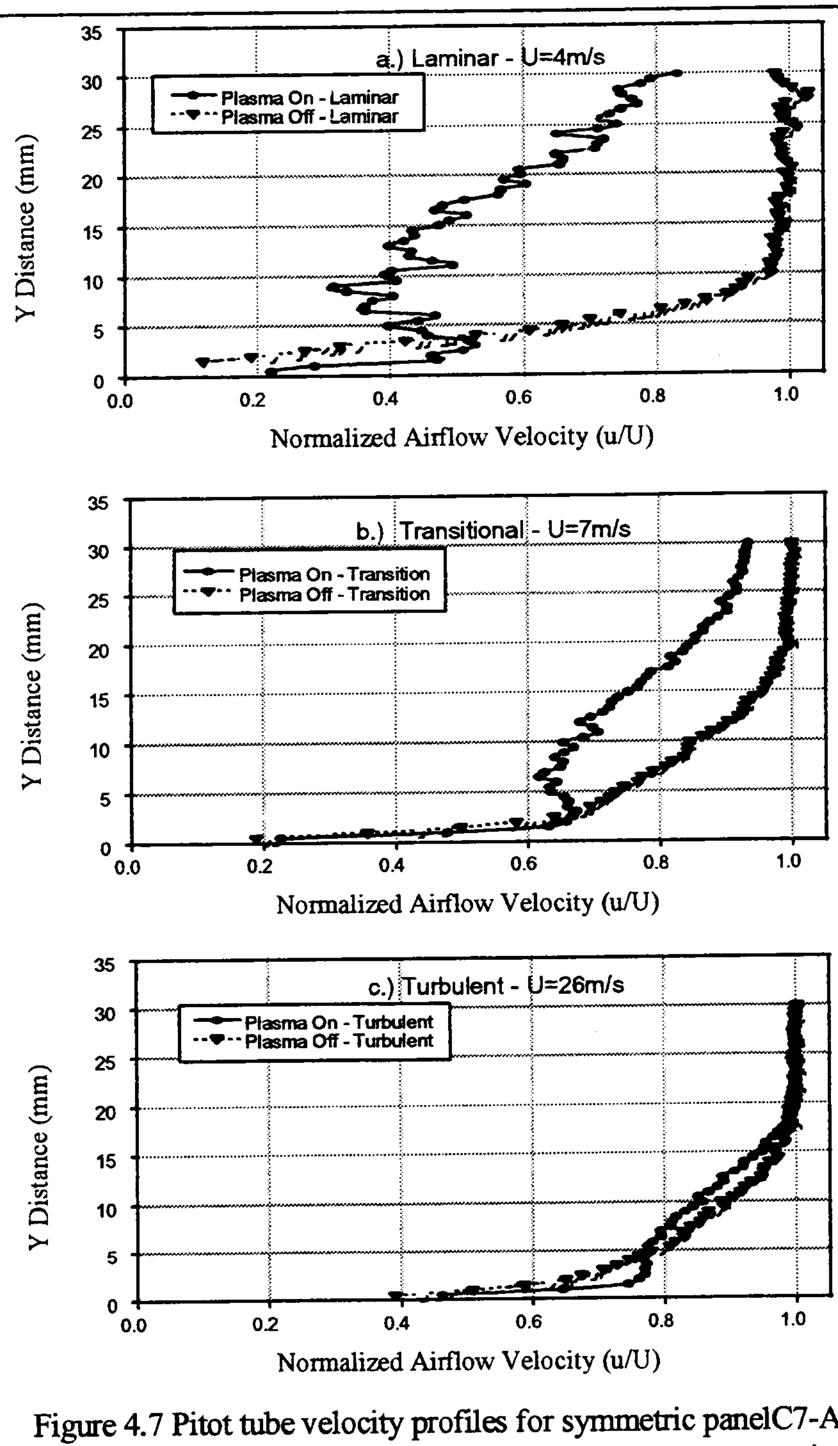

Figure 4.7 Pitot tube velocity profiles for symmetric panelC7-A with the pitot tube located downstream and behind a streamwise central RF strip that was operated at 5.1 kV and 3.0 kHz.

the airflow is increased, the ability of the OAUGDP panel to increase the boundary layer thickness diminishes. Also, for a sufficiently energized OAUGDP test panel, distinctive S-shaped (two inflection points) pitot velocity profiles result. These inflection points in the velocity profiles occur in all three airflow regimes for both positions of the pitot tube.

By moving the pitot tube probe tip laterally 5mm, from behind an RF electrode to between two RF electrodes, while still positioned 28 mm downstream of the plasma, both the magnitude of the velocity profile and boundary layer thickness is significantly altered. Figure 4.8a,b,c shows velocity profiles of figures 4.6 and 4.7 on the same graphs for the three boundary layer regimes. The difference in magnitude of the two velocity profiles while maintaining the dual inflection points can be interpreted as viewing different locations in vortical structures.

Pitot tube velocity profiles were also measured for a nearly identical RF electrode configuration rotated ninety degrees, so that the RF electrode and plasma strips were perpendicular to the airflow. Figure 4.9a,b,c show the pitot tube profiles for symmetric panel C7-C with the RF electrode strips spanwise to the airflow, operating conditions the same as the previous two figures, at 4.0 kV and 3.0 kHz. The pitot tube data for the spanwise symmetric panel (C7-C) are different from the stream-wise symmetric panel (C7-A), in that only the laminar case (figure 4.9 a) shows an increase in boundary layer thickness, and two inflection points in the airflow velocity ratios. The discrete nature of the plasma data in figure 4.9a is a problem with the instrumentation of a pressure gauge, which was corrected for subsequent runs. The grouping of datum appeared only to affect the smoothness of the profile. Constraints on research time did not allow that data set to

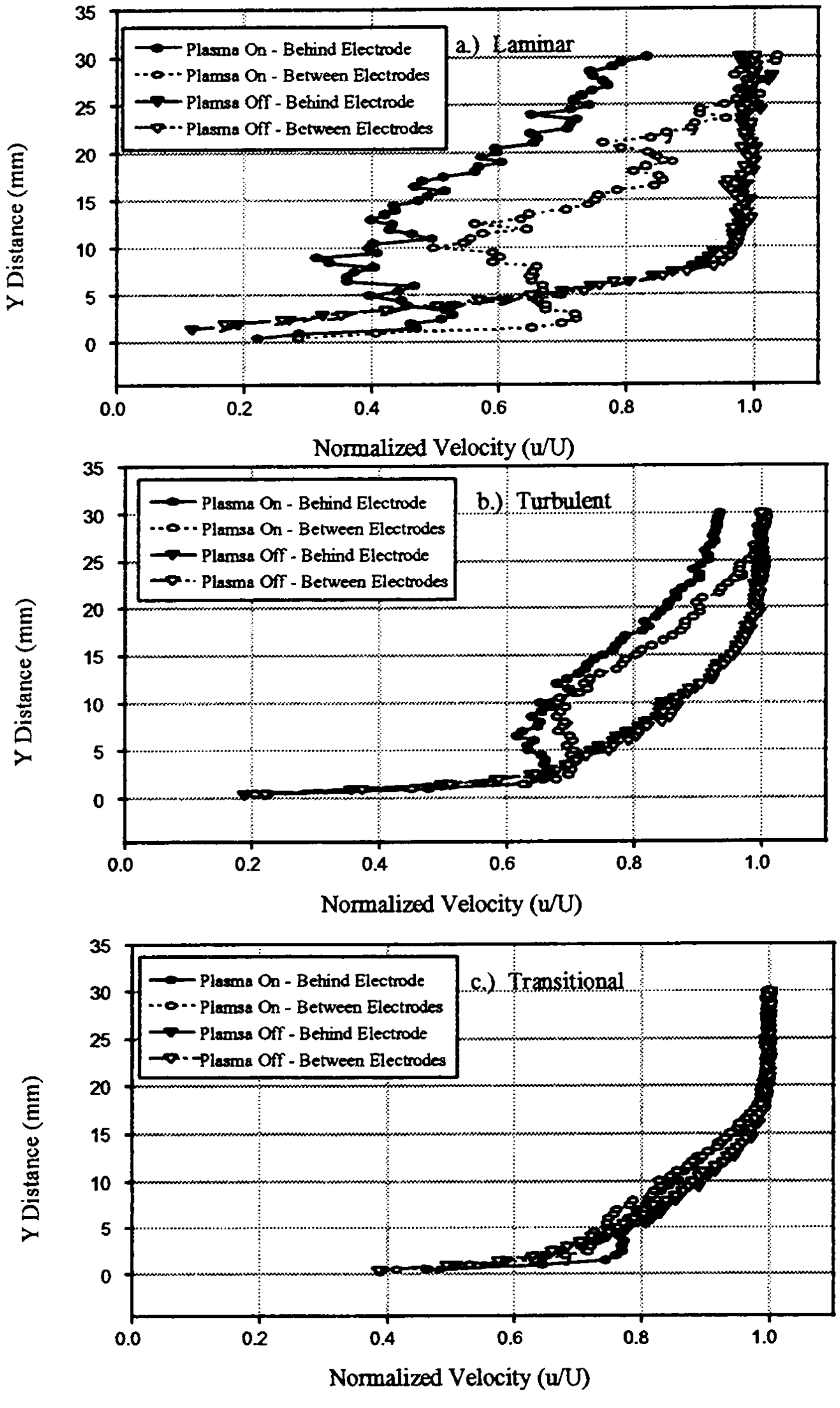

Figure 4.8 The combined plots of the pitot tube velocity profiles of figures 4.6 and 4.7.

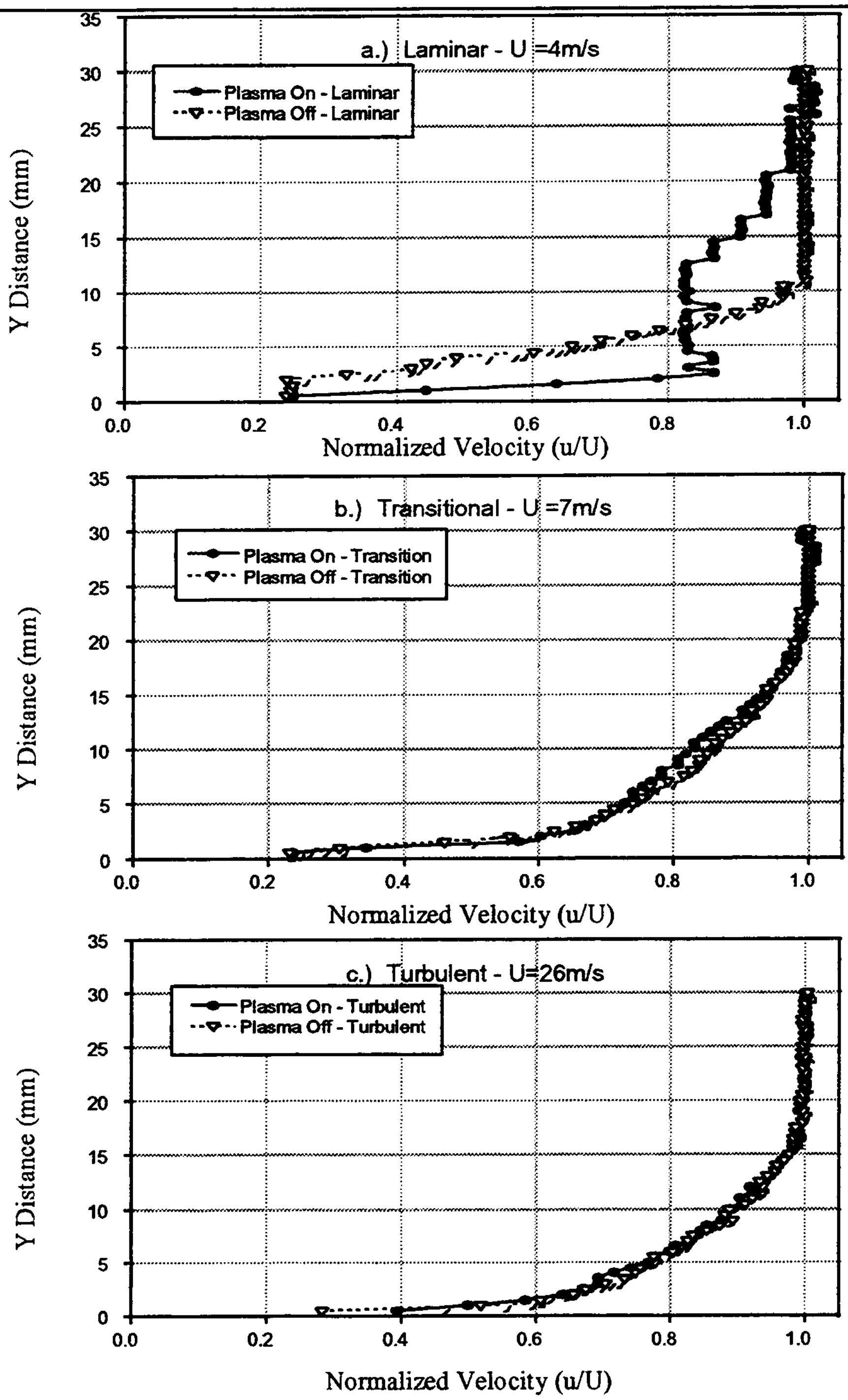

Figure 4.9 Pitot tube velocity profiles for symmetric panel C7-C with the pitot tube located downstream of the center of the span-wise electrodes.

be repeated. Figures 4.9 b & c show little or no variation from the plasma off condition of the test panel. This supports the idea that span-wise symmetric panels serve primarily to trip the airflow.

Smoke Injection Videos

Observing the interaction between OAUGD plasma and static air is crucial to understanding the OAUGD plasma – airflow interaction. This can be accomplished by watching smoke injection videos. As stated in chapter two, the OAUGDP induced motion in still air is due to a combination of the low pressure region above an RF electrode created by the paraelectric forces generated by the plasma. Figures 4.10 a, b are diagrams for the induced motion of static air for a.) a single symmetric RF electrode element and b.) an array of symmetric RF electrode strips.

Leading Edge Smoke Trail Visualizations

The smoke-wire visualization system reveals the interaction of an airflow with the induced paraelectric force generated by a test panel. Figure 4.11 shows a horizontal smoke-wire image for a single RF electrode element on a symmetric panel operated at 5.0 kV and 3.0 kHz. For this image, the airflow velocity was 4 m/s in the laminar regime and the smoke-wire was at a height of 2 mm above the surface of the test panel. The image shows initial movement of the smoke trails toward the RF electrode strip and then splitting of the airflow into two growing vortices as air is accelerated by the paraelectric forces of the plasma away from the RF electrode strip. Figure 4.12 shows a similar image for two symmetric RF electrodes.

Smoke-wire images were also taken of an array of symmetric RF electrode strips

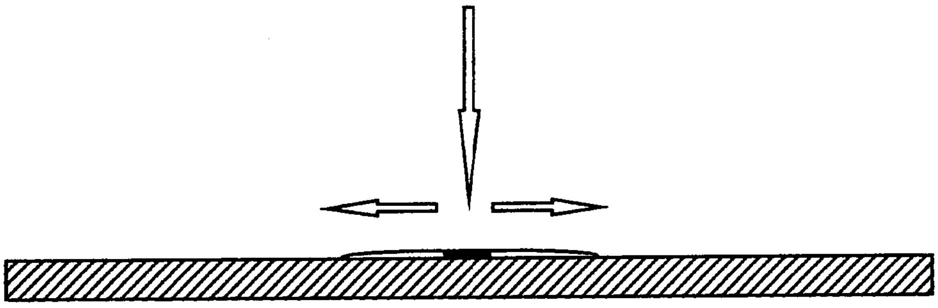

a.) A single symmetric RF electrode strip.

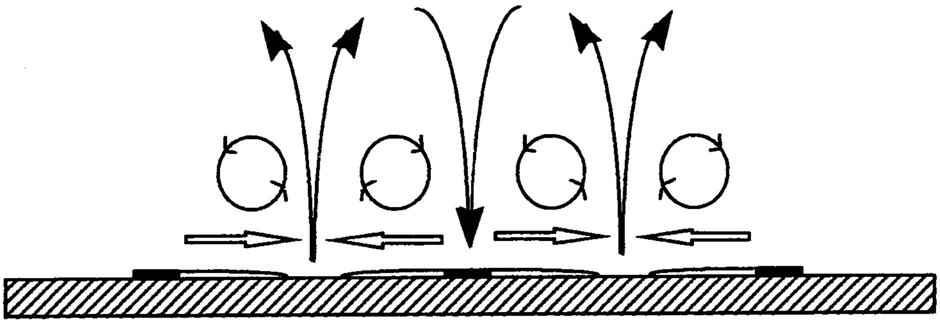

b.) An array of symmetric RF electrode strips.

Figure 4.10 Diagrams for the induced motion of the static air for smmetric RF electrode strips.

(C7-A). Figure 4.13 shows the behavior of the smoke trails for C7-A energized at 3 kV and 3 kHz. Figure 4.14 shows the behavior of the smoke trails of C7-A when energized at a higher voltage, 5kV, but at the same frequency 3.0 kHz. The smoke wire in both cases was at a height of 5 mm and the airflow was in the laminar regime at 4 m/s. Both images show that the smoke trails first flow towards the electrodes, and then are drawn down towards the surface. The smoke trails then flow away from the RF electrode strip (due to paraelectric acceleration) to form vortical structures, which collide with the induced airflow from the adjacent electrode strip. This is the reason for the pocket-like structures observable in figures 4.13 and 4.14. The initial location and area of this pocket-like smoke structure depends on the height of the smoke trails and applied voltage. Figures 4.15 through 4.18 show the smoke trails for panel C7-A energized at 5.1 kV and 3.0 kHz and at heights of 2mm, 5 mm, 7.5 mm, and 9.5 mm.

As stated previously, the symmetric OAUGDP panel oriented perpendicular to the airflow trips an initially laminar airflow. Figures 4.19 shows this for a smoke wire at the height of 5 mm for two symmetric, spanwise electrodes energized at 5.0 kV and 3.0 kHz. Figures 4.20 and 4. 21 show this for panel C7-C when operated at 5.1 kV and 3.0 kHz with the smoke wire at a height of 2 mm and 5 mm. Images were taken for other heights and voltages but no coherent airflow structures were found.

Part II. – Asymmetric OAUGDP Panel

To a first approximation, the asymmetric panel is composed of a series of electrode strips with the OAUGDP generated only on one side of the strips. In practice, the asymmetric panels energized at a minimum applied voltage are perfectly asymmetric,

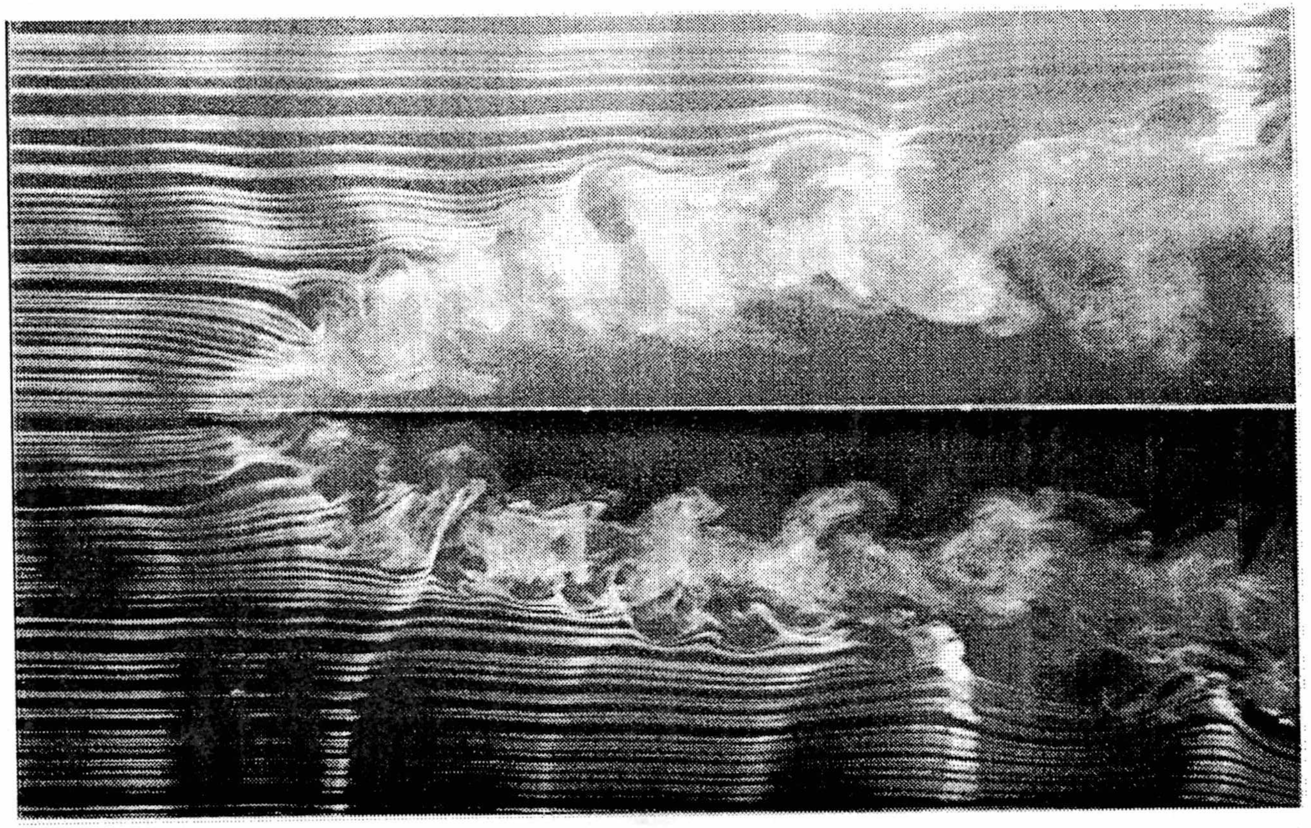

Figure 4.11 A horizontal digital image of a single RF electrodestrip energized at 5.0 kV and 3.0 kHz with the smoke trails generated at a height of 2mm.

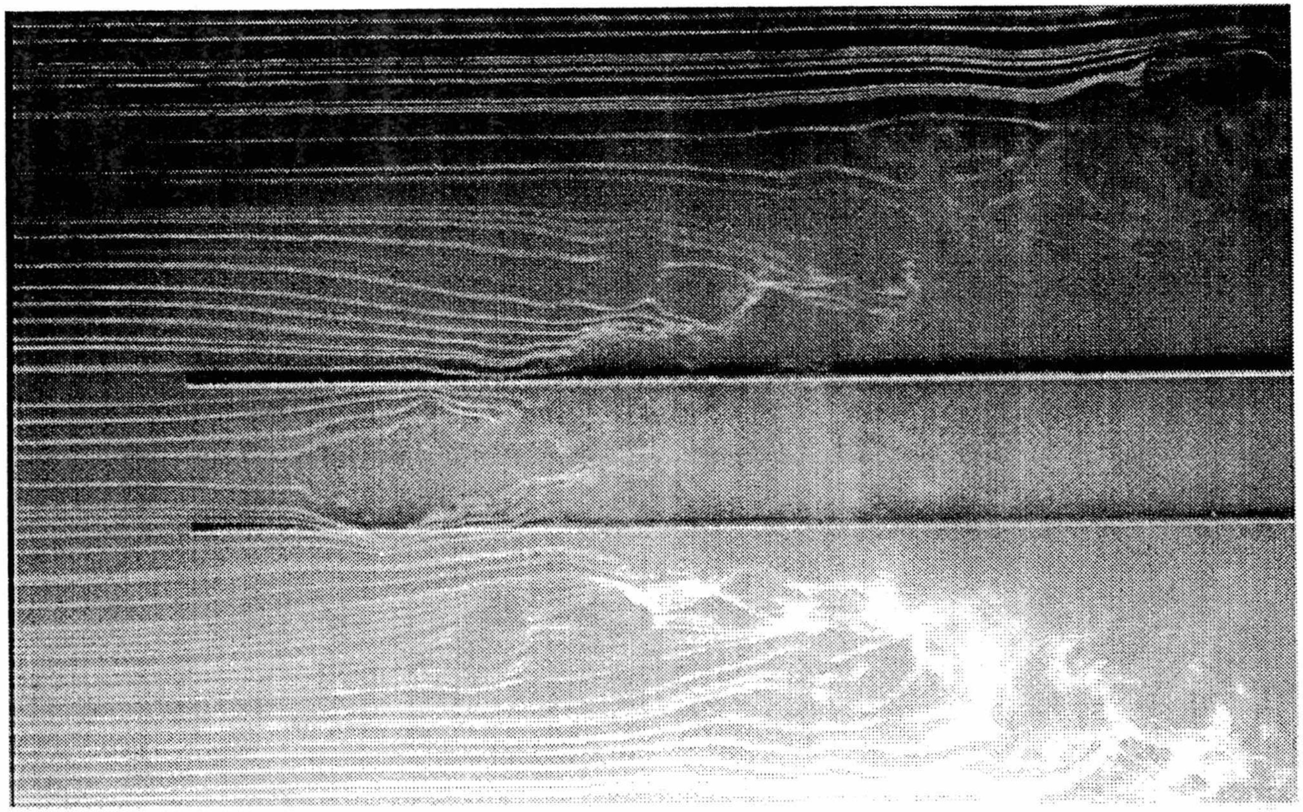

Figure 4.12 A horizontal digital image of a two RF electrode strips energized at 5.0 kV and 3.0 kHz with the smoke trails generated at a height of 2 mm.

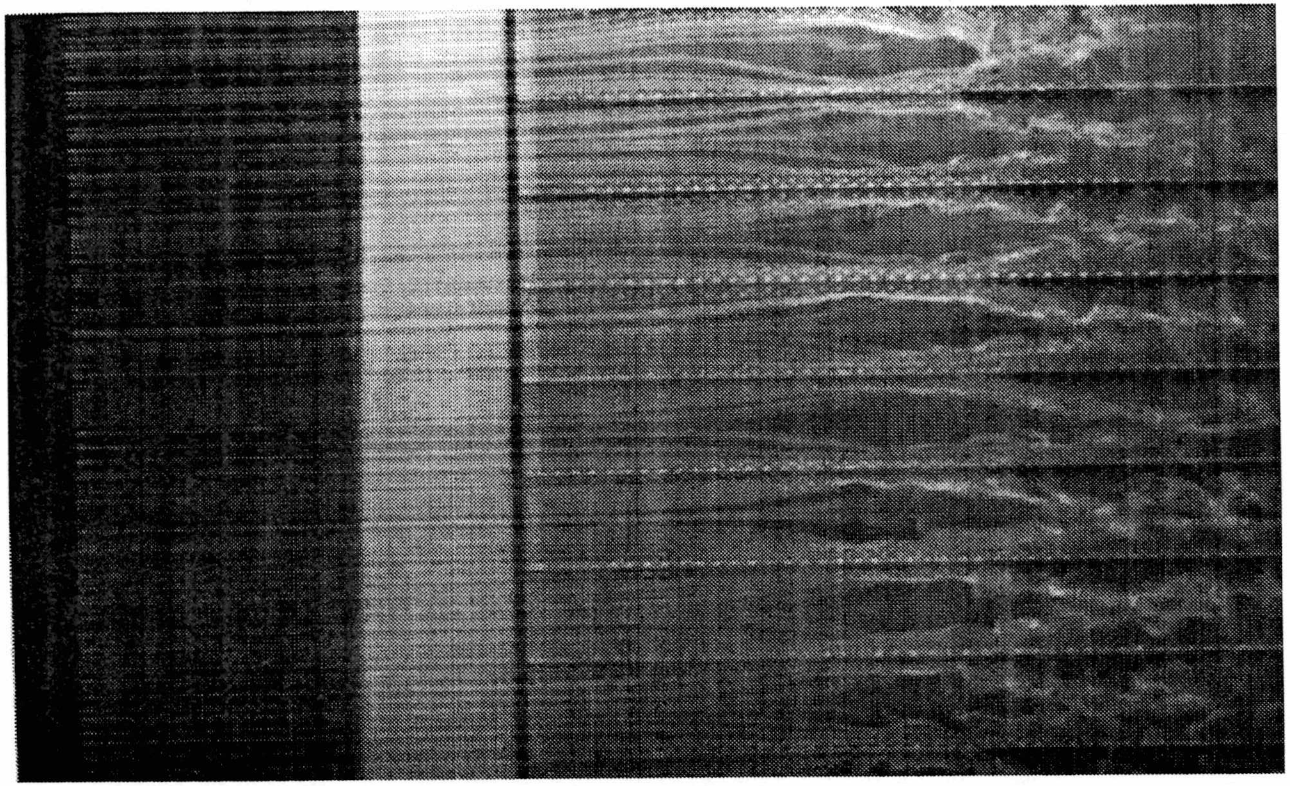

Figure 4.13 A horizontal digital image of symmetric panel C7-A energized at 3.0 kV and 3.0 kHz with the smoke trails generated at a height of 5 mm.

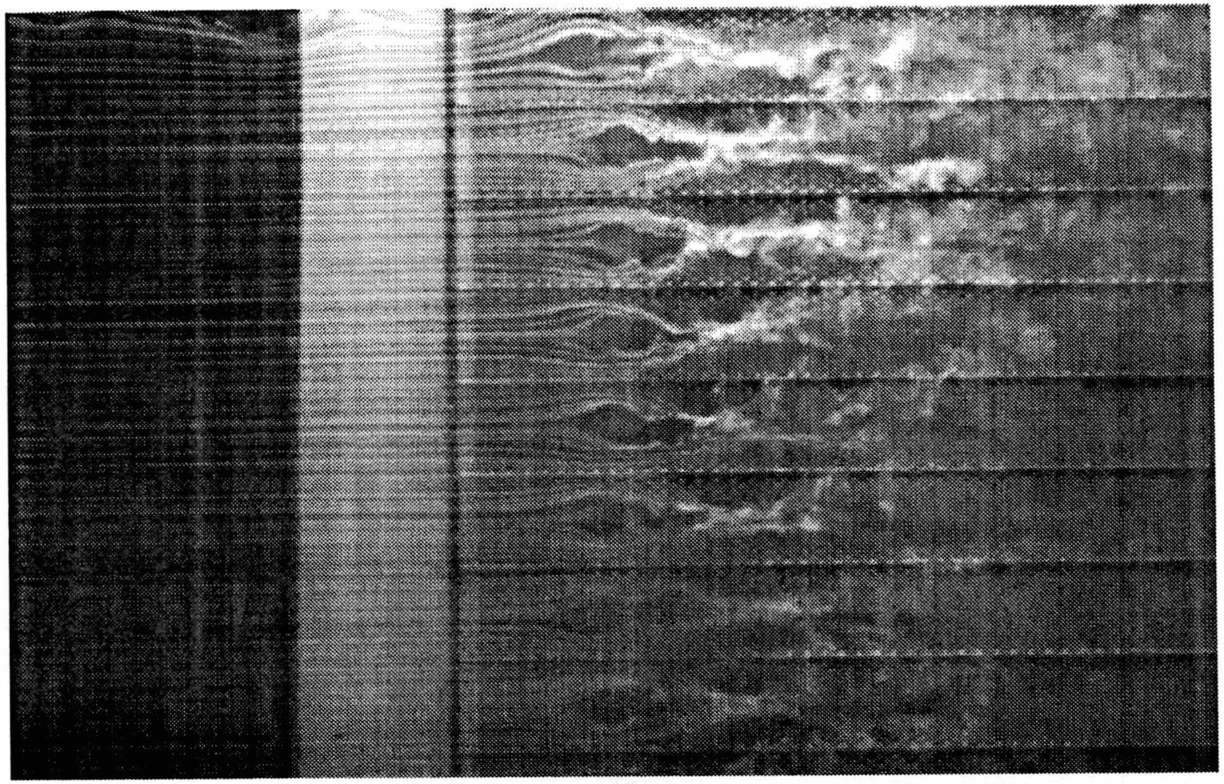

Figure 4.14 A horizontal digital image of symmetric panel C7-A energized at 5.0 kV and 3.0 kHz with the smoke trails generated at a height of 5 mm.

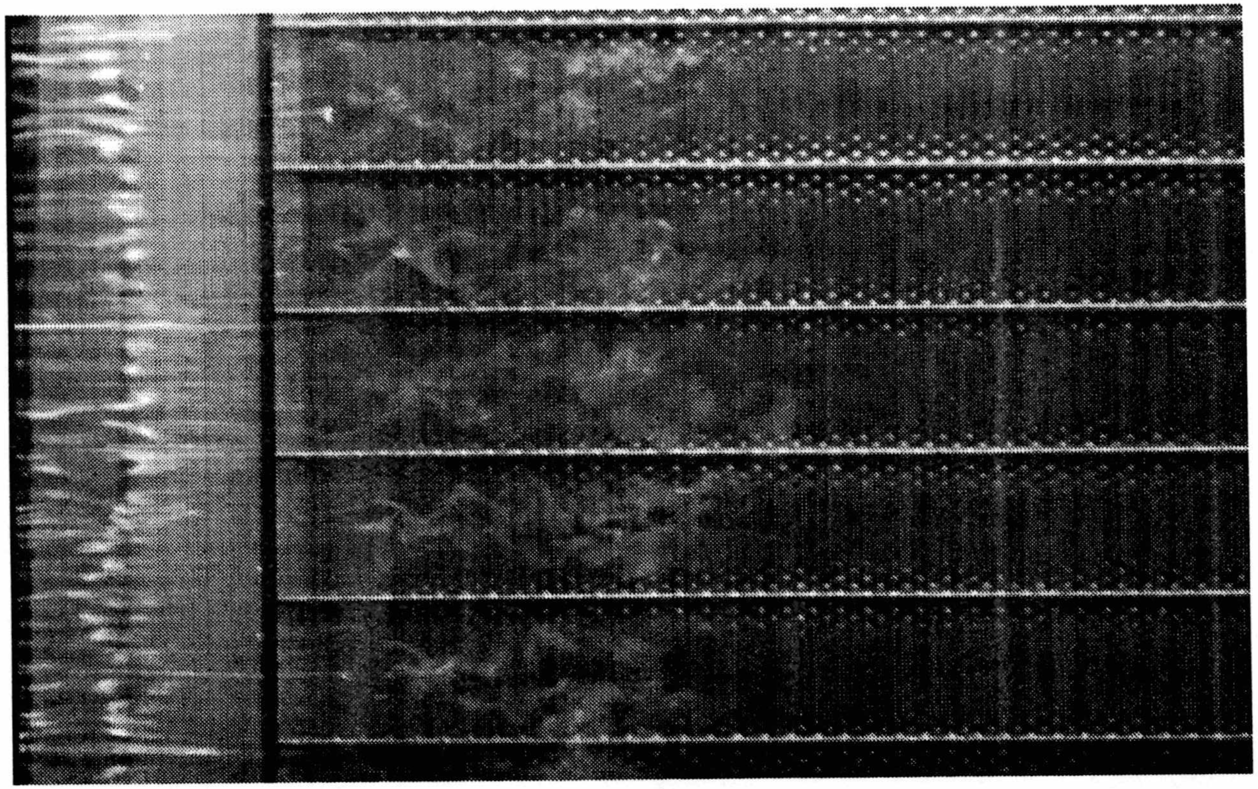

Figure 4.15 A horizontal digital image of symmetric panel C7-A energized at 5.0 kV and 3.0 kHz with the smoke trails generated at a height of 2 mm.

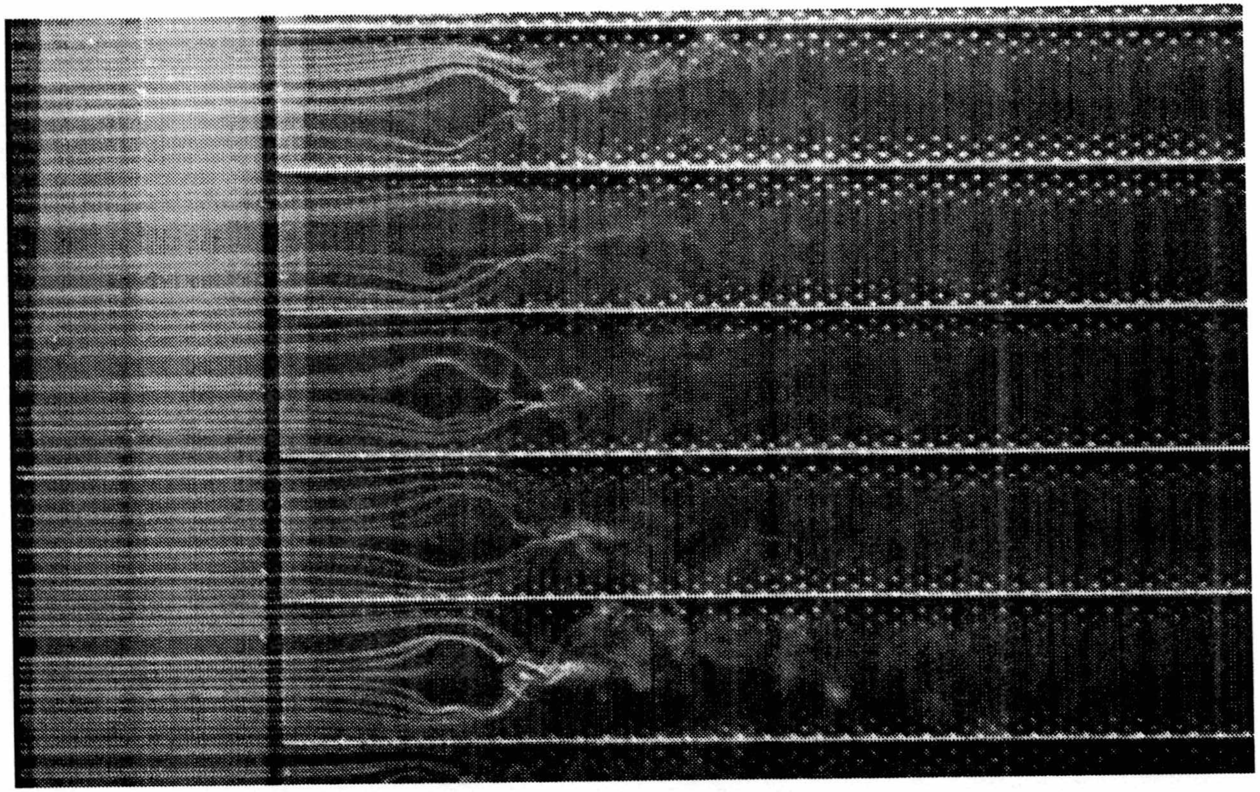

Figure 4.16 A horizontal digital image of symmetric panel C7-A energized at 5.0 kV and 3.0 kHz with the smoke trails generated at a height of 5 mm.

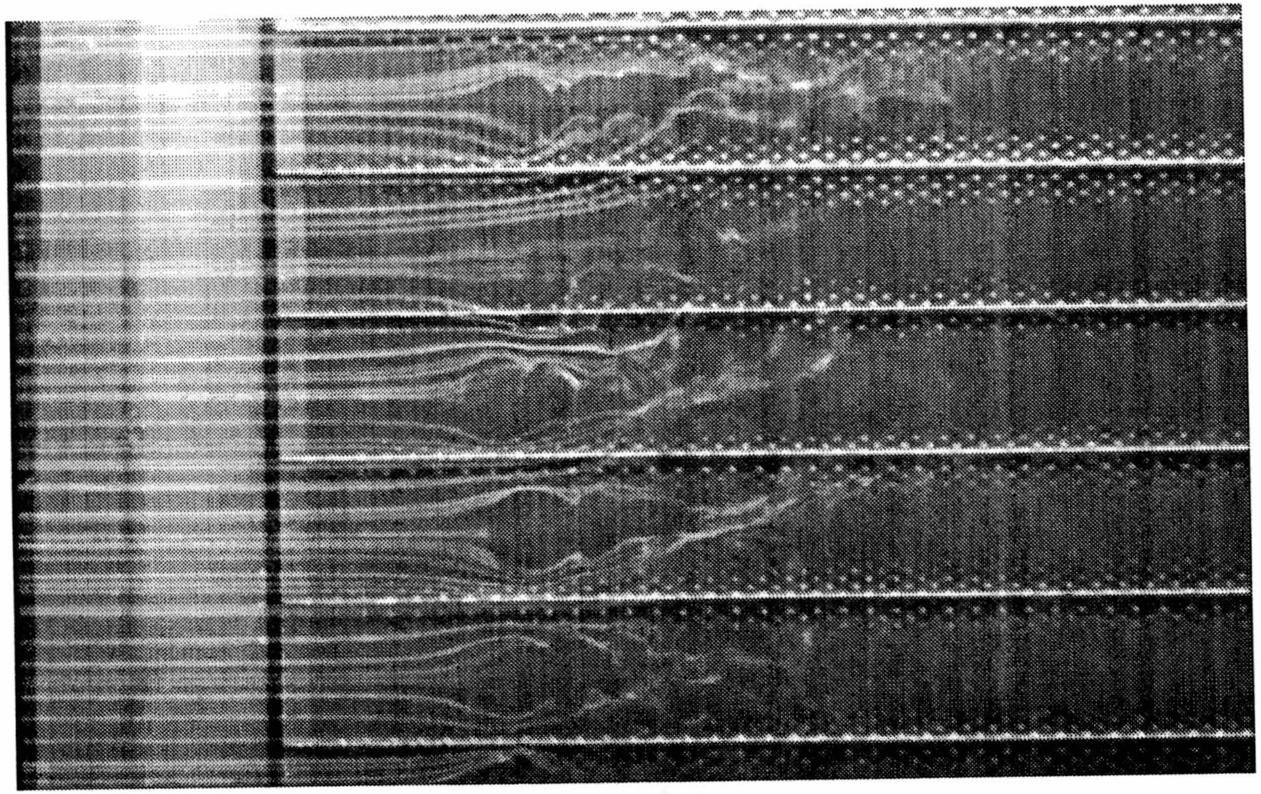

Figure 4.17 A horizontal digital image of symmetric panel C7-A energized at 5.0 kV and 3.0 kHz with the smoke trails generated at a height of 7.5 mm.

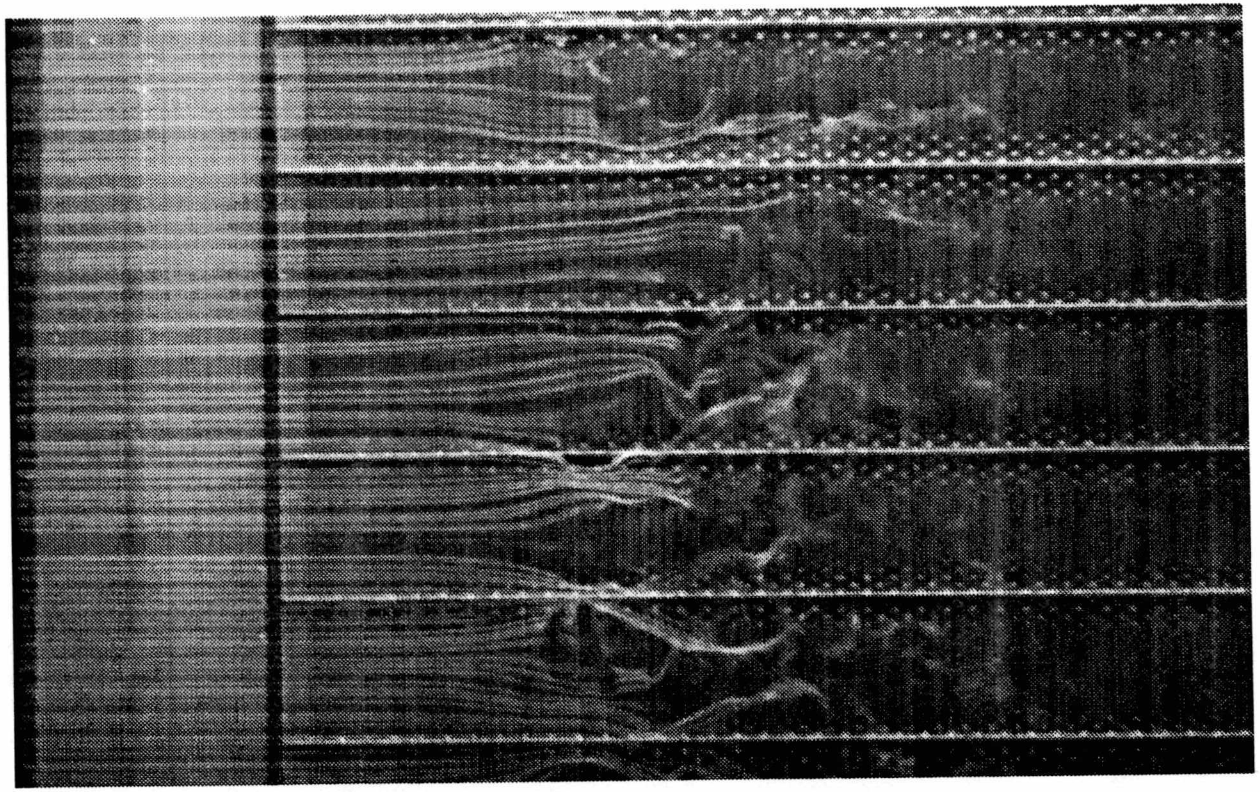

Figure 4.18 A horizontal digital image of symmetric panel C7-A energized at 5.0 kV and 3.0 kHz with the smoke trails generated at a height of 9.5 mm.

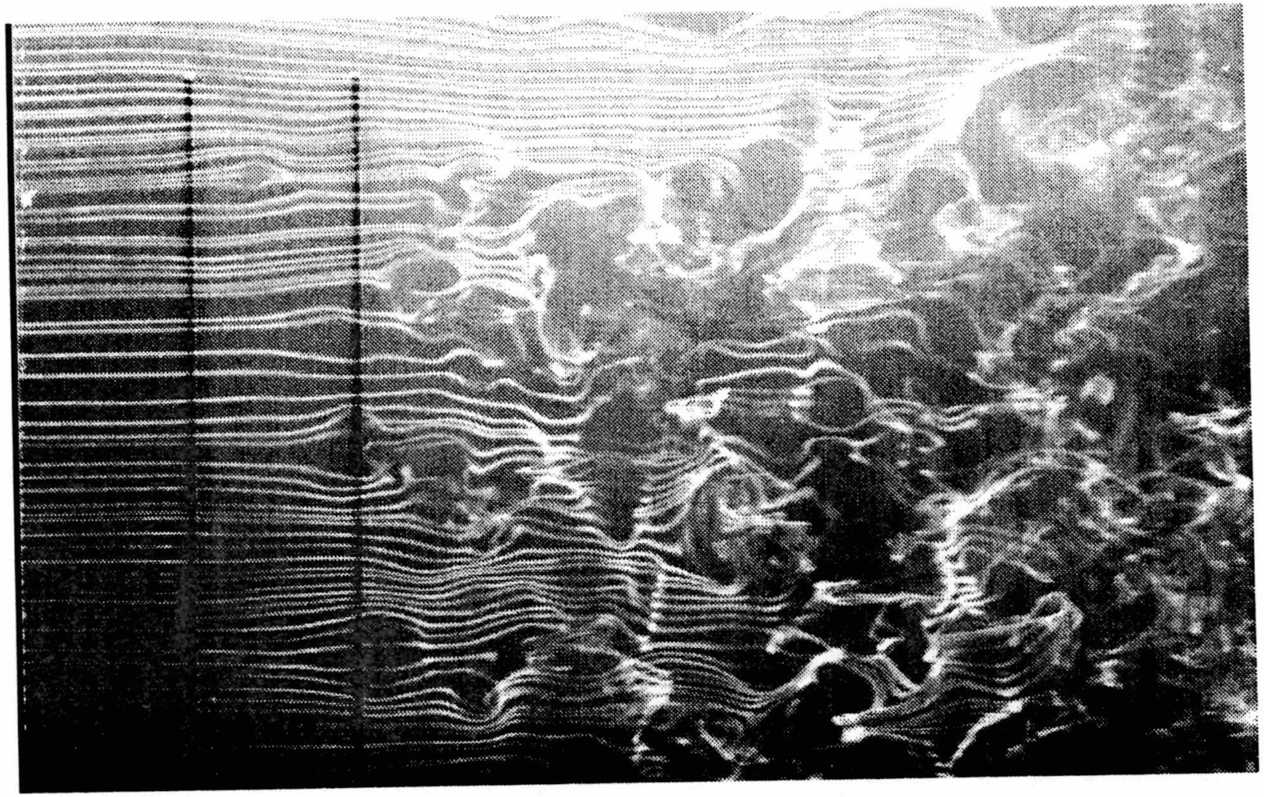

Figure 4.19 A horizontal digital image of two symmetric spanwise RF electrodes energized at 5.0 kV and 3.0 kHz with the smoke trails generated at a height of 5 mm.

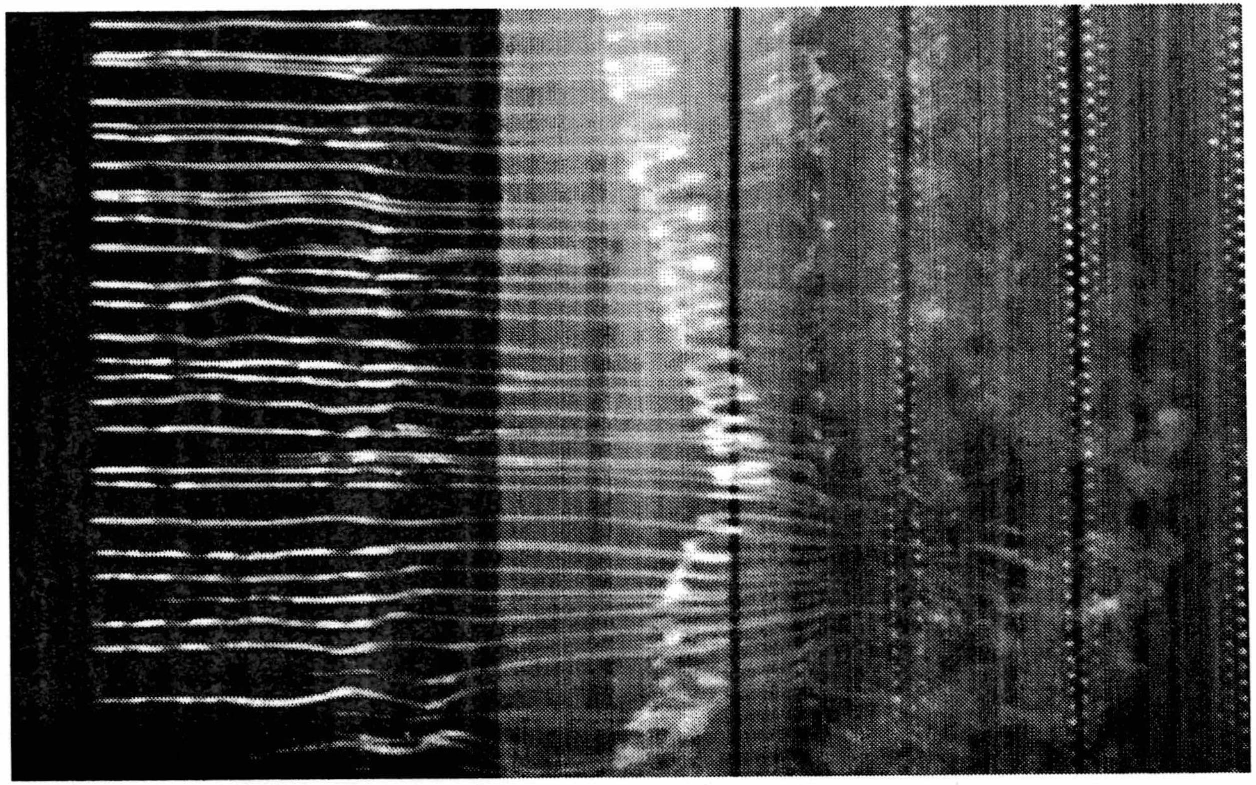

Figure 4.20 A horizontal digital image of symmetric panel C7-C energized at 5.0 kV and 3.0 kHz with the smoke trails generated at a height of 2 mm.

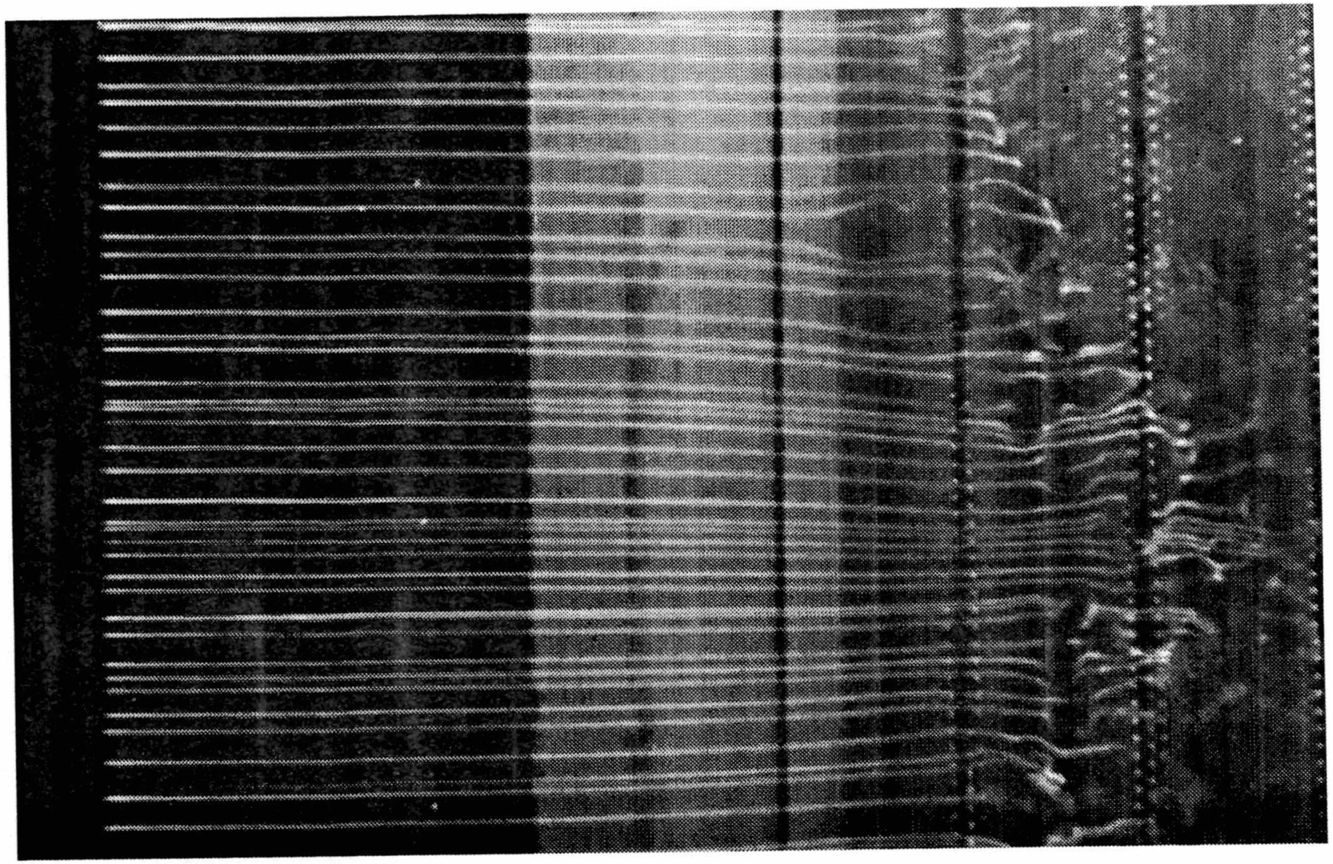

Figure 4.21 A horizontal digital image of symmetric panel C7-C energized at 5.0 kV and 3.0 kHz with the smoke trails generated at a height of 5 mm.

but at higher voltages the plasma is also generated on the side where plasma is not wanted. Previous data from symmetric panels shows that progressively stronger OAUGDP effects on the boundary layer occur with increasing applied voltage. Initial testing of the asymmetric panels shows the same behavior. Given that the asymmetric panels were developed at the end of the research contract, there was not time to develop optimized panels that remained perfectly asymmetric at the maximum voltage of the March Instruments power supply. The results that follow are for panels with a net asymmetric plasma generation, and are not optimized for this design concept. The ability of asymmetric OAUGDP panels to alter the airflow (magnitude of the lateral velocity) may be improved by designing panels that remain truly asymmetric. To understand the results that follow, the asymmetric OAUGDP must be envisioned as an airflow accelerator. This airflow acceleration is accomplished by a net asymmetric paraelectric force created by the combination of weak plasma generation to one side of the RF electrode strip and strong plasma generation on the other side of the RF electrode strip.

Drag Balance Results

With the problem of an electrostatic correction removed, then figure 4.22 shows for static airflow (wind tunnel off) the induced thrust (negative drag) as a function of the applied plasma voltage for the asymmetric panel E6-C. Given that the thrust begins when the plasma forms, the OAUGDP is the obvious cause for the flow acceleration.

Figure 4.23 shows the measured drag as a function of the airflow velocity for an asymmetric panel (E6-C) oriented so that the OAUGDP thrust is in the counter-flow (upstream) direction. The panel was operated at 4 kV and 3 kHz. Included in this figure

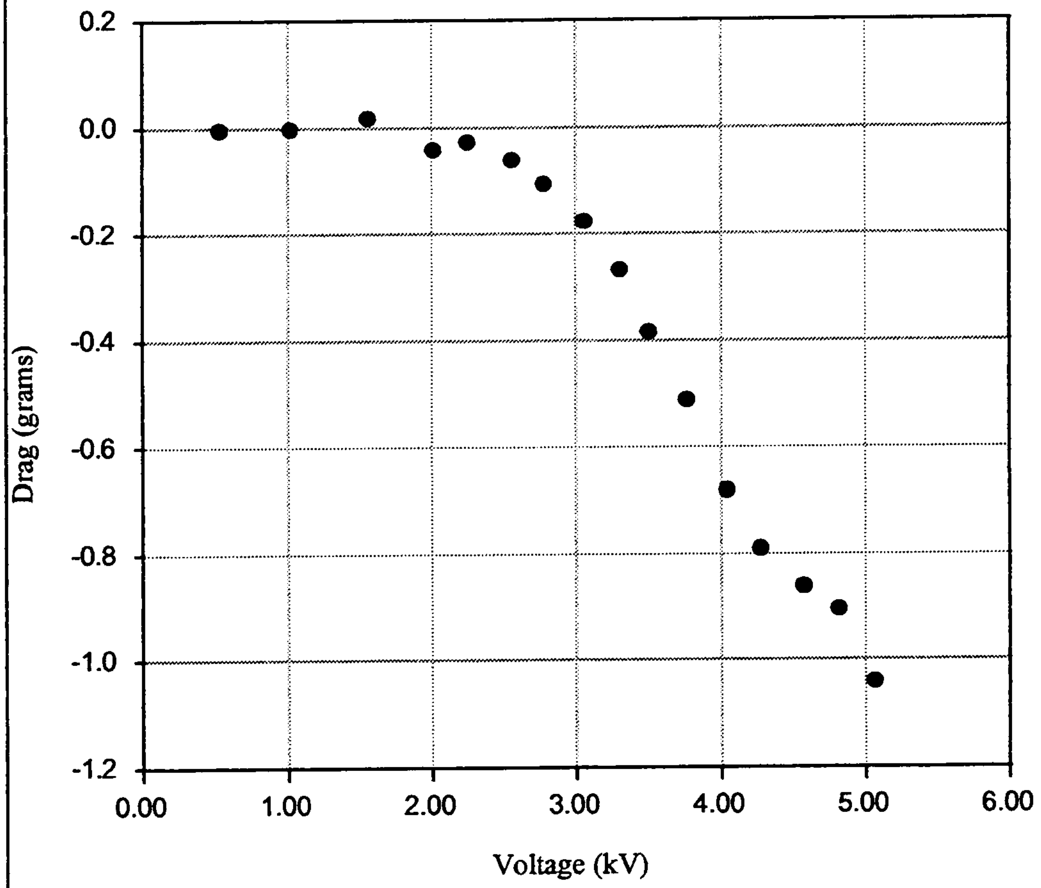

Figure 4.22 A graph of the drag (thrust) versus voltage for asymmetric panel E6-C.

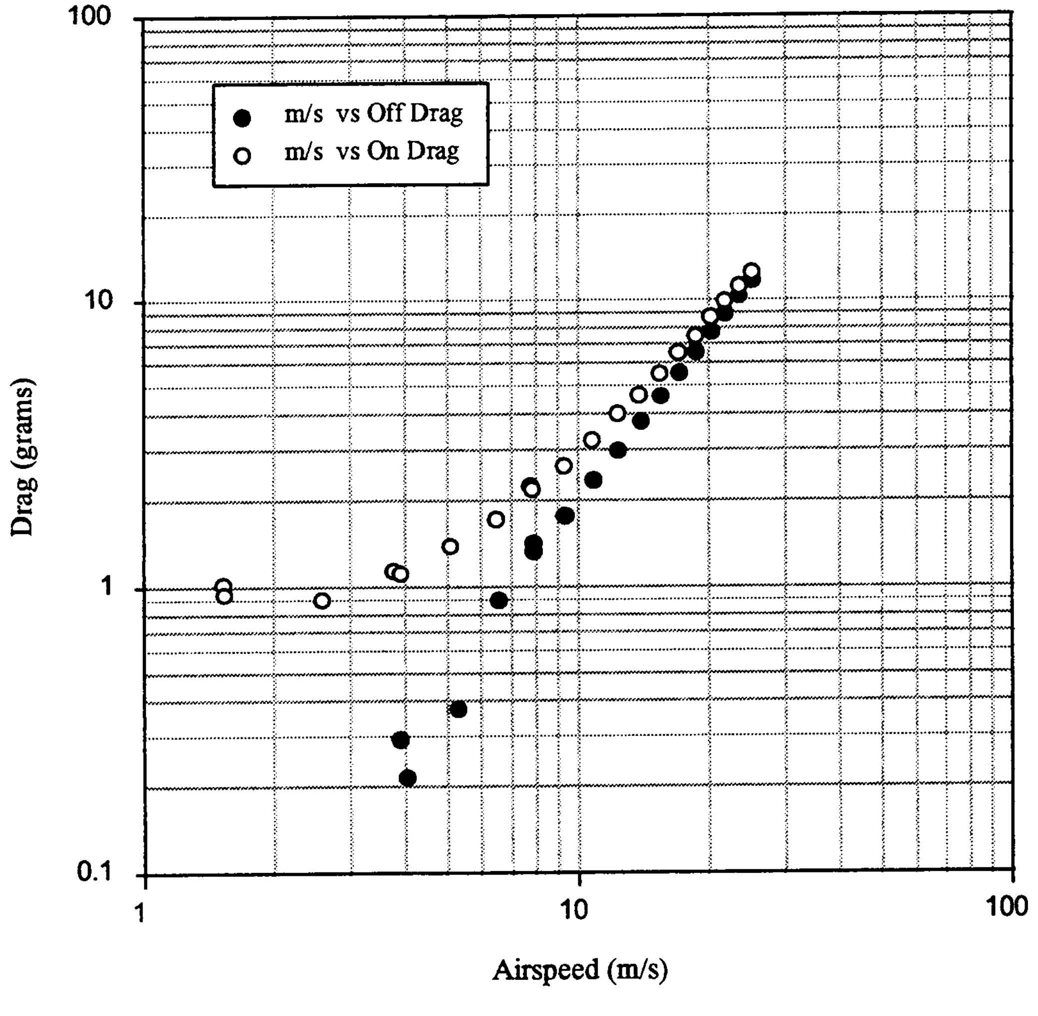

Figure 4.23 A graph of the drag versus airspeed for the asymmetric panel with the thrust oriented counter-flow.

is the drag data showing the plasma off. From this figure, it is evident that a counter-flowing asymmetric OAUGDP panel also increases the aerodynamic drag. Figure 4.24a shows a figure similar to 4.23 for the same panel and operation conditions except that it has been rotated 180 degrees so that the panel's thrust is in a co-flow (downstream) direction. The result evident is drag reduction. For velocities less than 7 m/s the measured "drag" was actually thrust, which could not be shown on the logarithmic-plot but is shown on a linear plot in figure 4.24b .

Drag versus airflow velocity data were also taken for an asymmetric panel oriented such that the paraelectric thrust was perpendicular to the airflow. Figure 4.25 shows that this configuration increases the aerodynamic drag. The magnitude of this increase can be as large as that of a symmetric panel.

Pitot Probe Results

The pitot tube velocity profile data further support the concept that the asymmetric panel acts as a gas flow accelerator. Figure 4.26 shows three pitot tube profiles for E6-C taken at 3 kV, 4 kV, and 5 kV in static air (with the wind tunnel off). The probe was located at the same position used for testing the symmetric panels (28 mm from the last electrode and in the center of the tunnel). The airflow maximum velocity is not located at the panel surface, which is covered with plasma, because the probe tip is 28 mm from the plasma edge. Also evident is that the "free stream" airflow velocity is up to ~0.5 m/s at distance of 30 mm above the surface of the aft test plate. Recall that for these velocities and a laminar flow, the boundary layer thickness was about 10 mm. Furthermore, if the maximum airflow velocity is plotted as a function of the applied

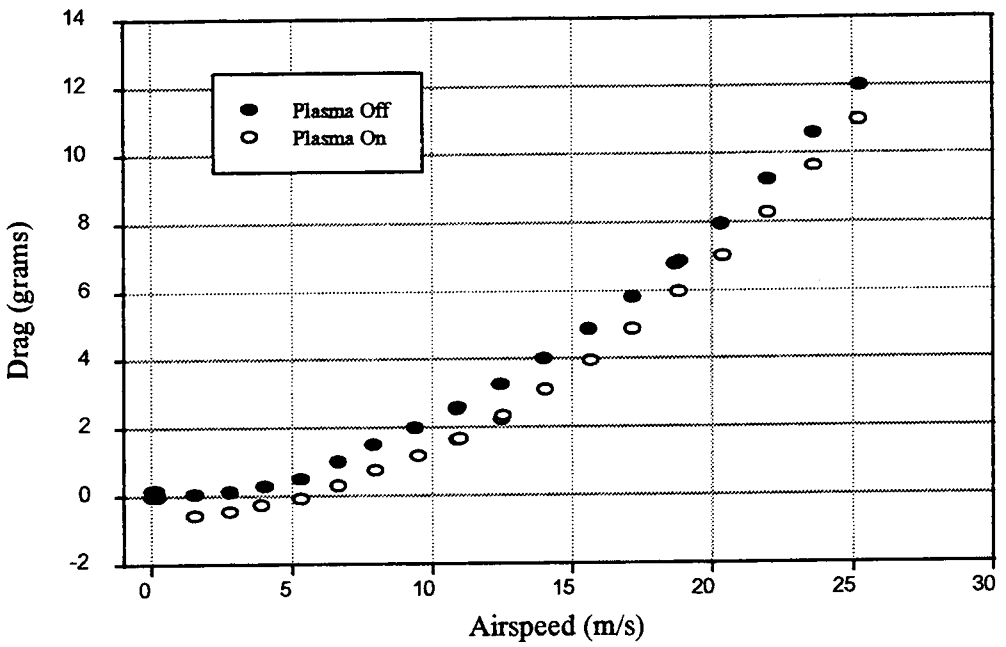

a.) Linear graph.

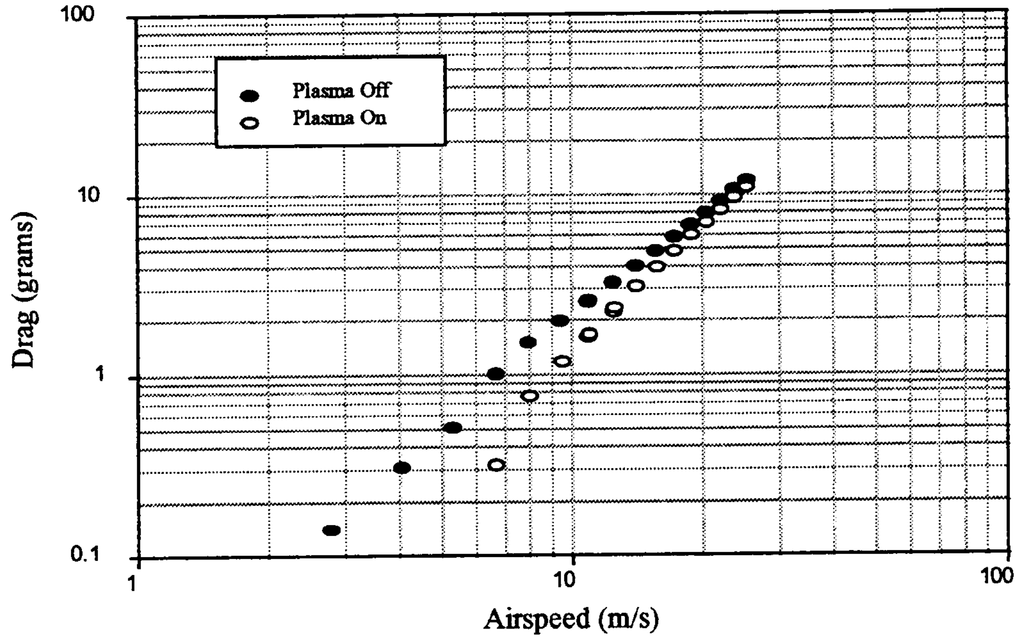

b.) Logrithmic graph.

Figure 4.24 Graphs of the drag versus airspeed for an asymmetric panel with the thrust oriented co-flow.

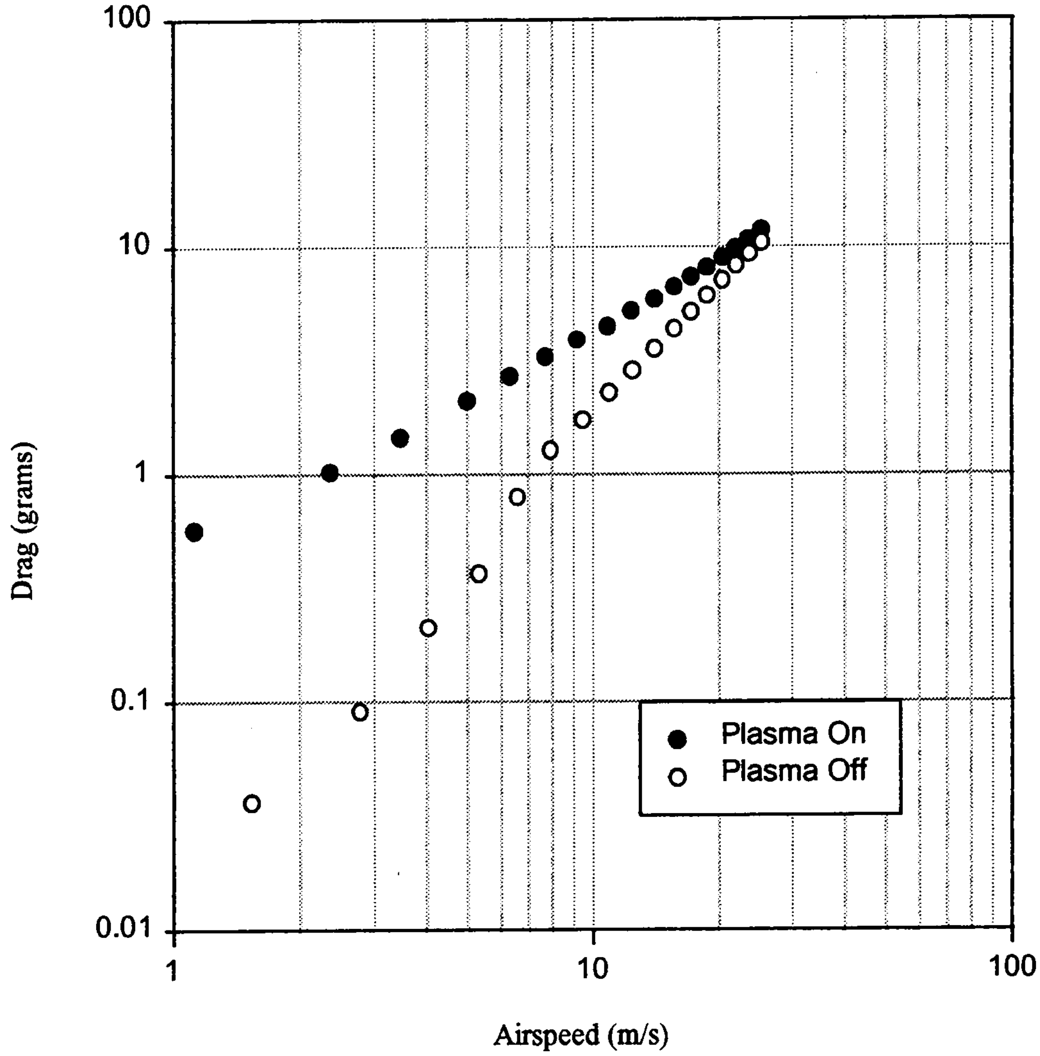

Figure 4.25 A graph of the drag versus airspeed for an asymmetric panel with the thrust perpendicular to the flow.

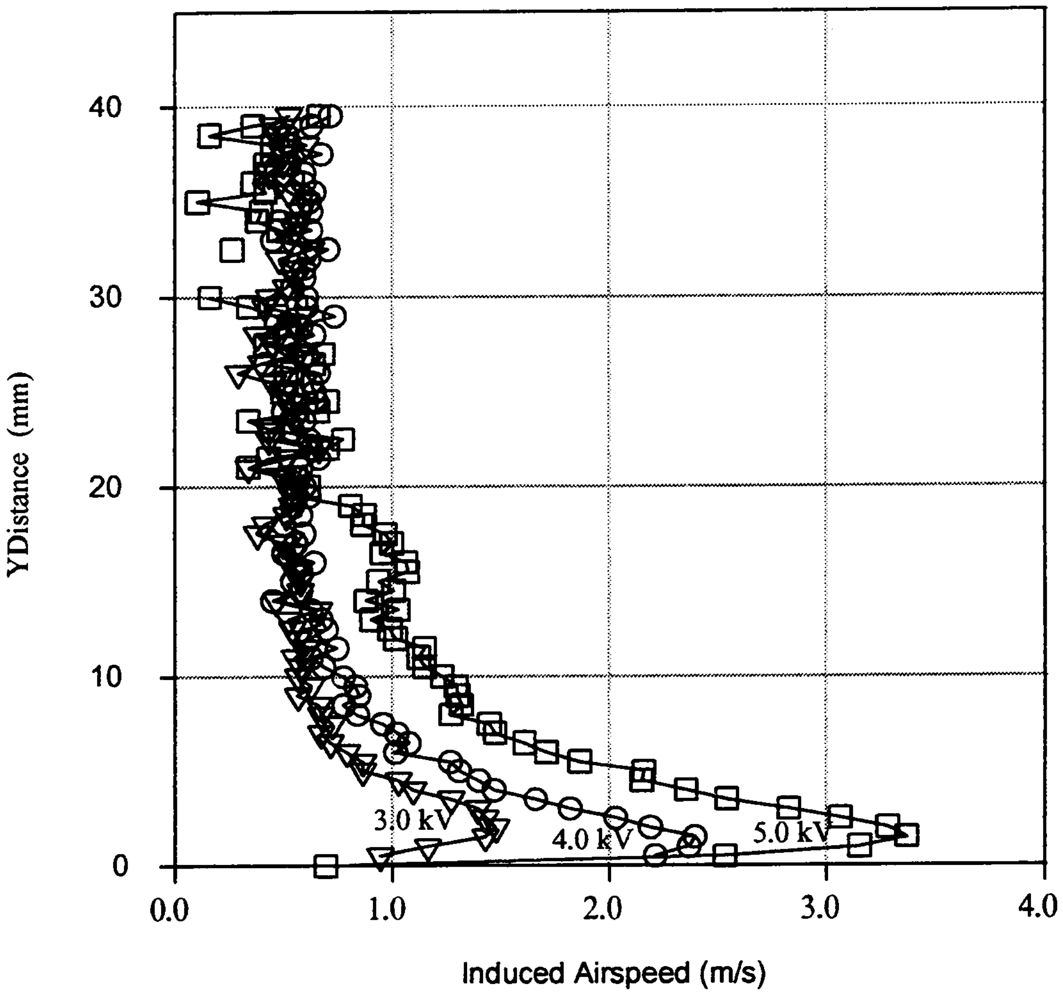

Figure 4.26 The pitot tube velocity profiles of the induced motion of static air for the voltages of 3.0 kV, 4.0 kV and 5.0 kV.

voltage, figure 4.27, a linear relationship between the maximum induced velocity and voltage is observed.

Pitot tube profiles were also taken for free stream airflow velocities identical to those in the previous symmetric panel test, at 4 m/s, 7 m/s, and 26 m/s. Figure 4.28a,b,c shows the profiles for the asymmetric panel E2-A counter-flow oriented, and operated at 4 kV and 3 kHz. Depending on the velocity of the airflow, figures 4.28a,b,c show a slight thickening of the boundary layer, but do not show the two inflection points observed in the symmetric panel pitot tube profiles.

Similar profiles were taken for the asymmetric panel E2-A, co-flow oriented and operated at the same conditions as figure 4.28a,b,c. In figure 4.29a,b,c the pitot tube profiles show that the asymmetric co-flow OAUGDP panel thins the aerodynamic boundary layer. While the boundary layer is thinner when the plasma is present, hot-wire anemometry done at a point downstream of the test panel showed that the airflow was turbulent. This probably results from a combination of the asymmetric panel not being optimized, and the laminar flow undergoing a sudden acceleration when encountering the energized asymmetric OAUGDP panel.

Smoke Injection Videos

Figures 4.30a,b,c are diagrams for the induced motion of static air for a.) a single asymmetric electrode strip b.) an array of asymmetric electrode strips, and c.) an array of energized asymmetric strips well above the initiation voltage.

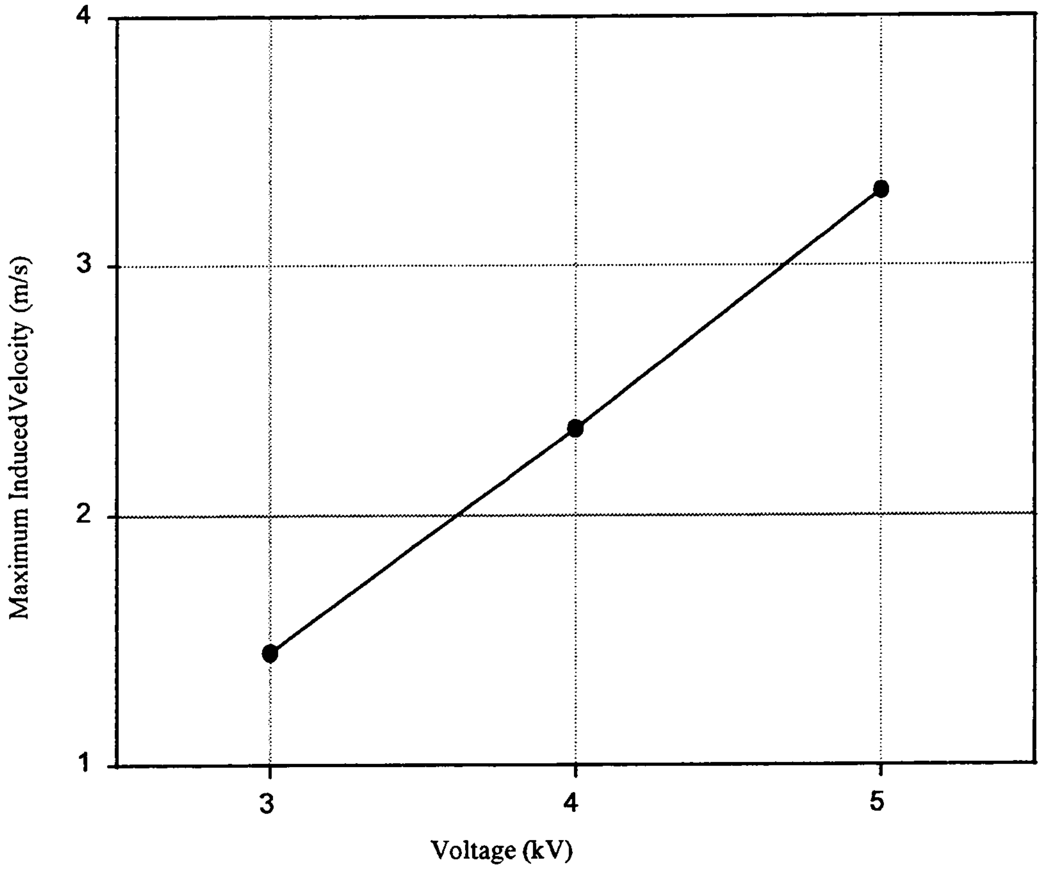

Figure 4.27 A linear graph of the maximum induced velocity versus voltage for the asymmetric panel E6-C.

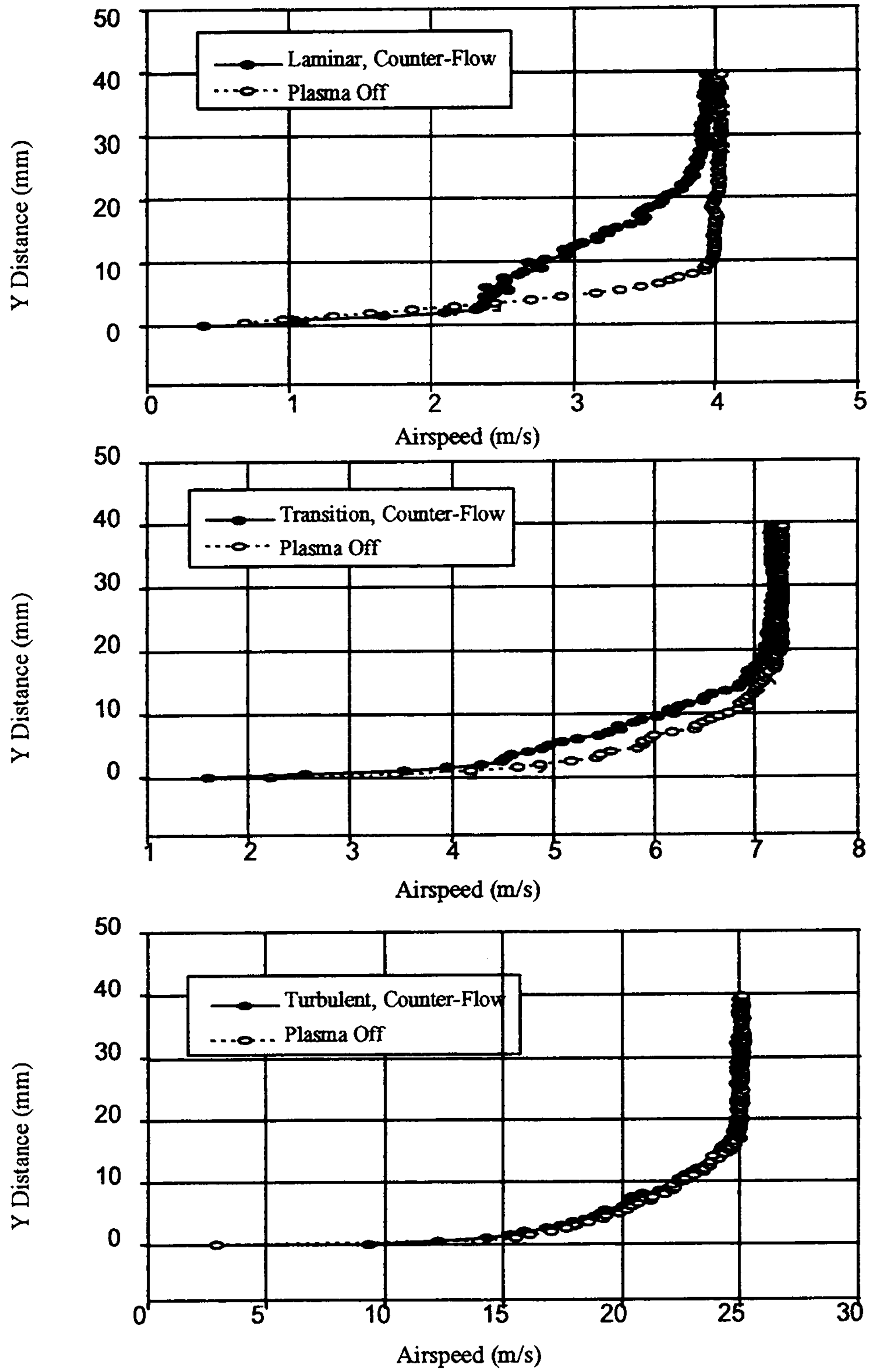

Figure 4.28 The pitot tube velocity profiles for the counter-flow oriented asymmetric panel E6-C energized at 4.0 kV and 3.0 kHz.

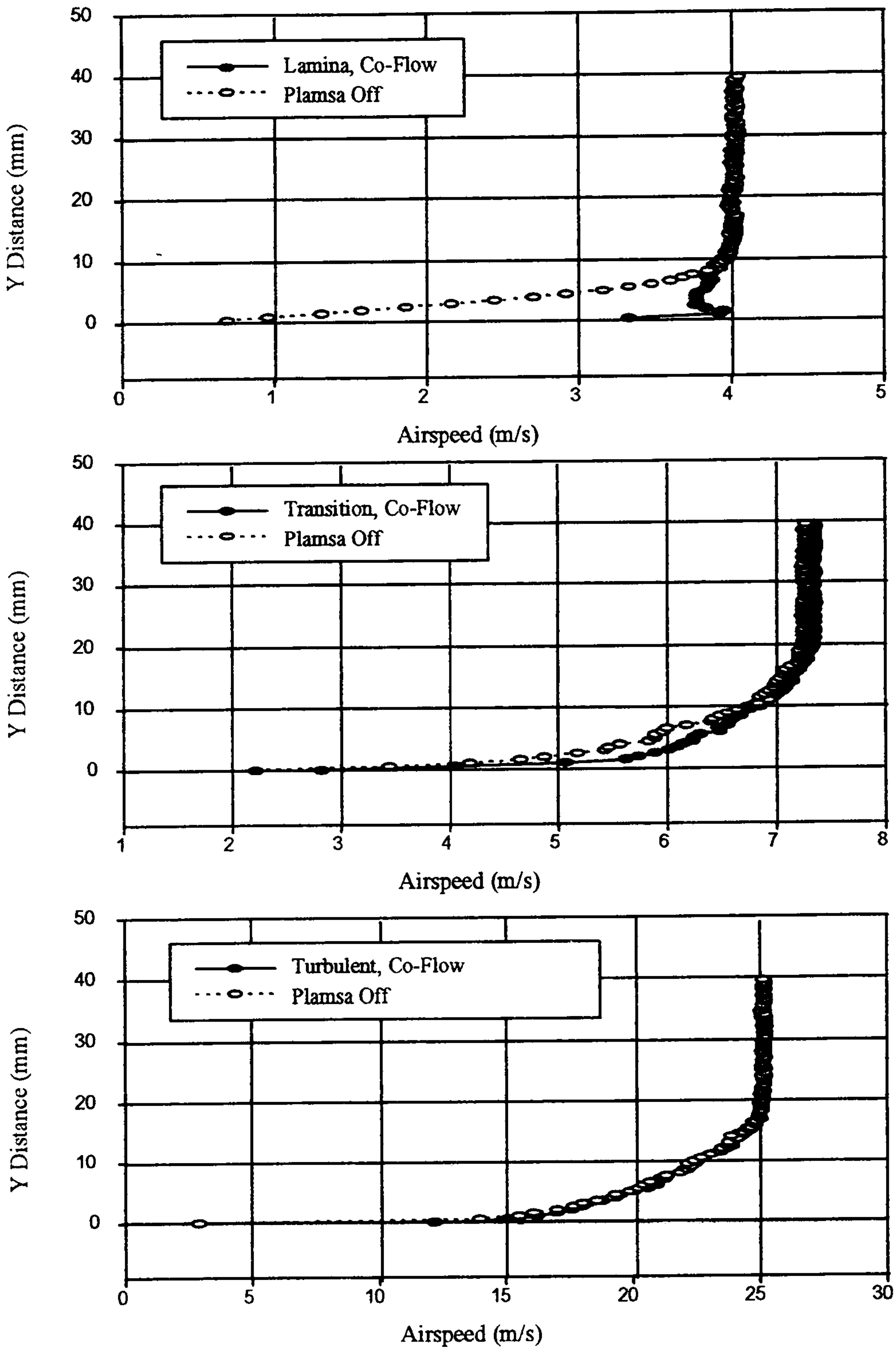

Figure 4.29 The pitot tube velocity profiles for the co-flow oriented asymmetric panel E6-C energized at 4.0 kV and 3.0 kHz.

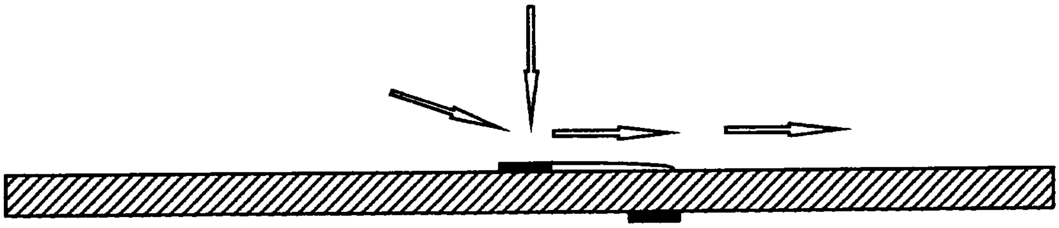

a.) A single asymmetric RF strip.

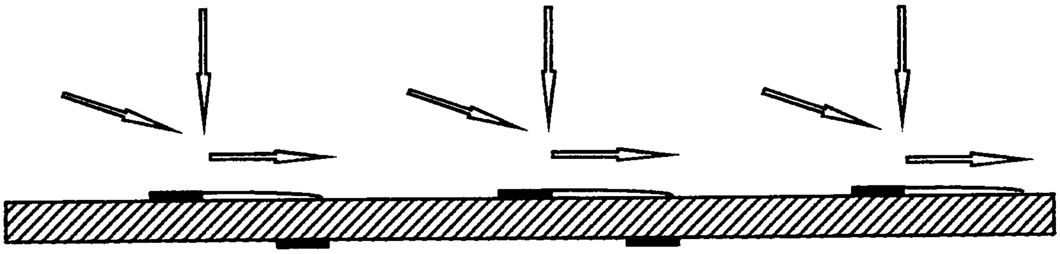

b.) An array of optimized asymmetric RF strips.

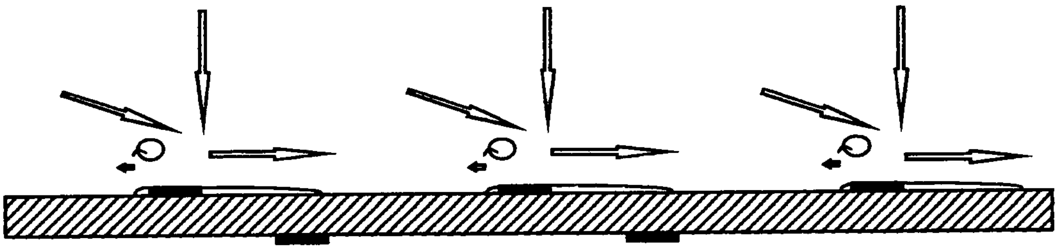

c.) An array of over energized asymmetric RF strips.

Figure 4.30 Diagrams of the induced motion of static air for asymmetric RF strips.

Leading Edge Smoke Trail Visualizations

Smoke trail visualizations were done for an asymmetric OAUGDP panel for three electrode configurations, including counter-flow, co-flow, and perpendicular orientations. In figure 4.31 a counter-flow image of panel E2-A shows the smoke trails entering the panel but abruptly being stopped. The operating conditions for this figure were 5.0 kV at 3.0 kHz, with the smoke wire at a height of 2 mm. Figure 4.32 shows a vertical smoke trail digital image of E2-A oriented co-flow. With the wire located near the center of the wind tunnel and the asymmetric panel energized at 4.0 kV and 3.0 kHz, this figure shows that the airflow is turbulent (confirming data taken by the hot-wire anemometer), though the drag balance observed a reduction in drag. Figure 4.33 shows a digital smoke wire image of E2-A perpendicularly oriented and energized at 4.0 kV and 3.0 kHz. Turbulent mixing of the airflow is shown but no coherent structures were seen when examined at different smoke-wire heights.

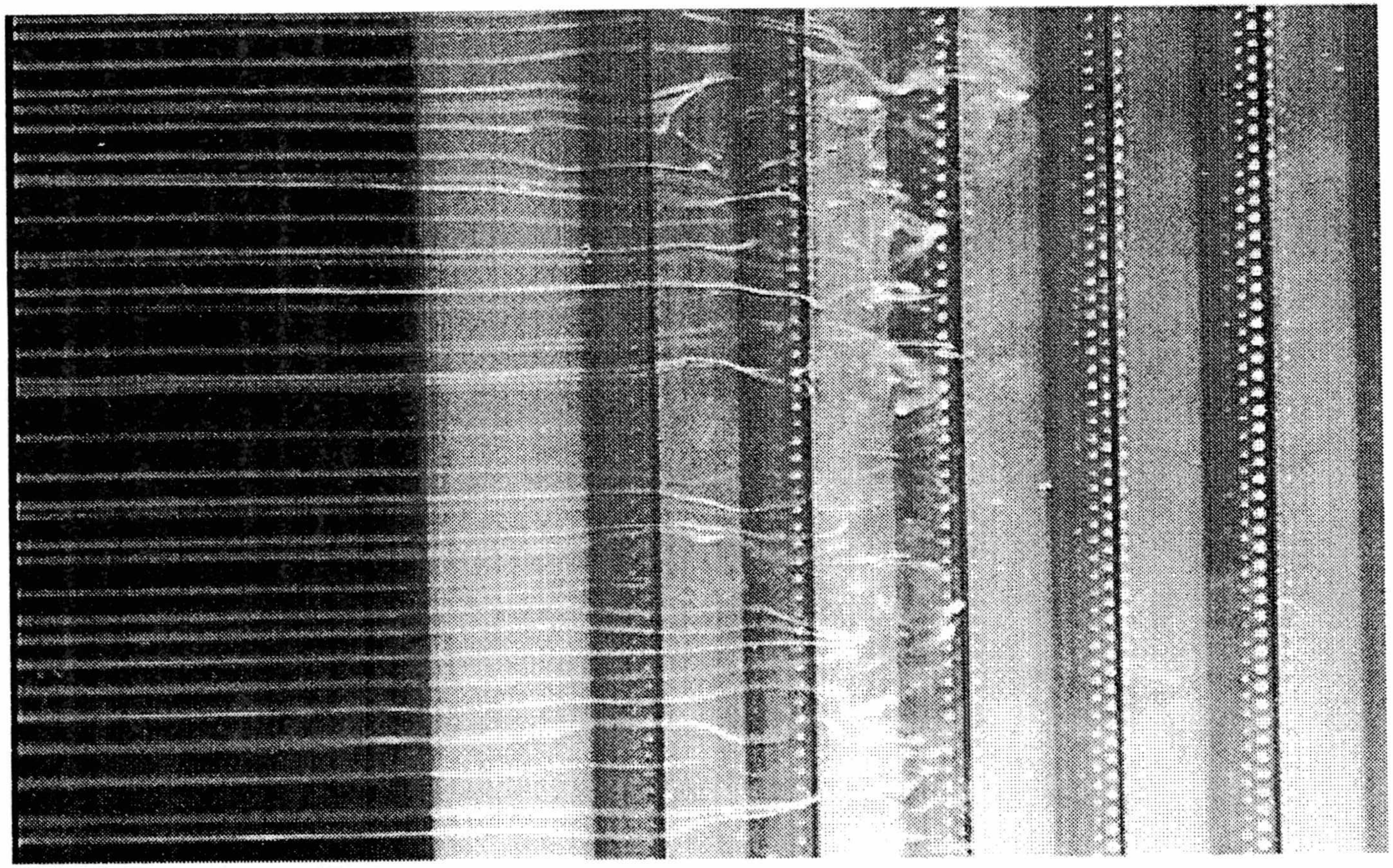

Figure 4.31 A horizontal digital image of asymmetric panel E2-A energized at 4.0 kV and 3.0 kHz with the thrust oriented counter-flow.

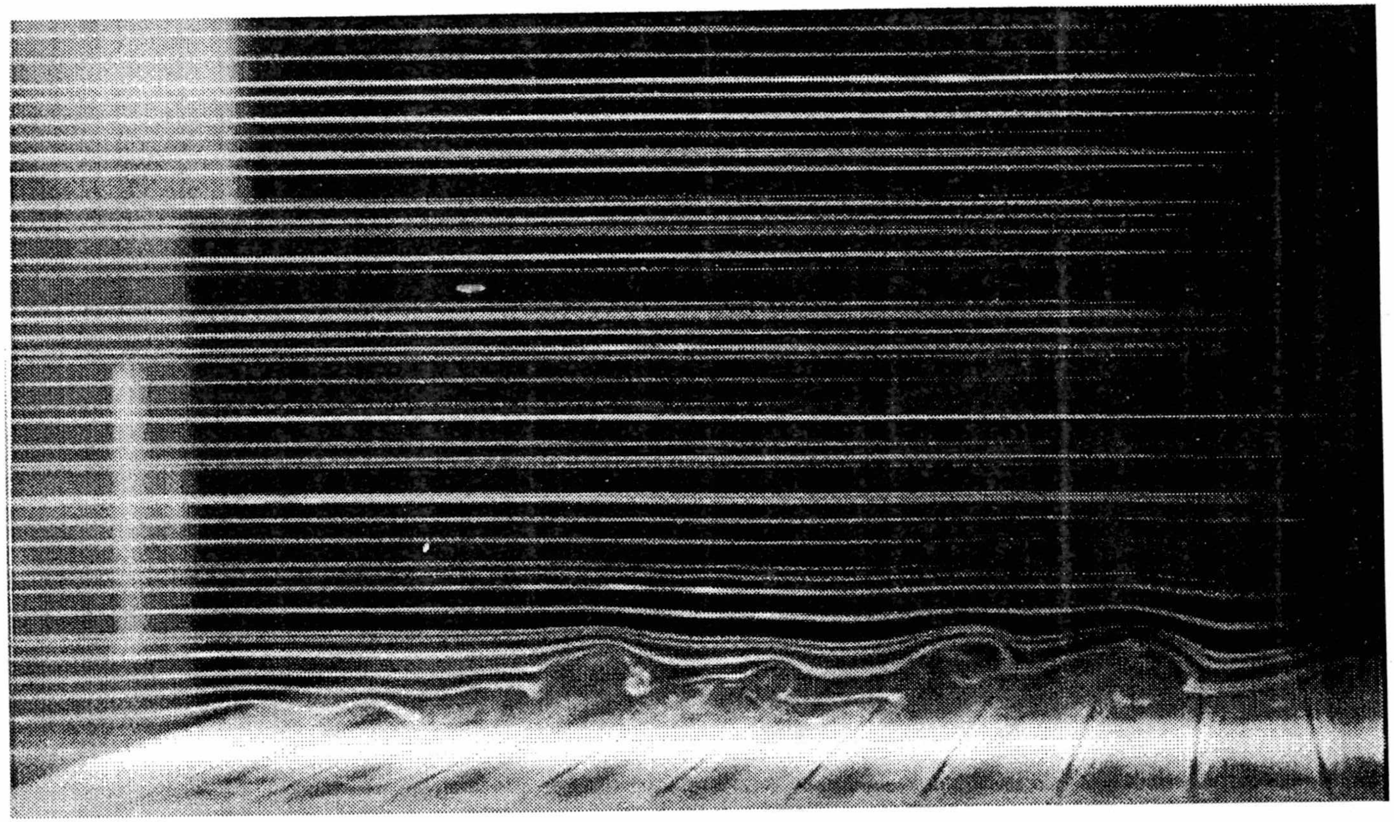

Figure 4.32 A vertical digital image of the asymmetric panel E2-A energzied at 4.0 kV and 3.0 kHz with the thrust oriented co-flow.

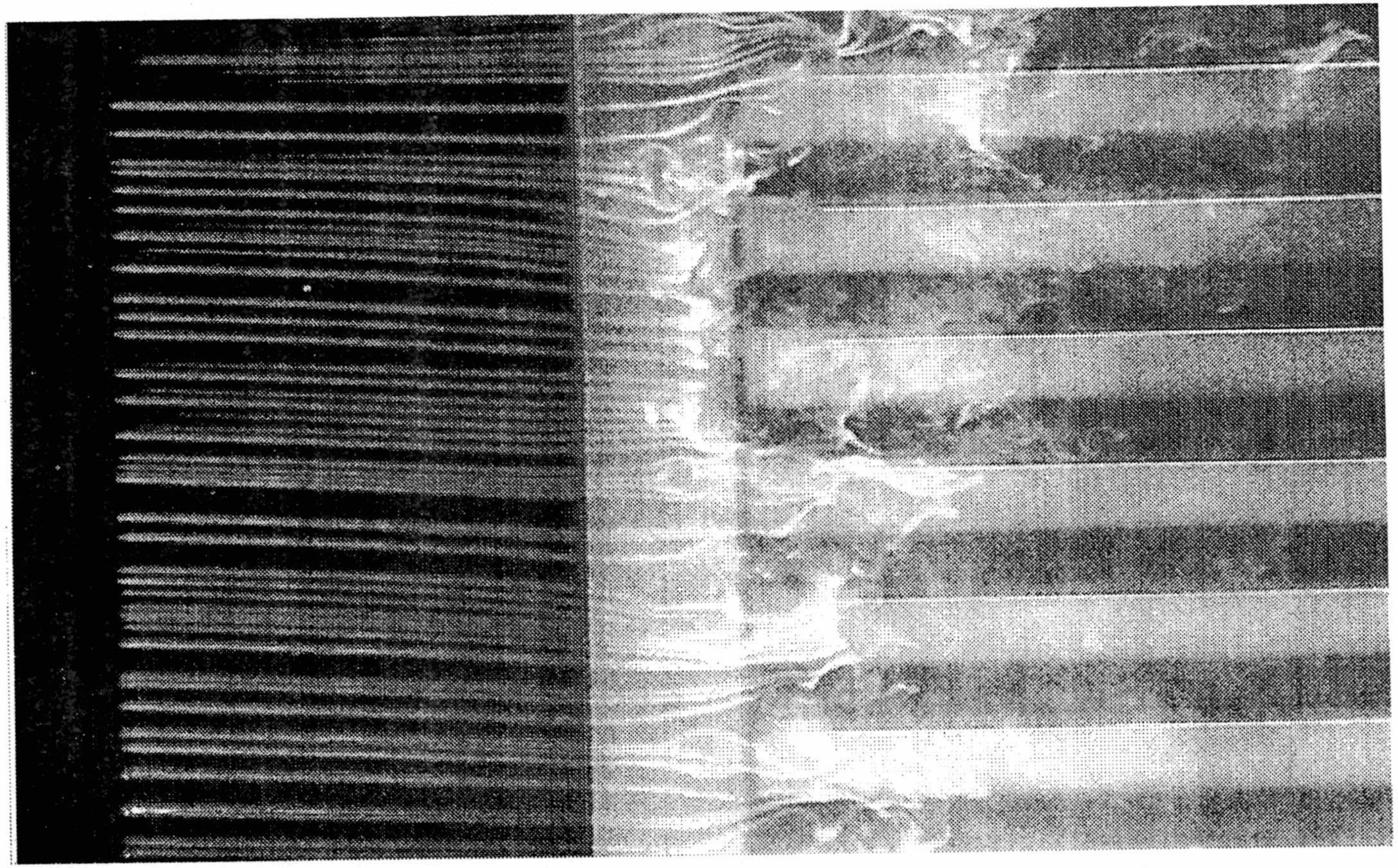

Figure 4.33 A horizontal image of the asymmetric panel E2-A energized at 4.0 kV and 3.0 kHz with the thrust oriented perpendicular to the flow.

Part V

Conclusion

Accuracy of Data

The accuracy of the experimental used in for the aerodynamic measurements was described in "Boundary layer flow control with a One Atmosphere Uniform Glow Discharge Surface Plasma" by J. R. Roth, S. P. Wilkinson and the author as follows:

> The primary experimental data measured during this investigation were pressure (for velocity) and force (for drag). Pressures were measured with capacitive or piezoelectric transducers with better than 0.1% accuracy and read on 5 ½ digit digital voltmeters with an order of magnitude or better accuracy than the pressure transducers. Given additional sources of error such as the data reduction model, probe alignment and position, probe viscous effects, and electronic voltage offsets and noise, the overall accuracy is still estimated to be within no more than ± 2% of the actual value, which was adequate for the current tests. The force on the drag balance was measured with an elastic piezoresistive force sensor with two active resistor elements. Two passive resistors were added to complete a bridge circuit. The bridge offset was amplified, filtered with a 4th order Butterworth low pass filter at 0.5 Hz, and calibrated against an applied streamwise force. The resultant resolution was about 10 milligrams. The absolute, systematic error is estimated to be less than 5% of the actual value and much better for comparative measurements (Roth et al, 1998).

The electrical diagnostic equipment, the Tektronix 1000X High Voltage Probe and the Pearson Electronics Current Monitor, were accurate to ± 3% and +1,%, respectively. Both instruments were operated well within their defined limits.

Heat and the OAUGDP Panels

There are at least four reasons why the observed effects are not due to heating. 1.) The OAUGD plasma is a collection of charged particles in the presence of strong electric fields. Charged particles are accelerated in electric fields. The aerodynamic effects are only observed when the plasma is present. 2.) Preliminary investigation of the downstream temperature of an energized test panel showed only a rise of several degrees Celsius after several minutes (Roth et al, 1998). The panels were operated for the shortest time intervals necessary to gather the data point (~5 seconds in most cases). The amount of added heat in this short time interval is insufficient to explain the results of the measurements. 3.) The asymmetric panel is a lateral gas flow accelerator once the plasma is generated. Any heating would lead to buoyancy forces rising upward, not propagating laterally. There is no reason to assume that the driving mechanism for the symmetric panel is any different from that of the asymmetric panel. This implies that the increase or decrease in drag observed for the test panels is the result of EHD body forces of the OAUGDP interacting with the neutral gas. 4.) A spanwise oriented symmetric panel and a spanwise oriented asymmetric panel can have identical plasma strip orientations and surface area, and yet the induced motion in the airflow is very different. If the measured results were due to heating this would not be true.

Discussion and Summary

The generation of a One Atmosphere Uniform Glow Discharge Plasma on one or both sides of an RF electrode strip results in a paraelectric body force due to Lorentzian collisions between the charged particles of the OAUGDP and the neutral gas. These collisions result in the transfer of momentum to the airflow. A simple estimate of the paraelectric induced velocity to a neutral gas can be formulated by setting the electrostatic pressure ($1/2\ \varepsilon_o E^2$) equal to a stagnation pressure ($1/2\ \rho v_o^2$) and solving for the induced velocity:

$$v_o = E\,(\varepsilon_o / \rho)^{0.5}$$

where ρ is equal to the density of air (Roth, 1998). For an electric field, $E = 10^6$ V/m, permitivity of free space, $\varepsilon_o = 8.85 \times 10^{-12}$, and density of air, $\rho = 1.3$ kg/m^3, the induced velocity, v_o, is 2.6 m/s. Both this expression and figure 4.26 show the induced air velocity has a linear dependence on voltage.

The exact electrohydrodynamic effect from the generation of strips of OAUGDP on the boundary layer is primarily dependent on 1.) the generation of the OAUGDP being symmetric or asymmetric, 2.) the orientation of the of the OAUGDP strips, 3.) the width of the OAUGDP strips (determined by the voltage), and 4.) the gap distance between the RF electrodes. In all generating configurations of the OAUGDP, except the co-flow orientation of an asymmetric panel, the magnitude of the aerodynamic drag increased, depending on the orientation and type of panel and airflow regime.

The symmetric panel oriented parallel to the airflow generates coherent vortical structures, with the resulting increase in drag dependent on gap distance of the RF electrodes and the voltage. The vortical structures also produced the two inflection points in the pitot tube velocity profiles for the symmetric panel. The asymmetric panel oriented parallel to the airflow, also generates a similar increase in drag, though smoke wire visualization showed no coherent structures. Pitot tube velocity profiles and an explanation for the similar increase in drag over all three airflow regimes, despite the absence of coherent airflow structures, were not pursued due to time constraints.

Both the symmetric panel oriented perpendicularly and the asymmetric panel counter-flow oriented show an increase in the drag by tripping the laminar flow. In pitot tube velocity profiles for both these configurations, the boundary layer was thickened in the laminar regime but the two inflection points were missing. Smoke-wire visualization of these panel configurations only shows a turbulent mixing of the smoke trails.

The co-flow oriented asymmetric OAUGDP panel has been shown to reduce the aerodynamic drag and thin the boundary layer, but changes the airflow from laminar to turbulent. This transition from laminar airflow to turbulent airflow is presumed to be due to the sudden acceleration of the of laminar airflow or from weak plasma generation in the counter-flow direction.

The final result of this study is that the OAUGDP is a technically viable method of EHD control of an aerodynamic boundary layer. The method of generating a surface layer of OAUGDP yields an airflow actuator that is inexpensive, flexible, reliable, rugged, potentially retrofitable, and requires low amounts of power. For these reasons, the possible OAUGDP methods of altering an aerodynamic boundary layer also show technological promise.

References

Bushnell, D. M. (1997): "Application Frontiers of 'Designer Fluid Mechanics' - Visions versus Reality or an Attempt to Answer the Perennial Question 'Why isn't it Used?'", AIAA Paper 97-2110, 28th AIAA Fluid Dynamics Conference, June 29 - July 2, 1997, Snowmass Village, CO.

Carr A., and Roth J. R. (1996a): "Characteristics of a One Atmosphere Uniform Glow Discharge Plasma", IEEE Paper 2HP-23, 23rd IEEE Conference on Plasma Science, June 3-5.

Carr A., and Roth J. R. (1996b): "Comparison of parallel-plate and flat-plate configurations of a One Atmosphere Uniform Glow Discharge Plasma (OAUGDP)", APS Paper 7HP-30, 38th Annual Meeting of the APS Division of Plasma Physics, APS Bulletin, Series II, Vol. 41, No. 7, p. 1539.

El-Khabiry S., and Colver G. M. (1997): "Drag Reduction by DC Corona Discharge Along an Electrically Conductive Flat Plate for Small Reynolds Number Flow", Phys. Fluids, Vol. 9, No. 3 (1997) pp. 587-599.

Falkenstein Z. and Coogan J. (1996): "Microdischarge behaviour in the silent discharge of nitrogen-oxygen and water - air mixtures", Journal of Applied Physics, Phys. 30, pp. 817-825.

Hefner J. and Bushnell N. (1989): "Viscous Drag Reduction", in Viscous Drag Reduction in Boundary Layers, AIAA Progress in Astronautics and Aeronautics, Vol. 123, Seabass A. R., ed., ISBN 0--930403-66-5, pp. 457-476.

Kimura M., Tung S., Ho C., Jiang F., Tai Y. (1997): "MEMS for Aerodynamic Control", AIAA Paper 97-2118, 28th AIAA Fluid Dynamics Conference, June 29 - July 2, 1997, Snowmass Village, CO.

Lachowicz C. T., Yao C. S., Wlezien R. W. (1998): "Scaling of an Oscillatory Flow Control Actuator", AIAA Paper 98-0330, 36th AIAA Aerospace Sciences Meeting and Exhibit, January 12 - 15, 1998, Reno, NV.

Massines F. (1998), Ben Gadri R., Rabehi A., Decomps Ph., Segur P. : "Mechanisms of a Glow Discharge at Atmospheric Pressure Controlled by Dielectric Barrier", Journal of Applied Physics, Vol. 83, No. 6, pp. 2950-2957.

Roth J. R. (1998): "Boundary Layer Flow Control with a One Atmosphere Uniform Glow Discharge Surface Plasma ... Part I: Electrohydrodynamic Flow Control", AIAA Paper 98-0328 (Oral presentation thereof), 36th AIAA Aerospace Sciences Meeting and Exhibit, Reno NV, January 13, 1998.

Roth J. R., Sherman D. M., Wilkinson S. P.(1998): "Boundary Layer Flow Control with a One Atmosphere Uniform Glow Discharge Surface Plasma", AIAA Paper 98-0328, 36th AIAA Aerospace Sciences Meeting and Exhibit, Reno NV, January 13, 1998.

Roth J. R., Tsai P.P., and Liu C.(1995a): "Steady-state, Glow Discharge Plasma and Applications Thereof", U.S. Patent #5,387,842, Issued February 7, 1995.

Roth J. R., Tsai P.P., Liu C., and Laroussi M., and Spence P.D. (1995b): "One Atmosphere Uniform Glow Discharge Plasma", U.S. Patent #5,414,324, Issued May 9, 1995.

Roth, J. R. (1995c): Industrial Plasma Engineering. Volume 1 - Principles, Institute of Physics Publishing, Bristol and Philadelphia, ISBN 0-7503-0318-2, 1995, pp. 453-461.

Roth, J. R. (1997): "Method and Apparatus for Covering Bodies with a Uniform Glow Discharge Plasma and Applications Thereof", U.S. Patent #5,669,583, Issued September 23, 1997.

Spence P.D., Liu C., Roth J.R. (1993): "Preliminary Measurements of the Plasma Properties of a One Atmosphere Uniform Glow Discharge Plasma", APS Bulletin, Vol. 38, No. 10, p. 1901.

Tong H., Yongmin K., and Roth J. R. (1995): "Characteristics of a One Atmosphere Uniform Glow Discharge Plasma in Air", APS Paper 5S-24, 37th Annual Meeting of the APS Division of Plasma Physics, APS Bulletin, Vol. 40, No. 11, P. 1774.

Tsinober, A. (1989), "MHD Flow Drag Reduction", in Viscous Drag Reduction in Boundary Layers, AIAA Progress in Astronautics and Aeronautics, Vol. 123, Seabass A. R., ed., ISBN 0–930403-66-5, pp. 327-349.

Walsh M. (1989), "Riblets", in Viscous Drag Reduction in Boundary Layers, AIAA Progress in Astronautics and Aeronautics, Vol. 123, Seabass A. R., ed., ISBN 0--930403-66-5, pp. 203-261.

Wygnanski I. (1997): "Boundary Layer and Flow Control by Periodic Addition of Momentum (Invited)", AIAA Paper 97-2117, 4th AIAA Sheer Flow Control Conference, June 29 July 2, 1997, Snowmass Village, CO.

Zhang Y.S, and Kuo S., (1989): "Bragg Scattering of EM Waves by microwave produced periodic plasma layers", International Conference on Plasma Science, 1989, Buffalo, NY.

Appendix

Table of OAUGDP Test Panels and Characteristics

Panels are designated in the following format:

1.) Letter

B Panel designs with electrodes on the same side of the panel.

C Panel designs with symmetric electrode patterns.

D Panel designs with electrode patterns designed for DC acceleration.

E Panel designs with asymmetric electrode patterns.

2.) A panel design number (not all designs were fabricated).

3a.) Letter A or B if the panel's electrodes are to be oriented streamwise to the airflow.

3b.) Letter C or D if the panel's electrodes are to be oriented spanwise to the airflow.

Table of Panel Designs and Parameters*

Panel Designation	Width of Upper Electrodes	Width of Lower Electrodes	Spacing Between Upper Electrodes	Spacing Between Electrode Patterns
C1- A or C	2	2	8	4
C2- A or C	1	Sheet Electrode	4	Sheet Electrode
C5- A or C	0.5	Sheet Electrode	6.5	Sheet Electrode
C7- A or C	0.5	Sheet Electrode	10.5	Sheet Electrode
E2- A	0.5	4	8.5	2.5
E6- C	0.5	3.5	8.5	2.5

* This table applies only to OAUGDP panels mentioned in the text and figures.

VITA

Daniel Max Sherman was born in Corpus Christi, Texas on March 11, 1971. For most of his pre-collegiate education, he attended the public schools in Dayton, Tennessee but due to moving in the middle of his high school senior year, graduated from Hixson High School in Chattanooga, Tennessee in May of 1989. He entered the University of Tennessee, in Knoxville, in June of 1989 where in May of 1995 he received a Bachelor of Science with majors in engineering physics, mathematics, and psychology.

In October of 1995, he began a graduate research assistantship in the University of Tennessee Plasma Sciences Laboratory assisting with research involving the application of the One Atmosphere Uniform Glow Discharge Plasma with aerodynamic boundary layers. He entered the Master's degree program in Physics at The University of Tennessee, in Knoxville in January of 1996, officially receiving the Master's degree in August of 1998.

Though presently in Europe for a summer internship for research involving the application of the One Atmosphere Uniform Glow Discharge Plasma for plasma deposition, he will return to the University of Tennessee and its Plasma Sciences Laboratory in August 1998 to pursue a Doctorate of Science in Engineering Science with a focus in aerodynamics and computation fluid dynamics involving atmospheric plasma.